Project Report
ATC-375

Analysis of Ground-Based Radar Low-Altitude Wind-Shear Detection in OEP Terminal Airspace for NextGen

S. Huang
J.Y.N. Cho

2 December 2010

Lincoln Laboratory
MASSACHUSETTS INSTITUTE OF TECHNOLOGY
LEXINGTON, MASSACHUSETTS

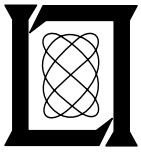

Prepared for the Federal Aviation Administration,
Washington, D.C. 20591

1. Report No.	2. Government Accession No.	3. Recipient's Catalog No.
ATC-375		

4. Title and Subtitle	5. Report Date
Analysis of Ground-Based Radar Low-Altitude Wind-Shear Detection in OEP Terminal Airspace for NextGen	2 December 2010
	6. Performing Organization Code

7. Author(s)	8. Performing Organization Report No.
Suilou Huang and John Y.N. Cho	ATC-375

9. Performing Organization Name and Address	10. Work Unit No. (TRAIS)
MIT Lincoln Laboratory 244 Wood Street Lexington, MA 02420-9108	11. Contract or Grant No. FA8721-05-C-0002

12. Sponsoring Agency Name and Address	13. Type of Report and Period Covered
Department of Transportation Federal Aviation Administration 800 Independence Ave., S.W. Washington, DC 20591	Project Report
	14. Sponsoring Agency Code

15. Supplementary Notes

This report is based on studies performed at Lincoln Laboratory, a center for research operated by Massachusetts Institute of Technology, under Air Force Contract FA8721-05-C-0002.

16. Abstract

To support the Next Generation Air Transportation System (NextGen), the Reduce Weather Impact Sensor RightSizing program is identifying and analyzing gaps in the current sensor network coverage relative to the Four-Dimensional Weather Data Cube Single Authoritative Source performance requirements. In this study, we look for shortfalls in low-altitude wind-shear sensing by ground-based radars and lidar in the NextGen super-density operations (SDO) terminal airspace. Specifically, 2D gridded wind-shear visibility (an upper bound to detection probability) data are generated for microbursts and gust fronts separately for different sensors, namely the Terminal Doppler Weather Radar, Next Generation Weather Radar, Airport Surveillance Radar-9 with Weather Systems Processor, and Doppler lidar.

17. Key Words	18. Distribution Statement
	This document is available to the public through the National Technical Information Service, Springfield, VA 22161.

19. Security Classif. (of this report)	20. Security Classif. (of this page)	21. No. of Pages	22. Price
Unclassified	Unclassified	88	

This page intentionally left blank.

EXECUTIVE SUMMARY

To support the Next Generation Air Transportation System (NextGen), the Reduce Weather Impact (RWI) Sensor RightSizing program is identifying and analyzing gaps in the current sensor network coverage relative to the Four-Dimensional Weather Data Cube (4D Wx Cube) Single Authoritative Source (SAS) performance requirements. In this study, we look for shortfalls in low-altitude wind-shear sensing by ground-based radars and lidar in the NextGen super-density operations (SDO) terminal airspace. Specifically, 2D gridded wind-shear visibility (an upper bound to detection probability) data are generated for microbursts and gust fronts separately for different sensors, namely the Terminal Doppler Weather Radar (TDWR), Next Generation Weather Radar (NEXRAD), Airport Surveillance Radar-9 (ASR-9) with Weather Systems Processor (WSP), and Doppler lidar. The 35 Operational Evolution Partnership (OEP) airports are chosen to represent the SDO terminals.

The major findings are as follows:

1. Today's ground-based radar and lidar wind-shear sensors generally provide good microburst coverage inside a 10-km radius around the airport. The microburst visibility decreases with range such that over the entire SDO terminal airspace (100-km radius) the mean microburst visibility decreases to ~30%.
2. Because gust fronts in general are thicker in height than microburst outflows, they are observable by the same sensors to longer distances. The mean gust-front visibilities in the SDO terminal airspaces are ~95% (50-km radius) and ~70% (100-km radius).
3. Specific OEP airports with significantly worse low-altitude wind-shear coverage than the average results discussed above are HNL, LAS, LAX, PDX, PHX, SAN, SEA, SFO, and SLC. These terminal airspaces have mean wind-shear visibilities of < 20% (microburst) and < 40% (gust front) over the entire 100-km radius. The causes for the deficits are not having a TDWR (the best wind-shear sensor), terrain blockage, NEXRADs that are located too high above the terminal ground level, or a combination of these factors.
4. The 0.5-km horizontal resolution requirement for the SDO terminal airspace will not be met by ground-based wind-shear radars and lidar at the farther reaches of the terminal airspace.
5. The current gust-front product update period is tied to the radar volume scan period, so it will not satisfy the 1-min NextGen 4D Wx Cube SAS requirement with today's TDWR (5 min) and NEXRAD (4-10 min) volume scan periods. The ASR-9 WSP and lidar gust-front update periods are short enough (1 min) as are the microburst update periods for all sensors considered.
6. The requirement to measure the vertical extent of wind shears with ±50-ft accuracy is not met with today's sensor products (measurements of the height of wind-shear phenomena are not attempted). Radars cannot make vertical measurements with such accuracy and resolution; lidars may be able to, but they have very limited range.

7. There is currently no product that tracks the motion of microbursts as required by NextGen. However, such a product can likely be developed using the already available sensor data.

The wind-shear coverage gaps identified are mainly caused by the fact that the phenomena of interest are restricted to very low altitudes and the range of the ground-based sensors are limited by the Earth's curvature everywhere and severe terrain blockage at certain sites. To cover the gaps, data from additional sensors (either existing ones that are not used for this purpose now and/or newly acquired sensors) are necessary. To satisfy all of the NextGen 4D Wx Cube SAS low-level wind-shear observation requirements is likely to be a very costly enterprise. However, one should take a careful look at the concept of NextGen flight operations to determine if blanket coverage of low-level wind-shear detection is truly necessary over the entire SDO terminal airspace. For example, how would a microburst alert 100 km from the airport be used?

The various wind-shear sensors have varying performance characteristics as well as different levels of life-time cost, and the performance and cost are closely related. Therefore, the deployment strategy in the past has been based on careful cost/benefit analyses. For example, TDWRs (best performance, highest cost) were not deployed at LAX, PDX, SAN, SEA, and SFO, because the occurrence rates of convective wind shears are very low at those west coast locations. And, thus, their low-level wind-shear coverage is significantly worse than in the other OEP terminal airspaces. As the NextGen 4D Wx Cube SAS requirements currently stand, all SDO terminal airspaces need to be covered equally for low-level wind shears, regardless of the occurrence rate of such events. Perhaps such a blanket coverage requirement is warranted under the new NextGen flight operations concept, but that is the type of issue that needs to be investigated in the future.

TABLE OF CONTENTS

This page intentionally left blank.

LIST OF ILLUSTRATIONS

LIST OF TABLES

This page intentionally left blank.

1. INTRODUCTION

Low-altitude wind shear is recognized as an aviation danger thanks to intensive research in the late 1970s through late 1980s that was triggered by a series of fatal aircraft crashes during departure and arrival in airport terminal areas. In the 1990s and early 2000s, the Federal Aviation Administration (FAA) deployed the Terminal Doppler Weather Radar (TDWR), an advanced weather radar that was specially designed for low-altitude wind-shear surveillance, to provide protection at 46 major airports. Subsequently, wind-shear-related aviation accident rates in the United States have dropped by one order of magnitude, from ~1 fatal accident per decade to ~1 per century, with much of the credit going to the TDWR (Hallowell et al., 2009).

More recently the U.S. government launched an ambitious program to develop the Next Generation Air Transportation System (NextGen) to improve aviation efficiency. While the current low-altitude wind-shear surveillance is focused on the airport AREas Noted for Attention (ARENAs), wind-shear coverage expansion is listed as one of the aviation investment packages in the NextGen Network-Enabled Weather/Reduce Weather Impact (NNEW/RWI) Preliminary Portfolio Requirements (FAA, 2008). (The ARENAs consist of the runway length plus three nmi final on approach and two nmi on departure times a width of one nmi.) Common performance requirements for the NextGen Four-Dimensional Weather Data Cube (4D Wx Cube) Single Authoritative Source (SAS) are given in Table 1-1, where the super-density operations (SDO) terminal airspace is defined to be the volume of airspace within 100-km horizontal range of centerfield with height extending to the terminal airspace ceiling (FAA, 2009). Also in the same document, detailed performance requirements are listed for wind-shear observation, which are discussed in Section 3.4.

To make sure that weather observation capabilities will be able to meet the NextGen 4D Wx SAS requirements, the FAA initiated the Sensor RightSizing program to assess the gaps in the current sensor network for observing aviation-relevant weather phenomena. In the previous year, the RightSizing team investigated the ability of current sensors to meet the NextGen weather observation functional requirements (FAA, 2009a). This year, one of the goals is to identify and analyze gaps relative to the sensor performance requirements (FAA, 2009).

The focus of this study is to generate 2D low-altitude microburst and gust-front visibility data to show the current and potential coverage in SDO terminal airspaces. An SDO terminal is defined to be an airport with enplanements of at least 1% of all U.S. enplanements (Souders et al., 2010). Statistics from 2008 show 29 airports to fall into this category (FAA, 2009b). However, since these rankings fluctuate from year to year, we used the FAA's list of Operational Evolution Partnership (OEP) airports as a more stable alternative. The 35 OEP airports (the 29 SDO terminals plus six others) are major terminals that were selected in 2000 due to their significant impact on delays over the entirety of the National Airspace System (NAS). The sensors examined in this study include the TDWR, Weather Surveillance Radar-1988 Doppler (more commonly known as the Next Generation Weather Radar (NEXRAD)), Airport Surveillance Radar-9 (ASR-9) with Weather Systems Processor (WSP), and a Lockheed Martin Coherent Technologies (LMCT) Doppler lidar. A Cartesian-gridded data set is generated here in

accordance with the NextGen's spatial resolution requirements. In the end, we examine the wind-shear visibility results at each airport, along with the NextGen requirement for horizontal resolution of wind-shear detection, to see whether the NextGen performance requirements are met.

Note that NEXRAD is currently used for gust front detection but not microburst detection. Therefore, only the gust-front coverage results are currently valid for NEXRAD. The fastest volume update rate of about four minutes is thought to be too slow to capture microburst genesis at an operationally acceptable rate. This notion, however, is currently undergoing investigation at the Massachusetts Institute of Technology Lincoln Laboratory (MIT LL) using real data cases. Also, implementation of a proposed adaptive truncation of NEXRAD volume scans dubbed AVSET (automated volume scan evaluation and termination) (Chrisman 2009) could improve the update rate for the critical surface scan. Thus, the NEXRAD microburst visibility results given in this report can be seen as potential gap fillers for OEP terminals.

Table 1-1. NextGen 4D Wx Cube SAS Performance Requirements Above Surface

Location Above Surface		Super-Density Terminal Airspace		En Route Airspace		Global Airspace		Designated En Route Terminal Airspace		Designated Global Terminal Airspace	
Weather Type		Convective	Other	Convective	Other	Convective	Other	Convective	Other	Convective	Other
Horizontal Resolution		1/2 km	½ km	1 km	4 km	10 km	10 km	1 km	4 km	10 km	10 km
Horizontal Accuracy		1/4 km	¼ km	1/2 km	2 km	5 km	5 km	1/2 km	2 km	1/2 km	5 km
Vertical Resolution	≥ 5000 ft AGL	500 ft	500 ft	500 ft	500 ft	500 ft	500 ft	500 ft	500 ft	500 ft	500 ft
	< 5000 ft AGL	100 ft	100 ft					100 ft	100 ft	100 ft	100 ft
Vertical Accuracy	≥ 5000 ft AGL	250 ft	250 ft	250 ft	250 ft	250 ft	250 ft	250 ft	250 ft	250 ft	250 ft
	< 5000 ft AGL	50 ft	50 ft					50 ft	50 ft	50 ft	50 ft
Update Period		1 min	5 min	2 min	5 min	10 min	20 min	1 min	5 min	2 min	20 min

2. METHODOLOGY

To investigate terminal airspace coverage, we first identify the ground-based wind-shear sensors near the OEP airports. The sensor identification (ID) code and its distance to the airport are listed in Table 2-1. Twenty nine out of the 35 OEP airports are equipped with TDWR. Four airports that do not have a TDWR are covered by the ASR-9 WSP. One airport, LAS, has both TDWR and lidar due to the presence of severe road clutter and occurrence of dry microbursts. Two airports, SAN and SFO, do not have a TDWR, ASR-9 WSP, or lidar, although SFO is equipped with a Low-Level Wind-Shear Alert System (LLWAS). LLWAS was not included in this quantitative study, because it is an in-situ local-coverage system that has negligible impact on overall SDO terminal airspace coverage as currently deployed. For example, the DEN LLWAS is the only LLWAS that covers all of the ARENAs (Cho and Hallowell, 2008), but that still translates to merely 0.4% of the SDO terminal airspace area. Also, out of the 35 OEP airports, only nine (ATL, DEN, DFW, LGA, MCO, ORD, SFO, STL, and TPA) are equipped with LLWAS. We will, however, include LLWAS in the potential gap filler discussion (Section 3.5).

In this study, all airports are associated with only the nearest NEXRAD. In fact, no more than one radar per radar type is assigned to each airport. In reality, there can be more than one TDWR or NEXRAD that potentially contribute to wind-shear detection within the 100-km radius around an airport. For example, the four TDWRs in the Potomac region (ADW, BWI, DCA, and IAD) are spaced close enough to likely yield useful wind-shear data to each other's future terminal airspace domains. This is likewise true in south Florida (FLL, MIA, PBI), Dallas (DAL and DFW), Chicago (MDW and ORD), and New York City (EWR and JFK). (Many TDWR airports, however, are spaced too far apart for such data sharing.) More than one NEXRAD may also produce usable wind-shear data per airport. If necessary, we can extend our study in the future to incorporate all possible weather radars, perhaps even non-FAA radars and in situ systems, to examine effective (and cost-efficient) gap filling measures. For now, we simply identify very basic gaps relative to the spatial resolution and coverage requirements of the NextGen 4D Wx Cube SAS.

The wind-shear coverage is evaluated by a quantity called wind-shear visibility (Cho and Martin, 2007). It is defined as the probability that a sensor can distinguish a wind-shear (i.e., microburst and gust front) velocity signal from noise and clutter in a given resolution volume. It does not include the probability of the wind-shear detection algorithm to correctly classify a macroscopic collection of these pixels as a microburst/gust-front event. Thus, the wind-shear visibility value is an upper bound to the probability of detection.

The wind shear visibilities for different sensors are calculated based on the wind-shear detection performance model developed at MIT LL (Cho and Hallowell, 2008). The radar signal processing, beam blockage, ground clutter, range folding, partial beam filling, and microburst and gust-front reflectivity and outflow height distributions are all considered in this model. Terrain data from the Shuttle Radar Topography Mission (SRTM), Digital Terrain Elevation Data (DTED), and Digital Feature Analysis Data (DFAD) are compiled to generate accurate

terrain blockage and ground clutter maps with improved representation of tall buildings and road clutter (Huang et al., 2009). The resulting wind-shear visibility is ranked from 0 (not visible) to 1 (100% visible) at each grid point in the area of interest.

Table 2-1. Ground-Based Wind-Shear Sensors Closest to the OEP Airports

	Sensor I.D.			Distance to Airport (km)			
Airport	TDWR	ASR-9 WSP	NEXRAD	TDWR	NEXRAD	ASR-9 WSP	LIDAR
ATL	ATL		FFC	15.3	33.3		
BOS	BOS		BOX	23.6	46.7		
BWI	BWI		LWX	10.1	73.5		
CLE	CLE		CLE	18.9	0.9		
CLT	CLT		GSP	14.7	122.1		
CVG	CVG		ILN	18.0	83.7		
DCA	DCA		LWX	12.3	40.6		
DEN	DEN		FTG	19.5	13.8		
DFW	DFW		FWS	21.7	43.7		
DTW	DTW		DTX	17.5	55.0		
EWR	EWR		DIX	14.0	85.3		
FLL	FLL		AMX	20.7	57.5		
HNL	LAS	HNL	HMO	4459.8	79.7	0.6	
IAD	IAD		LWX	16.7	3.9		
IAH	IAH		HGX	23.5	62.2		
JFK	JFK		OKX	10.3	81.2		
LAS	LAS		ESX	14.8	48.2		0.7
LAX	LAS	LAX	SOX	394.8	72.7	1.1	
LGA	JFK		OKX	20.9	85.6		
MCO	MCO		MLB	9.6	73.2		
MDW	MDW		LOT	15.1	34.2		
MEM	MEM		NQA	16.3	34.8		
MIA	MIA		AMX	20.5	23.7		
MSP	MSP		MPX	22.5	27.8		
ORD	ORD		LOT	20.5	44.2		
PDX	SLC	PDX	RTX	1005.4	31.9	2.2	
PHL	PHL		DIX	17.0	71.5		
PHX	PHX		IWA	14.1	35.6		
PIT	PIT		PBZ	21.5	4.6		
SAN	LAS		NKX	0.0	24.8		
SEA	SLC	SEA	ATX	1096.9	83.9	0.4	
SFO	LAS		MUX	676.7	66.6		
SLC	SLC		MTX	20.3	65.9		
STL	STL		LSX	12.9	28.6		
TPA	TPA		TBW	12.9	32.6		

The relevant sensor parameters used in the model are listed in Table 2-2. Note that performance improvements due to the radar upgrades planned in the programmed service life extension programs (SLEPs) are assumed (which mainly impacts the maximum clutter suppression figures). The specifications and settings for the current LMCT Doppler lidar at LAS are used in the model (Hannon, 2004; R. Frankel, person communication).

Table 2-2. Ground-based Sensor Parameters Used in the Wind-Shear Visibility Model

Parameter	TDWR	NEXRAD	ASR-9 WSP	LIDAR
Beamwidth (azimuth x elevation)	0.55°x0.55°	0.925°x0.925°	1.4°x4.8°	10 cm[1]
Range Resolution (km)	0.15	0.25	0.12	0.10
Min. Doppler Obs. Range (km)	0.5	~0.5	~0.5	0.3
Max. Doppler Obs. Range (km)	90	300	111	10[2]
Beam Elevation Angle	0.3°	0.5°	2°	2°
Max. Clutter Suppression (dB)	60	60	60	N/A
Min. Detectable dBZ @ 50 km	-11	-10	7	N/A

[1] Collimated beam diameter.
[2] Current cut-off range; could be extended with an upgrade to the signal processing system.

The initial model output is in polar coordinates because that is how a radar "sees" an object. For comparisons with the FAA performance requirements, we convert the wind-shear visibility results to Cartesian coordinates with equal spacing. Further, the radar areal-resolution maps are also generated in Cartesian coordinates to address the FAA requirements for horizontal resolution of the wind-shear sensor measurements. In addition to the entire SDO terminal airspace, we also assess the wind-shear visibilities for areas closer to the airport, i.e., within 10 and 50-km radii to obtain better insight about the wind-shear coverage of different sensors.

This page intentionally left blank.

3. RESULTS AND DISCUSSION

In this section, we first give an overview of the NextGen 4D Wx Cube SAS SDO terminal airspace wind-shear performance requirements, i.e., the wind-shear product horizontal (or areal) resolution and accuracy. We then present the results of the wind-shear visibilities for each airport. To obtain more detailed information within the terminal airspace, we break it down to regions within 10, 50, and 100-km radii around the airport. Finally, we comment item by item on whether each NextGen wind-shear requirement is met or likely to be met.

3.1 AREAL RESOLUTION OF WIND-SHEAR SENSORS

Some remarks need to be made about the NextGen horizontal resolution requirements in Table 1-1 and later in Table 3-4. Radar measurement is polar coordinate oriented. Hence, how fine the instrument can measure can be evaluated by the 2D range-azimuth resolution, which is known for each type of radar. This parameter, along with the maximum range at which the radar produces Doppler data, are listed in Table 3-1 for all sensors. For the lidar, we use the current maximum range limit (10 km). To go beyond this range, its signal processing hardware needs to be upgraded. The azimuth resolutions are approximate, based on the angular span of coherent integration.

Table 3-1. Resolution and Maximum Range of Wind-Shear Sensors

Sensor	Range-Azimuth Resolution (km/°)	Maximum Range (km)
TDWR	0.15/1	90
NEXRAD	0.25/1	300
ASR-9 WSP	0.116/1.4	111
Lidar	0.10/1	10

However, the NextGen 4D Wx Cube SAS horizontal resolution requirements are only given in one dimension (0.5 km for SDO airspace (Table 1-1)). Therefore, it is necessary to assume a relationship between the 2D radar/lidar resolution and 1D requirement. Here we assume that the horizontal resolution value can simply be squared to yield an equivalent areal resolution requirement (0.25 km^2). It is also possible to take the worst-case horizontal resolution of the sensor (i.e., the greater of the range or azimuth dimension) as the metric (see discussion in Section 2 of Cho (2010)). This is a point that needs to be discussed with the requirements definition team.

The fraction of the SDO airspace area where the NextGen areal-resolution requirement (as we interpret it) for wind-shear detection is met is listed in Table 3-2 for different radii around the airports. The results show that at the current sensor locations and current range, TDWR can cover the 10 and 50-km radius areas with adequate resolution. Also for the area out to 100-km range, which is beyond TDWR's maximum range, there is still $\geq 75\%$ of the area with areal

resolution satisfying the requirement. NEXRAD can provide adequate resolution for 19 airports within a 10-km radius (≥ 90%). At 50-km radius around the airport, only 4 airports (CLE, DEN, IAD, and PIT) have nearly complete coverage with adequate resolution. At the same range, the rest of the airports have 12%–82% of properly covered areas. Inside a 100-km radius, NEXRAD is expected to provide 7%–33% area with adequate areal resolution for the airports. For ASR-9 WSP-equipped airports, the compliance rates are similar to the TDWR-covered airports. The lidar also has adequate resolution fraction similar to TDWR and ASR-9 WSP within 10-km range. The airports with overall worst wind-shear resolution are SAN and SFO, which rely solely on the NEXRAD for weather radar coverage. (Note, again, that in the discussion of NEXRAD coverage, only gust front products are currently generated, not microburst products.)

To summarize, TDWR and ASR-9 WSP-equipped airports have about three quarters of the area where the areal resolution is sufficient for NextGen (without taking into account the actual wind-shear visibility). For airports without either of these two primary terminal weather radars (SAN and SFO), only ~30% of the area satisfies the NextGen resolution requirement. Therefore, to fully meet such a requirement, more sensors are needed to increase the wind-shear resolution in SDO terminal airspace. The situation is significantly worse if the alternate definition of radar horizontal resolution (the worse of either the range or azimuth resolution) is assumed. See the tables in Appendix A of Cho (2010) for further details.

Note that the definition of SDO airspace may be in flux. At a conference presentation more recent than the performance requirements document on which we based this study, a radius of 180 km was mentioned as defining SDO airspace (Souders et al., 2010). If this larger area is adopted for SDO airspace, then the coverage statistics reported here will become significantly worse overall. There is also the thinking that NextGen airspaces will be defined dynamically, i.e., their spatial dimensions my change in real time (J. Tauss, personal communication). In this case, the requirements definition process clearly becomes more complicated.

Table 3-2. Fraction in the 10, 50, and 100-km Radius Area Around the Airport with Areal Resolutions Meeting the NextGen 4D Wx Cube SAS SDO Airspace Requirements

	10km				50km			100km		
Airport	TDWR	NEXRAD	ASR-9 WSP	LIDAR	TDWR	NEXRAD	ASR-9 WSP	TDWR	NEXRAD	ASR-9 WSP
ATL	0.97	0.95	0	0	0.99	0.69	0	0.79	0.33	0
BOS	0.97	0.94	0	0	0.99	0.53	0	0.75	0.32	0
BWI	0.98	0.00	0	0	1.00	0.23	0	0.81	0.24	0
CLE	0.98	0.97	0	0	0.99	0.99	0	0.77	0.33	0
CLT	0.98	0.00	0	0	1.00	0.00	0	0.79	0.07	0
CVG	0.98	0.00	0	0	0.99	0.14	0	0.78	0.20	0
DCA	0.98	0.94	0	0	1.00	0.60	0	0.80	0.33	0
DEN	0.97	0.97	0	0	0.99	0.94	0	0.77	0.33	0
DFW	0.97	0.94	0	0	0.99	0.56	0	0.76	0.33	0
DTW	0.97	0.60	0	0	0.99	0.43	0	0.78	0.30	0
EWR	0.98	0.00	0	0	0.99	0.12	0	0.80	0.19	0
FLL	0.97	0.45	0	0	0.99	0.40	0	0.76	0.29	0
HNL	0	0.00	0.99	0	0	0.17	1.00	0	0.22	0.78
IAD	0.98	0.97	0	0	0.99	1.00	0	0.79	0.33	0
IAH	0.97	0.17	0	0	0.99	0.35	0	0.75	0.28	0
JFK	0.98	0.00	0	0	0.99	0.16	0	0.81	0.21	0
LAS	0.98	0.93	0	0.95	0.99	0.51	0	0.79	0.32	0
LAX	0	0.00	0.99	0	0	0.24	1.00	0	0.24	0.78
LGA	0.97	0.00	0	0	0.99	0.12	0	0.76	0.20	0
MCO	0.98	0.00	0	0	1.00	0.23	0	0.81	0.24	0
MDW	0.98	0.95	0	0	0.99	0.68	0	0.79	0.33	0
MEM	0.98	0.95	0	0	1.00	0.68	0	0.78	0.33	0
MIA	0.97	0.97	0	0	0.99	0.82	0	0.77	0.33	0
MSP	0.97	0.96	0	0	0.99	0.76	0	0.75	0.33	0
ORD	0.97	0.94	0	0	0.99	0.56	0	0.76	0.33	0
PDX	0	0.96	0.98	0	0	0.71	0.99	0	0.33	0.78
PHL	0.97	0.00	0	0	0.99	0.25	0	0.78	0.25	0
PHX	0.97	0.95	0	0	0.99	0.67	0	0.80	0.33	0
PIT	0.97	0.97	0	0	0.99	0.99	0	0.76	0.33	0
SAN	0	0.96	0	0	0	0.80	0	0	0.33	0
SEA	0	0.00	0.99	0	0	0.13	0.99	0	0.20	0.78
SFO	0	0.01	0	0	0	0.30	0	0	0.26	0
SLC	0.97	0.02	0	0	0.99	0.31	0	0.77	0.27	0
STL	0.98	0.96	0	0	0.99	0.76	0	0.80	0.33	0
TPA	0.98	0.96	0	0	1.00	0.70	0	0.80	0.33	0

3.2 ACCURACY OF WIND-SHEAR PRODUCTS

By definition, accuracy measures how well a wind-shear product replicates the truth. The truth could be the location, the actual wind velocity, the speed of the horizontal movement, the wind velocity loss/gain, etc., of the wind shear. Many factors can affect such accuracy, e.g., the

quality of the raw data (how strong the signal is compared to noise, how well the radar is calibrated, radar range-azimuth resolution) and how well the algorithm recognizes and tracks the wind shear. Although we can roughly estimate the measurement uncertainties from the manufacturer's specifications of the instruments and do some error propagation estimates on the software products, in the end we still need the observational truths such as the location and velocity loss/gain of the wind shear to validate our estimates. Wind shear events, especially microbursts, are small scale, short life span, violent, and infrequently occurring phenomena. As a result, any study concerning microbursts and gust fronts requires a long-term commitment. One such example is the scarce measurement data on microburst outflow heights. To validate the true location, wind speed loss, and the movement of a microburst, for example, we need field campaigns involving measurements of multiple ground-based radars and possibly in situ aircraft data at the same site, and observations of possible damage marks the microburst left on the ground. All these are difficult to achieve without sufficient financial support, careful planning, long-term monitoring, and participation of multiple institutions. Such knowledge of the accuracy of wind-shear products is currently lacking.

With that said, "eyeball" validation by subject matter experts of the performance of these wind-shear products, in the context of probabilities of detection and false alarm over the designated terminal areas, can be found in some previous studies (Allan et al., 1999; Evans and Weber, 2000; Cho and Hallowell, 2008; Huang et al., 2009). The current FAA requirement of microburst detection probability of 0.9 and false alarm rate of 0.1 are generally met by the TDWR over the airport ARENAs. Currently there is no specific accuracy requirement for gust front detection. Curiously, there are no detection and false alarm probability specifications for wind shear in the NextGen 4D Wx Cube SAS performance requirements.

3.3 WIND-SHEAR VISIBILITY

In addition to the characteristic reflectivity and outflow-height distributions of microbursts and gust fronts for an airport, whether and how much a wind-shear event is "visible" from a radar also depends on factors such as terrain blockage, ground clutter, the Earth's curvature, radar beam elevation angle, and radar characteristics (Cho and Martin, 2007; Huang et al., 2009). The effects of these factors can be seen in Figures 3-1 to 3-4, where the wind-shear visibilities are averaged over different radii around the individual airports.

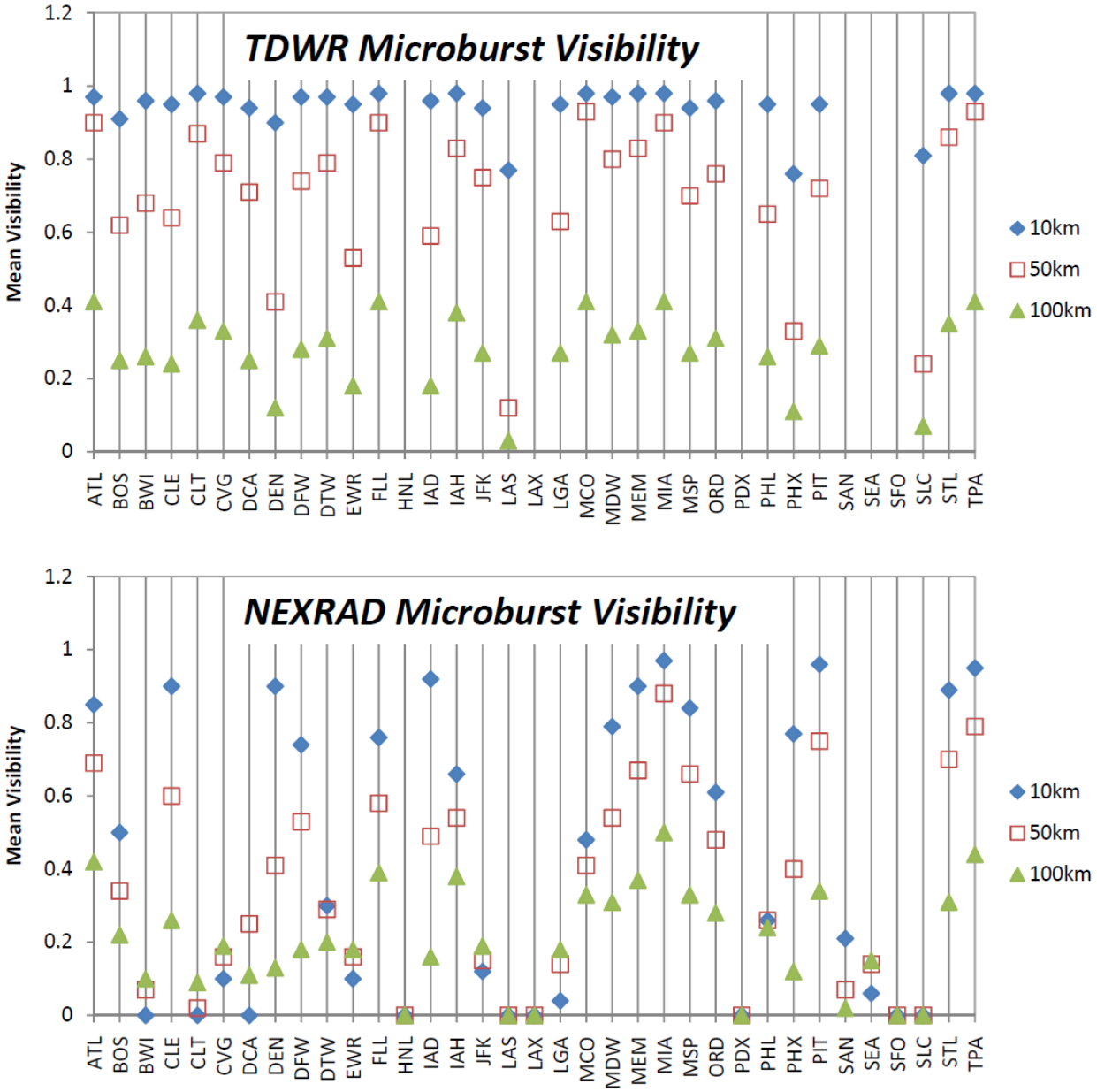

Figure 3-1. Mean microburst visibility over 10, 50, and 100-km radius disks around the airport. Top: TDWR. Bottom: NEXRAD.

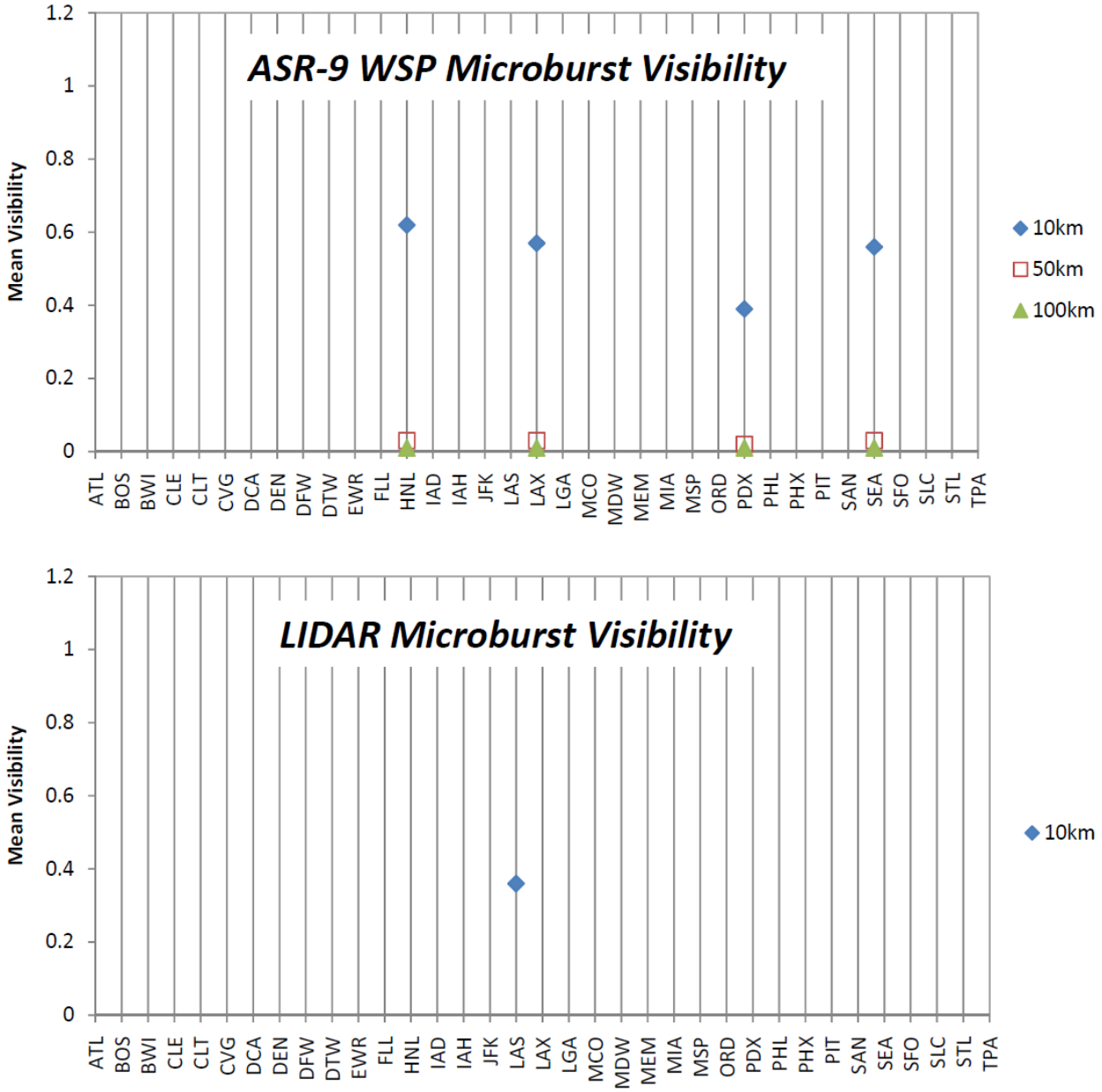

Figure 3-2. Mean microburst visibility over 10, 50, and 100-km radius disks around the airport. Top: ASR-9 WSP. Bottom: lidar.

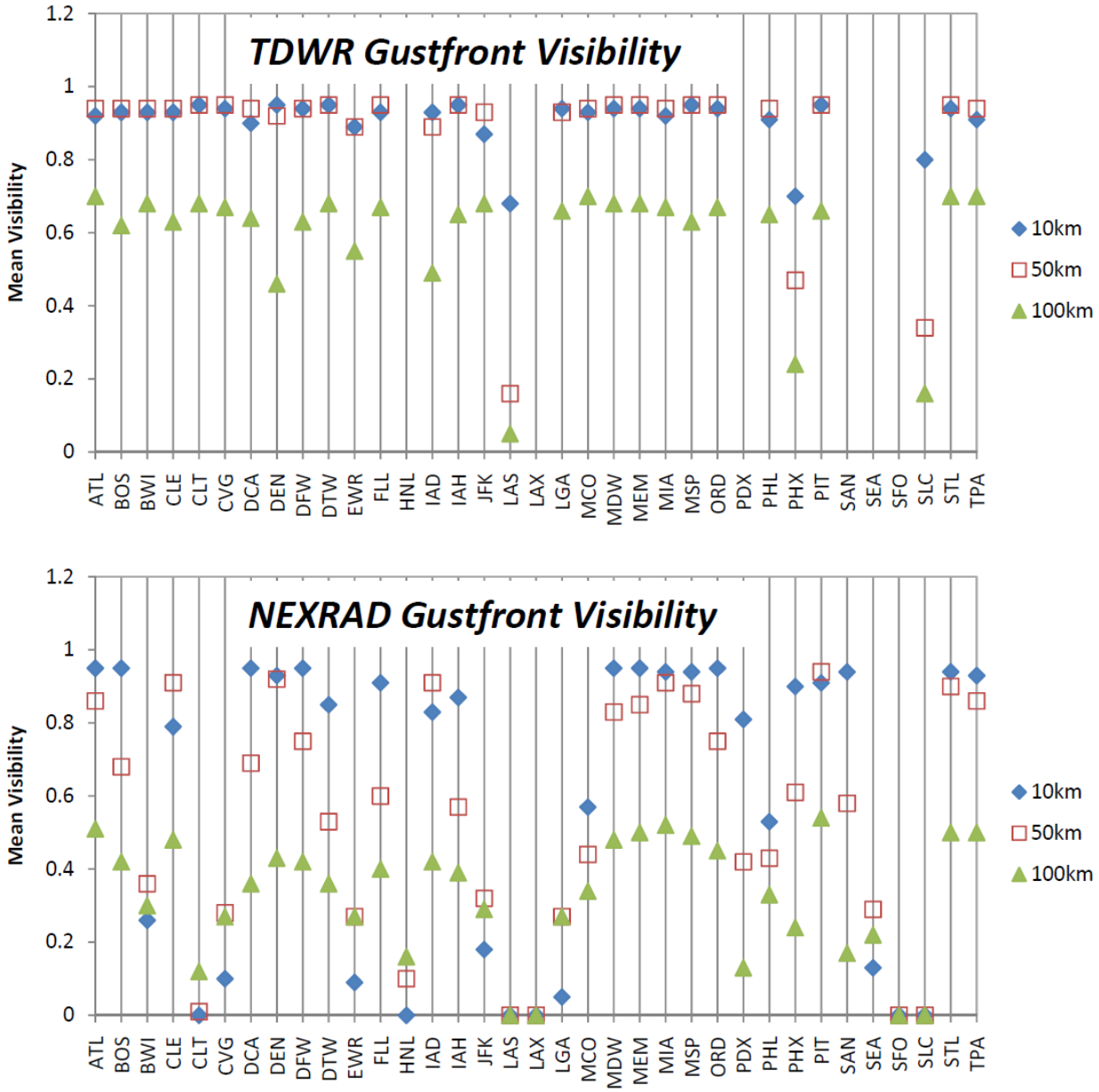

Figure 3-3. Mean gust-front visibility over 10, 50, and 100-km radius disks around the airport. Top: TDWR. Bottom: NEXRAD.

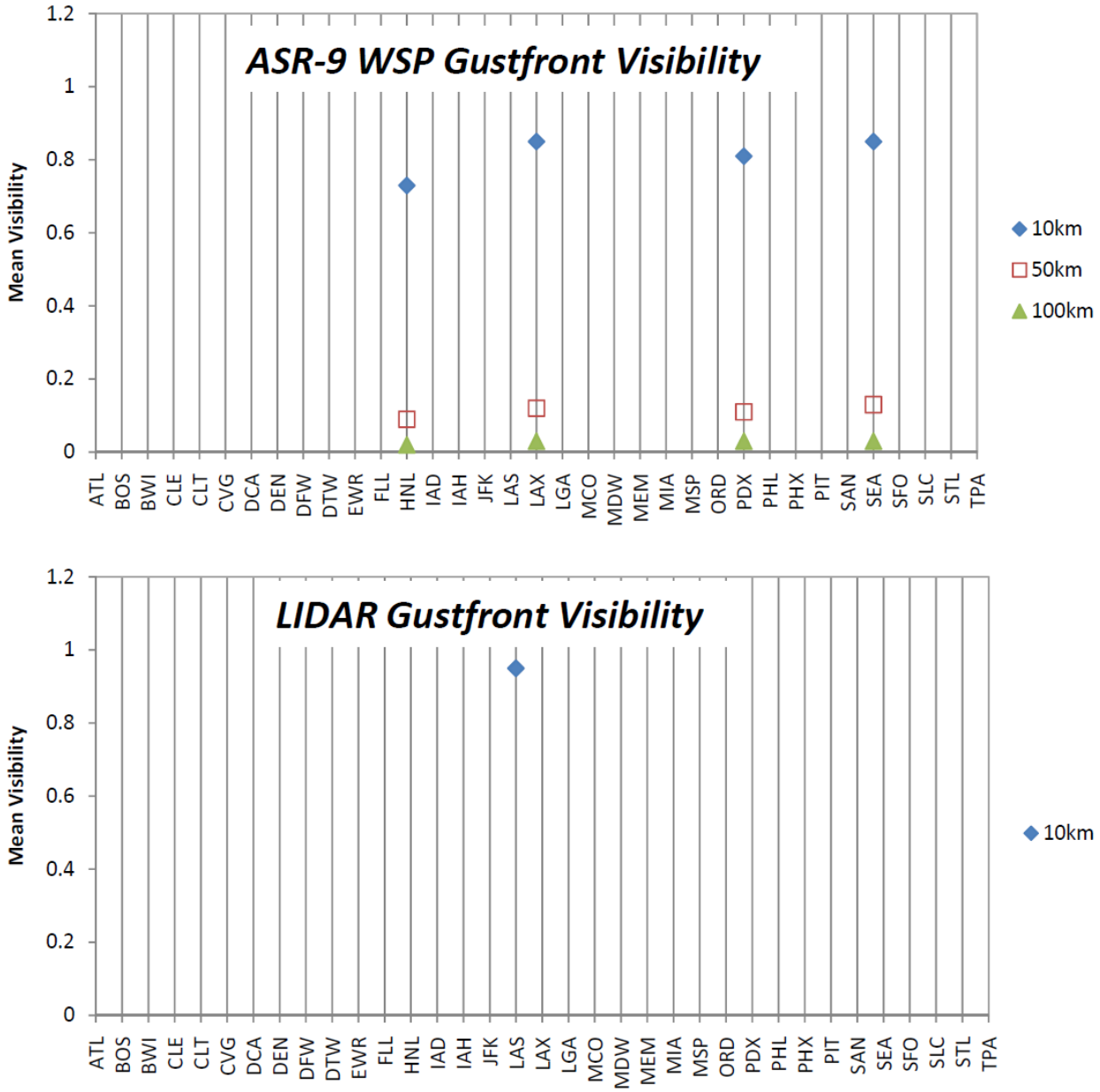

Figure 3-4. Mean gust-front visibility over 10, 50, and 100-km radius disks around the airport. Top: ASR-9 WSP. Bottom: lidar.

Since the TDWR and ASR-9 WSP (and lidar) are all near or at the airports, the Earth's curvature is not an issue for the airports that are covered by these sensors (except at far range). Yet, the rest of the factors play noticeable roles in the detection of wind shear. Take the ASR-9 WSP for example. It is not sensitive enough to "see" wind shear at long ranges, limited by its characteristic fan beam and rapid antenna rotation. As a result, its mean microburst and gust-front visibilities are reasonable over a 10-km range but are greatly reduced over a 50-km range (Figures 3-2 and 3-4). Over a 100-km radius disk, wind shears are nearly undetectable on

average by using an ASR-9 WSP. Therefore, even though the TDWR and ASR-9 WSP-equipped airports have similar fractional coverage with adequate areal resolution, a wind-shear event inside the airspace of former airports are more likely to be detected than in the airspaces of the latter airports.

The TDWR performs superbly at most airports, especially for microbursts, given that it was specifically designed and carefully sited for the detection of terminal wind-shear events. For most TDWR airports, the mean microburst visibility is better than 0.9 for an area that is 10-km radius around the airport. Even over a 100-km radius disk, the mean wind-shear visibilities are not negligible (Figures 3-1 and 3-3). However, the TDWR at some sites suffer from problems of beam blockage and road clutter, and the wind-shear visibilities are significantly lower than at the other TDWR airports. These airports are LAS (with mean microburst visibility over a 10-km radius of 0.81), PHX (0.76), and SLC (0.81). At LAS, the microburst detection rate had not been satisfying the FAA requirement of 0.9 even over the ARENAs, and that is why the lidar was installed there to supplement the wind-shear detection capability.

Compared to the TDWR and ASR-9 WSP, NEXRAD's wind-shear visibility is much more variable. This radar was not sited for airport terminal surveillance, so it can be far away from an OEP airport. Since all the factors mentioned above play active roles in determining wind-shear sensing performance, large variations in the NEXRAD wind-shear visibilities are seen for different airports (Figures 3-1 and 3-3). Such a noisy pattern is also evident in Figure 3-5, where mean microburst and gust-front visibilities are plotted against the airport-radar distance. It indicates that these variations cannot be explained solely by the airport-radar distance.

Radar-to-airport-distance-sorted plots of microburst and gust-front visibility (not shown) further reveal that not only do distant NEXRADs give poor visibilities (e.g., those with distance of over 80 km from the airports: BWI, CLT, CVG, EWR, HNL, JFK, LAX, LGA, and SEA), but also some NEXRADs that are 20–60 km away produce low numbers (DCA, LAS, PDX, SAN, SFO, and SLC). Figure 3-6 is a plot of mean microburst and gust-front visibility vs. the radar observable floor, i.e., the minimum height a wind-shear event can be observed at the airport by the sensor. It further reveals the combined effect of the radar beam elevation angle and the Earth's curvature. If the altitude of the radar is much higher than the altitude of the ground around the terminal area, the default surface-scan beam elevation angle for NEXRAD (0.5°) is too large for some mid-distance airports, namely LAS, PDX, SAN, SFO, and SLC, that it causes the radar to overshoot low-level wind-shear events, especially microbursts. This finding suggests that in the future, it may be advisable to lower the beam elevation angle of some NEXRADs to optimize wind-shear detection, although negative antenna beam elevation angles can also increase ground clutter significantly (e.g., Huang et al., 2009). Note that gust-front visibility has a better correlation with distance than microburst visibility, indicating that the Earth's curvature is the main limiting factor for the detection of gust fronts (Figure 3-5).

The mean wind-shear visibility generally decreases with the radius around the airport, especially for microbursts (Figures 3-1 to 3-4, Appendices A and B). For example, an increase of the radius from 10 to 50 to 100 km results in a decrease of the mean microburst visibility from ~0.9 to ~0.7 to ~0.3 for TDWR, from ~0.5 to ~0.4 to ~0.2 for NEXRAD, and from ~0.5 to ~0.03 to ~0.01 for ASR-9 WSP. For gust fronts, which are thicker in altitude extent than microbursts

(and hence can be observed from farther away), there is not much change in the visibilities from TDWR and NEXRAD when the radius increases from 10 km to 50 km (~0.9 for TDWR and ~0.5–0.6 for NEXRAD). For ASR-9 WSP, however, the mean visibility is reduced from 0.8 to 0.1 with the same expansion of the radius. When the radius is increased to 100 km, the mean gust-front visibilities of all sensors are all reduced, to ~0.6, ~0.3, and ~0.03 for TDWR, NEXRAD, and ASR-9 WSP, respectively.

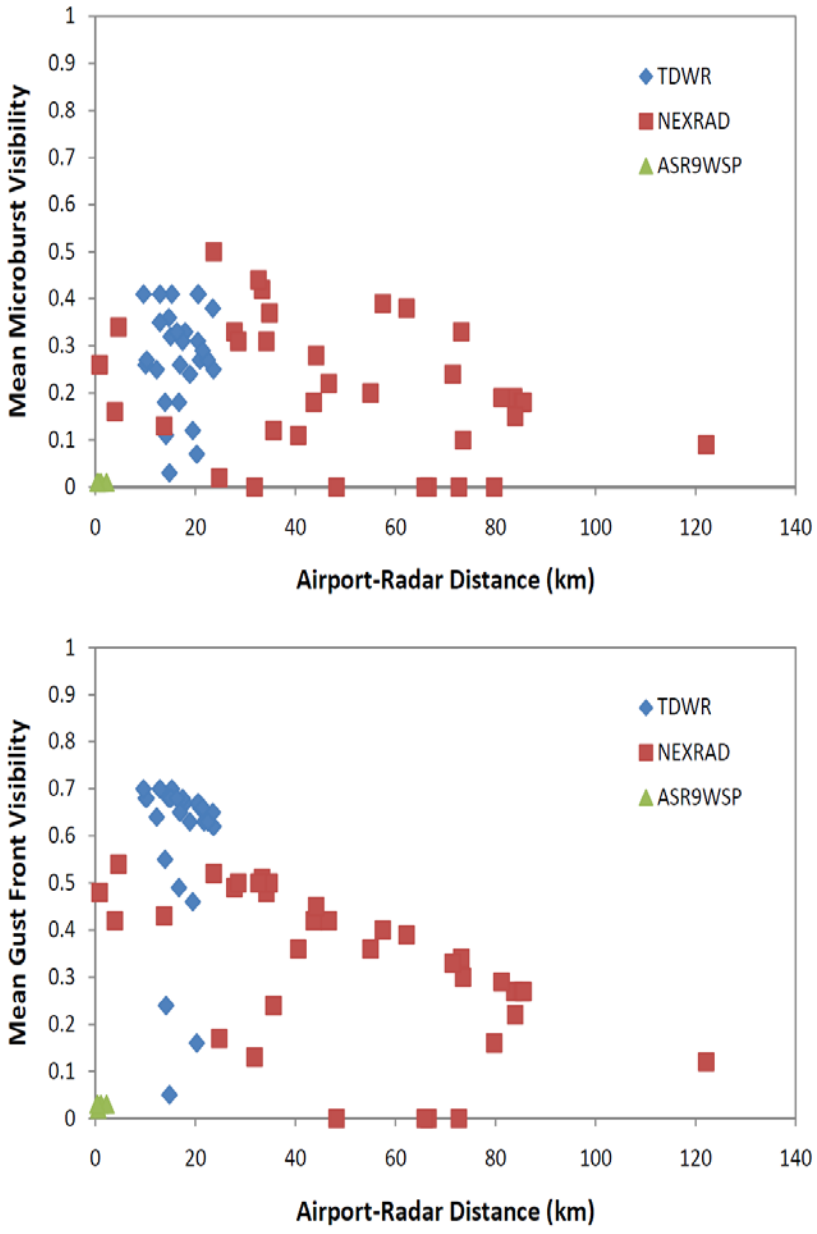

Figure 3-5. Mean microburst and gust-front visibilities over a 100-km radius disk around the airport versus the airport-radar distance.

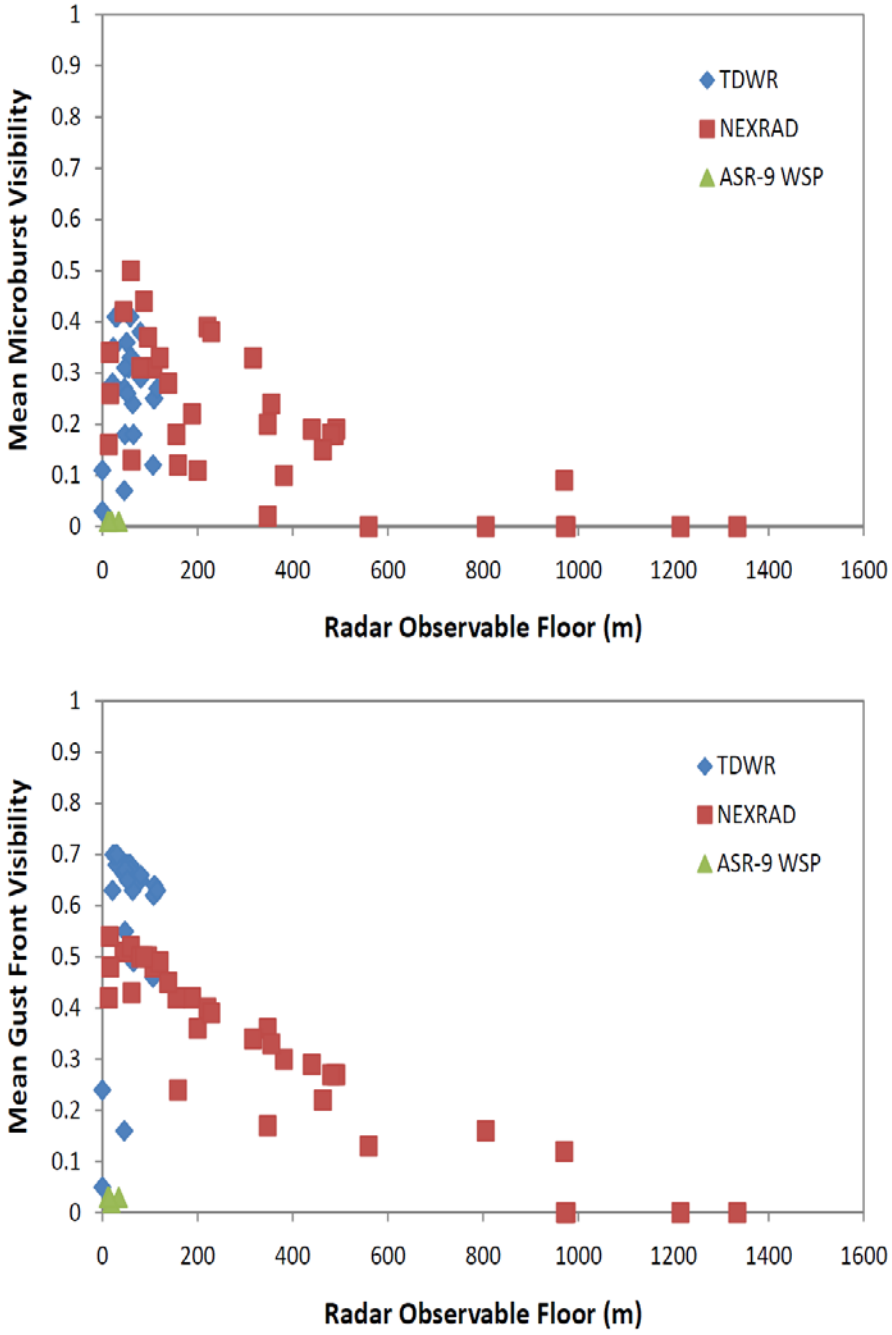

Figure 3-6. Mean microburst and gust-front visibilities over a 100-km radius disk around the airport versus the minimum observable altitude above the airport ground level.

The summary statistics (mean, standard deviation, minimum, and maximum) of the microburst and gust-front visibilities are listed in tables in Appendices A and B for individual sensors and airports. Note that the NextGen spatial resolution requirement is not considered in those tables.

Up to this point, we examined the visibility results for individual sensors only. For the best possible coverage, however, we need to make use of all available sensor data within the terminal airspace. To a certain extent, this is already done operationally. For example, the LAS TDWR and lidar wind-shear detection outputs are combined at the message level with the aim of maximizing detection rate and minimizing false alarms (R. Frankel, personal communication). In prototype mode, a gust-front mosaic algorithm was developed to take advantage of overlapping coverage by multiple TDWRs (Shaw et al., 2000). Fusion at the 2D base data level has potential for improving the detection products even more. Thus, in Figure 3-7 we present the "best" mean wind-shear visibility, where the average is taken over the best visibility from all available sensors at each resolution cell. This measure gives an indication of the extent to which existing sensor output might be combined to achieve better wind-shear coverage over the SDO terminal airspaces. Modest gains can be seen over the single-sensor results of Figures 3-1 to 3-4, especially at the 50 and 100-km radii cases. For the operationally critical 10-km radius case, PHX (microburst) and PDX (gust front) are able to exceed the 0.9 visibility level with sensor fusion, but not with single sensors. Note that, in this study, only the NEXRADs closest to each airport were considered. In some cases there may be other NEXRADs that could help cover different sections of the SDO terminal airspaces.

To account for the wind-shear visibility and the NextGen horizontal resolution requirement simultaneously, we can compile the best wind-shear visibility maps with acceptable areal resolution (Figures C-1 to C-35 in Appendix C). They are aids in visualizing the areas with good/poor wind-shear coverage, which sensor provides the most coverage, and in the case of NEXRAD for microburst coverage, how much of a gap can be filled if the NEXRAD were to be outfitted with a microburst detection algorithm and its scan strategies modified for timely detection. Obviously, for those areas with zero or poor coverage, other means of wind-shear detection need to be added to close the gaps. In addition, terrain blockage and ground clutter (e.g., LAS and SLC), as well as the Earth's curvature and radar beam-elevation angle effect (e.g., HNL, LAX, PDX, SAN, SLC, and SFO), are clearly seen for each airport.

Data in the composite maps can be further summarized by taking the mean over different radii (Table 3-3). The results are similar to those given in Figure 3-7, except that values (especially at 100-km radius) are somewhat reduced due to the loss of areas that did not meet the resolution criterion.

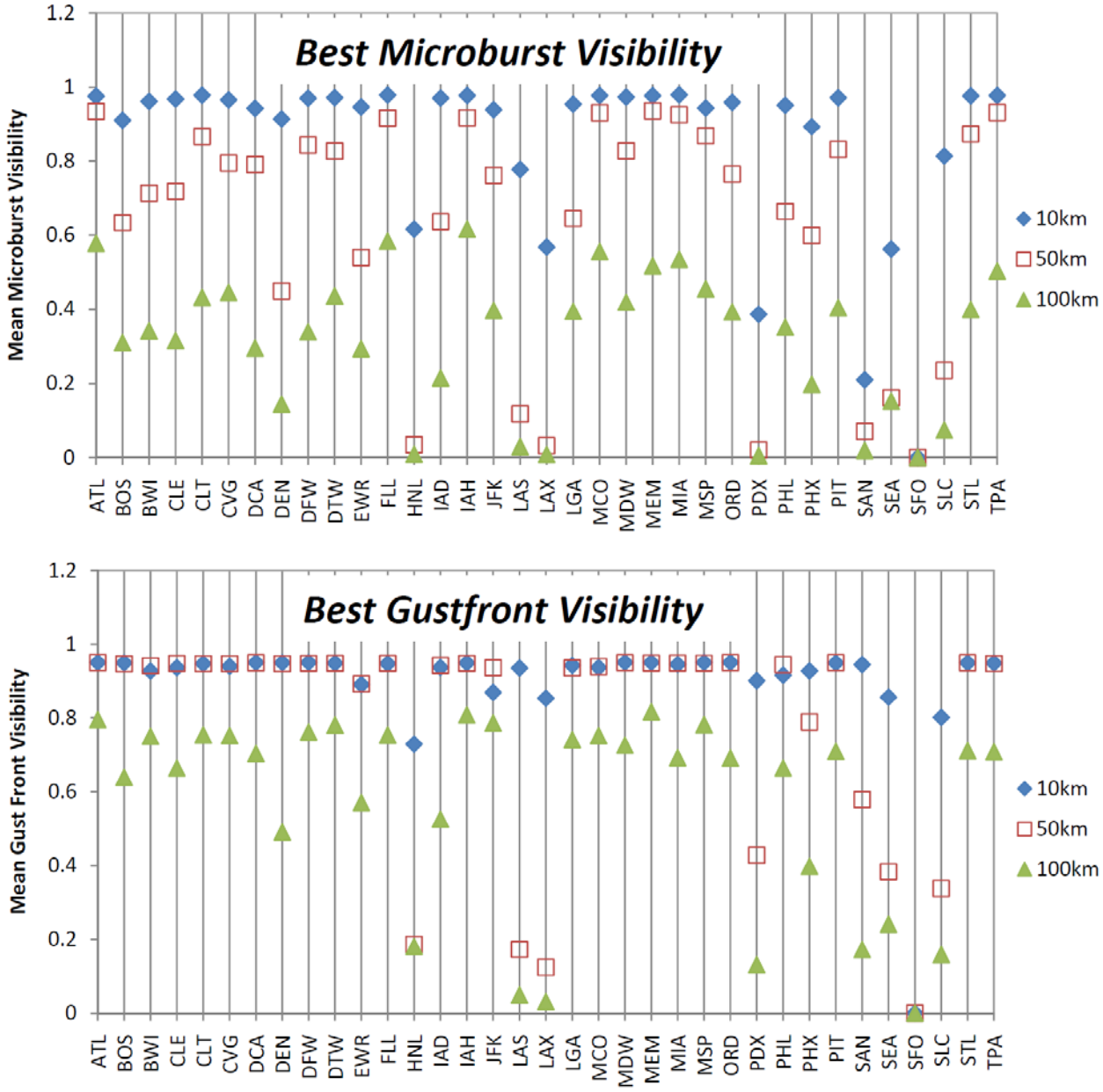

Figure 3-7. Mean best composite microburst (top) and gust-front (bottom) visibility over 10, 50, and 100-km radius disks around the airport. Before the spatial averaging is performed, the best visibility at each resolution cell (out of all the available radars and lidar) is selected.

Table 3-3. Mean Best Composite Microburst and Gust-Front Visibility Simultaneously Satisfying Areal Resolution Requirement of 0.25 km^2

Airport	Microburst			Gust Front		
	10 km	50 km	100 km	10 km	50 km	100 km
ATL	0.98	0.93	0.50	0.95	0.95	0.73
BOS	0.91	0.63	0.30	0.95	0.95	0.63
BWI	0.96	0.71	0.33	0.93	0.94	0.74
CLE	0.97	0.72	0.27	0.94	0.95	0.63
CLT	0.98	0.87	0.41	0.95	0.95	0.74
CVG	0.97	0.79	0.43	0.94	0.95	0.74
DCA	0.94	0.79	0.29	0.95	0.95	0.68
DEN	0.91	0.45	0.13	0.95	0.95	0.48
DFW	0.97	0.83	0.32	0.95	0.95	0.73
DTW	0.97	0.83	0.42	0.95	0.95	0.76
EWR	0.95	0.53	0.27	0.89	0.89	0.57
FLL	0.98	0.91	0.54	0.94	0.95	0.73
HNL	0.62	0.03	0.01	0.73	0.18	0.18
IAD	0.97	0.64	0.20	0.94	0.94	0.51
IAH	0.98	0.91	0.56	0.95	0.95	0.77
JFK	0.94	0.76	0.38	0.87	0.94	0.77
LAS	0.78	0.12	0.03	0.93	0.17	0.05
LAX	0.57	0.03	0.01	0.85	0.12	0.03
LGA	0.95	0.64	0.38	0.94	0.93	0.72
MCO	0.98	0.93	0.52	0.93	0.94	0.74
MDW	0.97	0.83	0.38	0.95	0.95	0.69
MEM	0.98	0.94	0.46	0.95	0.95	0.74
MIA	0.98	0.91	0.44	0.94	0.95	0.67
MSP	0.94	0.87	0.40	0.95	0.95	0.70
ORD	0.96	0.76	0.37	0.95	0.95	0.68
PDX	0.39	0.02	0.01	0.90	0.43	0.13
PHL	0.95	0.65	0.33	0.91	0.94	0.66
PHX	0.89	0.59	0.19	0.93	0.77	0.37
PIT	0.97	0.83	0.34	0.95	0.95	0.66
SAN	0.21	0.07	0.02	0.94	0.55	0.16
SEA	0.56	0.11	0.13	0.85	0.26	0.20
SFO	0.00	0.00	0.00	0.00	0.00	0.00
SLC	0.81	0.24	0.07	0.80	0.34	0.16
STL	0.98	0.87	0.36	0.95	0.95	0.70
TPA	0.98	0.93	0.44	0.95	0.95	0.70

At this point, let us take a step back and consider the reasons why some OEP airports currently have better wind-shear detection coverage than others. The FAA recognizes that the various wind-shear sensors have varying performance characteristics as well as different levels of lifetime cost, and that performance and cost are closely related. Therefore, the deployment strategy in the past has been based on careful cost/benefit analyses. For example, TDWRs (best

performance, highest cost) were not deployed at LAX, PDX, SAN, SEA, and SFO, because the occurrence rates of convective wind shears are very low at those west coast locations. For example, the microburst occurrence rate over the SFO ARENAs is estimated to be only 1% of the occurrence rate over the MCO ARENAs (Hallowell et al., 2009). Instead, lower-cost (and lower performance) systems like the WSP and LLWAS (or nothing) were installed there. In the absence of any ground-based wind-shear sensor as at SAN, there is still a measure of protection due to on-board predictive wind-shear (PWS) radars, and, of course, the pilot's own visual situation recognition capabilities. (The current fleet equipage rate of PWS radars for U.S. Part 121 aircraft varies from 15% to 100% depending on airline (Hallowell et al., 2009).) As the NextGen 4D Wx Cube SAS requirements currently stand, all SDO terminal airspaces need to be covered equally for low-level wind shears, regardless of the occurrence rate of such events. Perhaps such a blanket coverage requirement is warranted under the new NextGen flight operations concept, but that is the type of issue that needs to be investigated in the future.

Also, low-level wind-shear products are currently generated out to much shorter ranges from the airport than the NextGen SDO terminal airspace coverage requirement of 100 km. Will the NextGen flight operations concept depend on the availability of microburst alerts at 100 km from the airport? In order to provide such widespread coverage of low-altitude wind shear, multiple ground-based sensors per terminal airspace would be needed. Should there be different levels of wind-shear detection performance required depending on distance from the airport? As we move forward into the gap analysis and mitigation phase of the Sensor RightSizing program, we need to work more closely with the NextGen requirements definition team and the users of the weather observation products to prioritize the needs and develop realistic solutions to them.

3.4 ASSESSMENT OF THE NEXTGEN 4D WX CUBE SAS PERFORMANCE REQUIREMENTS

Low-level wind shear over the airport ARENAs is currently measured with the TDWR, ASR-9 WSP, LLWAS, and lidar (at LAS) at airports equipped with these sensors. The raw sensor data are channelled through the wind-shear algorithms to generate estimates of wind-shear location as well as speed loss/gain. A wind-shear alert is issued for airspeed loss of 15–30 kts in an ARENA. For airspeed loss of 30 kts or greater, a microburst alert is issued. Airspeed loss is detected by the microburst algorithm, and gain is detected by the gust-front algorithm. For the microburst detection algorithm, the update rates are 1 min (TDWR and lidar) and 28 sec (ASR-9 WSP). (NEXRAD currently does not have a microburst detection product.) For the gust-front detection algorithm, the update rates are 5 min (TDWR), 4-10 min (NEXRAD), and 1 min (ASR-9 WSP and lidar). The maximum ranges from the sensor for which microburst products are generated are 30 km (TDWR), 16 km (ASR-9 WSP), and 10 km (lidar). For gust front products, the corresponding ranges are 60 km (TDWR), 28 km (ASR-9 WSP), 10 km (lidar), and 70 km (NEXRAD). Thus, it is possible that the maximum range of product generation could be a further restriction to wind shear coverage on top of the visibility metric.

There are two major terminal-area wind-shear detection/prediction products available—those generated by the Microburst Detection Algorithm (MDA) and the Machine Intelligent Gust Front Algorithm (MIGFA) (Troxel and Pughe, 2002). Both were developed at MIT LL. The MDA is currently used in both the TDWR and ITWS (FAA, 2002). It processes the reflectivity

and wind data of a TDWR (and nearby Doppler weather radars for ITWS) to generate the reflectivity map, radial velocity map, and shear segment map in the event of a wind shear. The algorithm was later modified for the ASR-9 WSP in order to adapt to receiving data from the rapid-scanning fan-beam radar located right at the airport (Newell and Cullen, 1993). This version is called the Portable Automated Microburst Detection Algorithm (Portable AMDA). It is also used for the lidar at LAS.

Relative to these currently available products, an item-by-item evaluation of the NextGen 4D Wx Cube SAS performance requirements (Appendix D of FAA (2009)) is listed in Table 3-4. The difficulty in covering the entire SDO terminal airspace with the current operational sensors was well documented in the previous subsections, so that discussion is not repeated in this table.

Table 3-4. Assessment of the NextGen 4D Wx Cube SAS SDO Terminal Airspace Wind-Shear Performance Requirements

Item #	Performance Requirement	Comments/Assessment
459	The NextGen NAS shall periodically observe the occurrence of gust fronts in terminal airspace within an interval of 1 minutes or less.	The current reporting period is 5 min (TDWR), 4-10 min (NEXRAD), and 1 min (ASR-9 WSP and lidar), so only the latter sensor products meet the requirement.
462	The NextGen NAS shall determine the location of gust fronts at the surface of super-density terminal airspace with an accuracy of plus or minus 0.25 km.	See Section 3.2 for accuracy discussion.
470	The NextGen NAS shall measure the movement speed of gust fronts at the surface of super-density terminal airspace with an accuracy of plus or minus 5 nautical miles per hour.	MIGFA keeps track of past gust-front detections to estimate the velocity of movement. The accuracy of this estimate can vary with conditions and is not well characterized at this time.
477	The NextGen NAS shall determine the time of gust fronts within 100 km of super-density terminal airspace with an accuracy of plus or minus 1 minute.	See comments to #459 for the gust-front reporting periods. The accuracy of the reported beginning and ending times of gust fronts is not well characterized.
517	The NextGen NAS shall periodically observe the occurrence of low-level wind shear at super-density terminal airspace within an interval of 1 minute or less.	See comments to #459 for the gust-front reporting periods and #554 for the microburst reporting periods.
521	The NextGen NAS shall determine the location of low-level wind shear at super-density terminal airspace with a horizontal accuracy of plus or minus 0.25 km.	See Section 3.2 for accuracy discussion.

526	The NextGen NAS shall determine the vertical extent of low-level wind shear from the surface to 4,900 feet at super-density terminal airspace with an accuracy of plus or minus 50 feet.	Currently there is no such wind-shear product. See Cho (2010) for reasons why a vertical accuracy requirement of ±50 ft is unreasonable for radars. It may be possible with lidars, but they have very limited range.
530	The NextGen NAS shall calculate the change in wind speed of low-level wind shear at super-density terminal airspace with an accuracy of plus or minus 5 nautical miles per hour.	See Section 3.2 for accuracy discussion.
533	The NextGen NAS shall calculate the change in wind direction due to low-level wind shear at super-density terminal airspace with an accuracy of plus or minus 10 degrees.	See Section 3.2 for accuracy discussion.
538	The NextGen NAS shall determine the movement direction of low-level wind shear at super-density terminal airspace with an accuracy of plus or minus 10 degrees.	See comments for #470 and #572.
543	The NextGen NAS shall measure the movement speed of low-level wind shear at super-density terminal airspace with an accuracy of plus or minus 5 nautical miles per hour.	See comments for #470 and #577.
548	The NextGen NAS shall determine the beginning time of low-level wind shear at terminals with an accuracy of plus or minus 1 minute.	See comments to #459 for the gust-front reporting periods and #554 for the microburst reporting periods. The accuracy of the reported beginning and ending times of wind shear is not well characterized.
551	The NextGen NAS shall determine the ending time of low-level wind shear at terminals with an accuracy of plus or minus 1 minute.	See comments for #548.
554	The NextGen NAS shall periodically observe the occurrence of microbursts in the terminal airspace within an interval of 1 minute or less.	The update periods for the microburst product are 1 min (TDWR and lidar) and 28 sec (ASR-9 WSP), so this requirement is met where there is coverage.
557	The NextGen NAS shall determine the location of microbursts at super-density terminal airspace with a horizontal accuracy of plus or minus 0.25 km.	See Section 3.2 for accuracy discussion.
562	The NextGen NAS shall determine the maximum altitude (AGL) of microbursts in super-density terminal airspace with an accuracy of plus or minus 50 feet.	Currently there is no such microburst product. See Cho (2010) for reasons why a vertical accuracy requirement of ±50 ft is unreasonable for radars. It may be possible with lidars, but they have very limited range.

567	The NextGen NAS shall calculate airspeed loss or gain due to microbursts in super-density terminal airspace with an accuracy of plus or minus 5 nautical miles per hour.	See Section 3.2 for accuracy discussion.
572	The NextGen NAS shall determine the movement direction of microbursts in super-density terminal airspace with an accuracy of plus or minus 10 degrees.	Currently there is no such product for microburst, although the movement direction of microbursts could be derived from the current products.
577	The NextGen NAS shall measure the movement speed of microbursts in super-density terminal airspace with an accuracy of plus or minus 5 nautical miles per hour.	Currently there is no such product for microburst, although the movement speed of microbursts could be derived from the current products.
582	The NextGen NAS shall determine the beginning time of microbursts in terminals with an accuracy of plus or minus 1 minute.	See comments to #554 for the microburst reporting periods. The accuracy of the reported beginning and ending times of microbursts is not well characterized.
585	The NextGen NAS shall determine the ending time of microbursts at all terminals with an accuracy of plus or minus 1 minute.	See comments for #582.

3.5 POTENTIAL GAP-FILLING MEASURES

It is clear from our analysis that there will be significant gaps to fill if the current ground-based wind-shear sensing network of radars and lidar is tasked to meet the NextGen 4D Wx Cube SAS requirements. The difficulty in meeting the spatial resolution and accuracy requirements in general have already been addressed in an earlier report (Cho, 2010). For wind shear observations, again, the vertical accuracy requirement of ±50 ft (Table 3-4) would require an extremely dense network with a spacing of about 2 km for a 1.8°-beamwidth antenna, which is the beamwidth of the current Collaborative Adaptive Sensing of the Atmosphere (CASA) prototype radar (Hopf et al. 2009). This does not appear to be an economically viable option. (Note that the CASA concept calls for a network spacing of about 30 km.) A lidar with its narrow collimated beam could potentially provide such vertical resolution and accuracy with longer sensor spacing under clear conditions, but it will be severely limited by its inability to penetrate clouds and precipitation.

Ignoring the vertical resolution and accuracy problem for the moment, the horizontal resolution and wind-shear visibility gaps could be covered by incorporating data from additional sensors located optimally in or near the SDO airspace. In principle, LLWAS could be used to cover gap regions (although there would be no vertical coverage). However, each anemometer in an LLWAS network covers only ~4 km^2 (an estimate based on ARENA coverage provided by the current LLWAS Network Expansion (NE++) sensors), which translates to over 7,800 sensors to blanket the 100-km-radius SDO airspace surface. Thus, even filling in 30% of the SDO

terminal area surface would require over 2,300 anemometers, each needing installation real estate, electrical power, and communication capability. Modest coverage gains could be achieved for microburst detection by instituting a rapid surface scan strategy for NEXRADs (Section 3.3). And, as mentioned before, in regions where TDWRs are spaced relatively closely (such as in the Potomac), they can be used to help fill in coverage for each other's terminal airspace.

As for possible future radars, a CASA-type network of small (X-band) radars could potentially act as a gap filler, but we have not yet assessed the wind-shear detection performance of such a system. If today's weather and aircraft surveillance radars are to be replaced by a network of Multifunction Phased Array Radars (MPARs) and scaled-down terminal MPARs (Weber et al., 2007), we have an opportunity to site these new sensors for better coverage of SDO terminal airspace. The cost for achieving complete coverage, however, is likely to be quite high.

Other data sources should be explored. For example, private sector weather radars such as those operated by television (TV) broadcasting stations might be able to supplement SDO terminal wind-shear coverage if their owners can be persuaded to share the data. These radars are usually C-band systems with often high power ("megawatt" is an attractive marketing term in competing for viewers), although their ground clutter suppression capability may not be as good as the TDWR's or NEXRAD's (e.g., Huang et al., 2009). During severe weather they may be apt to be put into a rapid update mode (faster than the current NEXRAD scan strategies), which would be favorable for microburst detection (LaDue et al., 2010). Aircraft-based PWS radars may also help fill in wind shear coverage if their data can be properly processed and communicated to the 4D Wx Cube in a timely manner.

This page intentionally left blank.

4. CONCLUSIONS

Our analyses showed that the TDWR is the best low-altitude terminal wind-shear sensor examined, which is not surprising since it was designed specifically for this purpose and was carefully sited near the airports. Terminal microburst detection coverage can be augmented by NEXRAD if it happens to be located in or near the terminal airspace and an appropriately rapid surface-update scan strategy is implemented. For non-TDWR-equipped airports or where TDWR suffers from severe terrain blockage and ground clutter, wind shear coverage is made up partially by ASR-9 WSP (HNL, LAX, PDX, SEA) or lidar (LAS).

If we take the composite coverage of the radars and lidar included in this report and their horizontal resolutions into consideration, the best mean low-altitude wind-shear visibility inside the NextGen SDO terminal airspace ranges from 0 to 56% (with a median of 33%) for microbursts and 0 to 77% (median 68%) for gust fronts. The airport with the worst wind-shear coverage is SFO, where only LLWAS is available for fractional coverage of the ARENAs and the nearest NEXRAD is located too high to detect low-level wind shear. Terminal airspaces with < 20% mean visibility for microburst and < 40% mean gust-front visibility are HNL, LAS, LAX, PDX, PHX, SAN, SEA, SFO, and SLC. Analyses for smaller areas, i.e., 10 or 50-km radius around the airport, were also performed in this study. It was found that the wind-shear visibilities of such areas are significantly higher than those for the entire terminal airspace. Within a 50-km radius, the median value of the mean terminal airspace visibilities is 76% for microbursts and 95% for gust fronts. Within a 10-km range, it is 96% and 94%, respectively.

The findings of this study suggest that to meet the NextGen 4D Wx Cube SAS wind-shear detection requirements for the SDO terminal airspace, we need a ground-based sensor network with proper resolution that is denser than what is currently deployed. We also need to develop additional software to generate observational products that are specified by the NextGen 4D Wx Cube SAS. To characterize the accuracy of the current (and future) wind-shear products with respect to location, movement, velocity loss or gain, etc., extensive field studies are needed.

This page intentionally left blank.

REFERENCES

Allan, S.S., D.A. Grant, S.G. Gaddy, and M.J. Pottier, 1999: Review of NYC ITWS during the September 7, 1998 severe weather event. Project Rep. ATC-269, MIT Lincoln Laboratory, Lexington, MA, 31 pp.

Cho, J.Y.N. and B.D. Martin, 2007: Technical assessment of the impact of decommissioning the TDWR on terminal weather services. Project Rep. ATC-331. MIT Lincoln Laboratory, Lexington, MA, 58 pp.

Cho, J.Y.N., and R.G. Hallowell, 2008: Detection probability modeling for airport terminal wind-shear sensor. Project Rep. ATC-340. MIT Lincoln Laboratory, Lexington, MA, 64 pp.

Cho, J.Y.N., 2010: OEP terminal and CONUS weather radar coverage gap identification analysis for NextGen. Project Rep. ATC-369, MIT Lincoln Laboratory, Lexington, MA, 91 pp.

Chrisman, J.N., 2009: Automated volume scan evaluation and termination (AVSET): A simple technique to achieve faster volume scan updates for the WSR-88D. Preprints, *34th Conf. on Radar Meteorology*, Williamsburg, VA, American Meteorological Society, P4.4.

Evans, J.E., and M.E. Weber, 2000: Weather radar development and application programs. *Linc. Lab. J.*, **12**, 367–382.

FAA, 2002: Integrated Terminal Weather Systems (ITWS) algorithm description. DOT/FAA/ND-95-11 Rev. E, MIT Lincoln Laboratory, Lexington, MA.

FAA, 2008: NNEW/RWI Preliminary Portfolio Requirements. Version 1.0. September 2008.

FAA, 2009: Four-Dimensional Weather Data Cube Single Authoritative Source (SAS) Final Performance Requirements (fPR), Version 1.0. Federal Aviation Administration, Washington, DC.

FAA, 2009a: Sensor Network Assessment at NextGen IOC. RightSizing Project Team, AJP-6830, Federal Aviation Administration, Atlantic City, NJ, 64 pp.

FAA, 2009b: Primary and nonprimary commercial service airports (by rank order). http://www.faa.gov/airports/planning_capacity/passenger_allcargo_stats/passenger/media/cy08_primary_np_comm.pdf.

Hallowell, R.G., J.Y.N., Cho, S. Huang, and M.E. Weber, 2009: Wind-shear system cost-benefit analysis update. Project Rep. ATC-341, MIT Lincoln Laboratory, Lexington, MA, 171 pp.

Hannon, S.M., 2004: Pulsed Doppler lidar for terminal area monitoring of wind and wake hazards. Preprints, *11th Conf. on Aviation, Range, and Aerospace Meteorology*, Amer. Meteor. Soc., Hyannis, MA, P4.21.

Hopf, A.P., D.L. Pepyne, and D.J. McLaughlin, 2009: Topological considerations for a CONUS deployment of CASA-type radars. Preprints, *34th Conf. on Radar Meteorology*, Williamsburg, VA, American Meteorological Society, P8.4.

Huang, S., J.Y.N. Cho, M.F. Donovan, R.G. Hallowell, R.S. Frankel, M.L. Pawlak, and M.E. Weber, 2009: Redeployment of the New York TDWR: Technical analysis of candidate sites and alternative wind shear sensors. Project Rep. ATC-351, MIT Lincoln Laboratory, Lexington, MA, 84 pp.

LaDue, D.S., P.L. Heinselman, and J.F. Newman, 2010: Strengths and limitations of current radar systems for two stakeholder groups in the Southern Plains. *Bull. Amer. Meteor. Soc.*, **91**, 899-910.

Newell, O.J., and J.A. Cullen, 1993: ASR-9 microburst detection algorithm. Project Rep. ATC-197, MIT Lincoln Laboratory, Lexington, MA, 60 pp.

Shaw, J.D., B.A. Crowe, and S.W. Troxel, 2000: Developing a mosaicked gust front detection algorithm for TRACONS with multiple TDWRs. Preprints, *9th Conf. on Aviation, Range, and Aerospace Meteorology*, Orlando, FL, Amer. Meteor. Soc., 7.9.

Souders, C., T. Kays, S. Spincic, F. Bayne, C. Miner, S. Abelman, R. Showalter, J. Tauss, L. Leonard, E. Dash, and J. May, 2010: Next Generation Air Transportation System (NextGen) weather requirements: An update. Preprints, *14th Conf. on Aviation, Range, and Aerospace Meteorology*, Atlanta, GA, American Meteorological Society, J4.1.

Troxel, S. and W. Pughe, 2002: Machine Intelligent Gust Front Algorithm (MIGFA) for the WSP. Project Rep. ATC-274, MIT Lincoln Laboratory, Lexington, MA, 205 pp.

Weber, M.E., J.Y.N. Cho, J.S. Herd, J.M. Flavin, W.E. Benner, and G.S. Torok, 2007: The next generation multi-mission U.S. surveillance radar network. *Bull. Amer. Meteor. Soc.*, **88**, 1739–1751.

GLOSSARY

4D Wx Cube	Four-Dimensional Weather Data Cube
ADW	Andrews Air Force Base
AMDA	Automated Microburst Detection Algorithm
ARENA	AREa Noted for Attention
ASR-9	Airport Surveillance Radar-9
ATL	Atlanta Hartsfield International Airport
AVSET	Automated Volume Scan Evaluation and Termination
BOS	Boston Logan International Airport
BWI	Baltimore-Washington International Airport
CASA	Collaborative Adaptive Sensing of the Atmosphere
CLE	Cleveland-Hopkins International Airport
CLT	Charlotte/Douglas International Airport
CVG	Cincinnati-Northern Kentucky Airport
DAL	Dallas Love Field Airport
DCA	Ronald Reagan National Airport
DEN	Denver International Airport
DFAD	Digital Feature Analysis Data
DFW	Dallas-Fort Worth International Airport
DTED	Digital Terrain Elevation Data
DTW	Detroit Metro Wayne County Airport
EWR	Newark International Airport
FAA	Federal Aviation Administration
FLL	Fort Lauderdale-Hollywood International Airport
HNL	Honolulu International Airport
IAD	Washington Dulles International Airport
IAH	George Bush Intercontinental Airport
ID	Identification
ITWS	Integrated Terminal Weather System
JFK	New York John F. Kennedy International Airport
LAS	Las Vegas McCarran International Airport
LAX	Los Angeles International Airport
LGA	New York LaGuardia Airport
LLWAS	Low-Level Wind-Shear Alert System
LMCT	Lockheed Martin Coherent Technologies
MDA	Microburst Detection Algorithm
MCO	Orlando International Airport
MDW	Chicago Midway Airport
MEM	Memphis International Airport
MIA	Miami International Airport
MIGFA	Machine Intelligent Gust Front Algorithm
MIT LL	Massachusetts Institute of Technology Lincoln Laboratory

MPAR	Multifunction Phased Array Radar
MSP	Minneapolis-St Paul International Airport
NAS	National Airspace System
NEXRAD	Next Generation Weather Radar
NextGen	Next Generation Air Transportation System
NE++	Network Expansion
NNEW	NextGen Network Enabled Weather
OEP	Operational Evolution Partnership
ORD	Chicago O'Hare International Airport
PBI	Palm Beach International Airport
PDX	Portland International Airport
PHL	Philadelphia International Airport
PHX	Phoenix Sky Harbor International Airport
PIT	Greater Pittsburgh International Airport
RWI	Reduce Weather Impact
SAN	San Diego International Lindbergh Airport
SAS	Single Authoritative Source
s.d.	standard deviation
SDO	Super Density Operations
SEA	Seattle-Tacoma International Airport
SFO	San Francisco International Airport
SLC	Salt Lake City International Airport
SLEP	Service Life Extension Program
SRTM	Shuttle Radar Topography Mission
STL	Lambert St. Louis International Airport
TDWR	Terminal Doppler Weather Radar
TPA	Tampa International Airport
TV	Television
WSP	Weather Systems Processor

APPENDIX A
MICROBURST VISIBILITY SUMMARY STATISTICS

Mean, standard deviation (s.d.), minimum (min.), and maximum (max.) values of the microburst visibilities for ground-based wind-shear sensors in the 10, 50, and 100-km radius areas, respectively, around the individual OEP airports are listed in Tables A-1 (TDWR), A-2 (NEXRAD), A-3 (ASR-9 WSP), and A-4 (lidar, 10 km only). The areal resolution requirement is not considered in these tables.

Table A-1. Microburst Visibility for TDWR

Airport	RadarID	Radar-Airport Distance (km)	Beam El. Angle (deg)	Mean (S.d., Min, Max) 10km	50km	100km
ATL	ATL	15	0.3	0.97 (0.02 , 0.49 , 0.98)	0.90 (0.13 , 0 , 0.98)	0.41 (0.39 , 0 , 0.98)
BOS	BOS	24	0.3	0.91 (0.06 , 0.39 , 0.98)	0.62 (0.32 , 0 , 0.98)	0.25 (0.33 , 0 , 0.98)
BWI	BWI	10	0.3	0.96 (0.06 , 0 , 0.98)	0.68 (0.29 , 0 , 0.98)	0.26 (0.32 , 0 , 0.98)
CLE	CLE	19	0.3	0.95 (0.04 , 0.33 , 0.98)	0.64 (0.35 , 0 , 0.98)	0.24 (0.34 , 0 , 0.98)
CLT	CLT	15	0.3	0.98 (0.01 , 0.84 , 0.98)	0.87 (0.17 , 0 , 0.98)	0.36 (0.38 , 0 , 0.98)
CVG	CVG	18	0.3	0.97 (0.02 , 0.62 , 0.98)	0.79 (0.19 , 0 , 0.98)	0.33 (0.35 , 0 , 0.98)
DCA	DCA	12	0.3	0.94 (0.08 , 0.43 , 0.98)	0.71 (0.21 , 0 , 0.98)	0.25 (0.32 , 0 , 0.98)
DEN	DEN	19	0.3	0.90 (0.06 , 0.74 , 0.98)	0.41 (0.34 , 0 , 0.98)	0.12 (0.25 , 0 , 0.98)
DFW	DFW	22	0.3	0.97 (0.01 , 0.82 , 0.98)	0.74 (0.32 , 0 , 0.98)	0.28 (0.38 , 0 , 0.98)
DTW	DTW	17	0.3	0.97 (0.01 , 0.95 , 0.98)	0.79 (0.21 , 0 , 0.98)	0.31 (0.36 , 0 , 0.98)
EWR	EWR	14	0.3	0.95 (0.07 , 0.42 , 0.98)	0.53 (0.41 , 0 , 0.98)	0.18 (0.32 , 0 , 0.98)
FLL	FLL	21	0.3	0.98 (0.01 , 0.83 , 0.98)	0.90 (0.15 , 0 , 0.98)	0.41 (0.41 , 0 , 0.98)
HNL	*					
IAD	IAD	17	0.3	0.96 (0.04 , 0.57 , 0.98)	0.59 (0.36 , 0 , 0.98)	0.18 (0.31 , 0 , 0.98)
IAH	IAH	24	0.3	0.98 (0.01 , 0.80 , 0.98)	0.83 (0.21 , 0 , 0.98)	0.38 (0.39 , 0 , 0.98)
JFK	JFK	10	0.3	0.94 (0.09 , 0 , 0.98)	0.75 (0.25 , 0 , 0.98)	0.27 (0.34 , 0 , 0.98)
LAS	LAS	15	0.3	0.77 (0.21 , 0.09 , 0.98)	0.12 (0.29 , 0 , 0.98)	0.03 (0.15 , 0 , 0.98)
LAX	*					
LGA	JFK	21	0.3	0.95 (0.03 , 0.48 , 0.98)	0.63 (0.37 , 0 , 0.98)	0.27 (0.35 , 0 , 0.98)
MCO	MCO	10	0.3	0.98 (0.05 , 0 , 0.98)	0.93 (0.11 , 0 , 0.98)	0.41 (0.40 , 0 , 0.98)
MDW	MDW	15	0.3	0.97 (0.01 , 0.93 , 0.98)	0.80 (0.18 , 0 , 0.98)	0.32 (0.35 , 0 , 0.98)
MEM	MEM	16	0.3	0.98 (0.02 , 0.70 , 0.98)	0.83 (0.21 , 0 , 0.98)	0.33 (0.37 , 0 , 0.98)
MIA	MIA	21	0.3	0.98 (0.02 , 0.62 , 0.98)	0.90 (0.15 , 0 , 0.98)	0.41 (0.41 , 0 , 0.98)
MSP	MSP	22	0.3	0.94 (0.03 , 0.86 , 0.98)	0.70 (0.27 , 0 , 0.98)	0.27 (0.34 , 0 , 0.98)
ORD	ORD	21	0.3	0.96 (0.03 , 0.59 , 0.98)	0.76 (0.23 , 0 , 0.98)	0.31 (0.35 , 0 , 0.98)
PDX	*					
PHL	PHL	17	0.3	0.95 (0.06 , 0.47 , 0.98)	0.65 (0.35 , 0 , 0.98)	0.26 (0.34 , 0 , 0.98)
PHX	PHX	14	0.3	0.76 (0.39 , 0 , 0.98)	0.33 (0.45 , 0 , 0.98)	0.11 (0.29 , 0 , 0.98)
PIT	PIT	21	0.3	0.95 (0.03 , 0.82 , 0.98)	0.72 (0.25 , 0 , 0.98)	0.29 (0.34 , 0 , 0.98)
SAN	*					
SEA	*					
SFO	*					
SLC	SLC	20	0.3	0.81 (0.33 , 0 , 0.98)	0.24 (0.38 , 0 , 0.98)	0.07 (0.23 , 0 , 0.98)
STL	STL	13	0.3	0.98 (0.01 , 0.87 , 0.98)	0.86 (0.16 , 0 , 0.98)	0.35 (0.37 , 0 , 0.98)
TPA	TPA	13	0.3	0.98 (0.02 , 0.77 , 0.98)	0.93 (0.10 , 0 , 0.98)	0.41 (0.40 , 0 , 0.98)

* No TDWR

Table A-2. Microburst Visibility for NEXRAD

Airport	RadarID	Radar-Airport Distance (km)	Beam El. Angle (deg)	Mean (S.d., Min, Max) 10km	50km	100km
ATL	FFC	33	0.5	0.85 (0.24 , 0 , 0.97)	0.69 (0.32 , 0 , 0.98)	0.42 (0.36 , 0 , 0.98)
BOS	BOX	47	0.5	0.50 (0.18 , 0 , 0.70)	0.34 (0.34 , 0 , 0.98)	0.22 (0.30 , 0 , 0.98)
BWI	LWX	74	0.5	0 (0.01 , 0 , 0.11)	0.07 (0.16 , 0 , 0.81)	0.10 (0.24 , 0 , 0.98)
CLE	CLE	1	0.5	0.90 (0.14 , 0.29 , 0.98)	0.60 (0.35 , 0 , 0.98)	0.26 (0.30 , 0 , 0.98)
CLT	GSP	122	0.5	0 (0 , 0 , 0)	0.02 (0.04 , 0 , 0.26)	0.09 (0.20 , 0 , 0.94)
CVG	ILN	84	0.5	0.10 (0.04 , 0.04 , 0.19)	0.16 (0.20 , 0 , 0.76)	0.19 (0.29 , 0 , 0.98)
DCA	LWX	41	0.5	0 (0 , 0 , 0)	0.25 (0.36 , 0 , 0.98)	0.11 (0.24 , 0 , 0.98)
DEN	FTG	14	0.5	0.90 (0.08 , 0.35 , 0.98)	0.41 (0.31 , 0 , 0.98)	0.13 (0.23 , 0 , 0.98)
DFW	FWS	44	0.5	0.74 (0.06 , 0.38 , 0.86)	0.53 (0.32 , 0 , 0.98)	0.18 (0.31 , 0 , 0.98)
DTW	DTX	55	0.5	0.30 (0.07 , 0.17 , 0.45)	0.29 (0.27 , 0 , 0.97)	0.20 (0.27 , 0 , 0.98)
EWR	DIX	85	0.5	0.10 (0.04 , 0.04 , 0.21)	0.16 (0.19 , 0 , 0.69)	0.18 (0.28 , 0 , 0.98)
FLL	AMX	57	0.5	0.76 (0.07 , 0.60 , 0.89)	0.58 (0.34 , 0.01 , 0.98)	0.39 (0.40 , 0 , 0.98)
HNL	HMO	80	0.5	0 (0 , 0 , 0)	0 (0 , 0 , 0)	0 (0 , 0 , 0)
IAD	LWX	4	0.5	0.92 (0.11 , 0.33 , 0.98)	0.49 (0.41 , 0 , 0.98)	0.16 (0.29 , 0 , 0.98)
IAH	HGX	62	0.5	0.66 (0.07 , 0.51 , 0.80)	0.54 (0.33 , 0.01 , 0.98)	0.38 (0.39 , 0 , 0.98)
JFK	OKX	81	0.5	0.12 (0.06 , 0 , 0.23)	0.15 (0.18 , 0 , 0.74)	0.19 (0.28 , 0 , 0.98)
LAS	ESX	48	0.5	0 (0 , 0 , 0)	0 (0 , 0 , 0)	0 (0 , 0 , 0)
LAX	SOX	73	0.5	0 (0 , 0 , 0)	0 (0 , 0 , 0)	0 (0 , 0 , 0)
LGA	OKX	86	0.5	0.04 (0.05 , 0 , 0.20)	0.14 (0.18 , 0 , 0.68)	0.18 (0.28 , 0 , 0.98)
MCO	MLB	73	0.5	0.48 (0.10 , 0.28 , 0.66)	0.41 (0.34 , 0 , 0.98)	0.33 (0.38 , 0 , 0.98)
MDW	LOT	34	0.5	0.79 (0.09 , 0 , 0.91)	0.54 (0.33 , 0 , 0.98)	0.31 (0.31 , 0 , 0.98)
MEM	NQA	35	0.5	0.90 (0.06 , 0.72 , 0.97)	0.67 (0.28 , 0.14 , 0.98)	0.37 (0.33 , 0 , 0.98)
MIA	AMX	24	0.5	0.97 (0.03 , 0.31 , 0.98)	0.88 (0.13 , 0 , 0.98)	0.50 (0.36 , 0 , 0.98)
MSP	MPX	28	0.5	0.84 (0.07 , 0.07 , 0.95)	0.66 (0.24 , 0.07 , 0.98)	0.33 (0.31 , 0 , 0.98)
ORD	LOT	44	0.5	0.61 (0.07 , 0.47 , 0.77)	0.48 (0.30 , 0 , 0.98)	0.28 (0.31 , 0 , 0.98)
PDX	RTX	32	0.5	0 (0 , 0 , 0)	0 (0 , 0 , 0)	0 (0 , 0 , 0)
PHL	DIX	71	0.5	0.26 (0.06 , 0.15 , 0.40)	0.26 (0.25 , 0 , 0.91)	0.24 (0.31 , 0 , 0.98)
PHX	IWA	36	0.5	0.77 (0.24 , 0 , 0.93)	0.40 (0.39 , 0 , 0.98)	0.12 (0.27 , 0 , 0.98)
PIT	PBZ	5	0.5	0.96 (0.05 , 0.43 , 0.98)	0.75 (0.18 , 0 , 0.98)	0.34 (0.28 , 0 , 0.98)
SAN	NKX	25	0.5	0.21 (0.05 , 0 , 0.24)	0.07 (0.08 , 0 , 0.24)	0.02 (0.05 , 0 , 0.24)
SEA	ATX	84	0.5	0.06 (0.03 , 0.02 , 0.14)	0.14 (0.20 , 0 , 0.79)	0.15 (0.29 , 0 , 0.98)
SFO	MUX	67	0.5	0 (0 , 0 , 0)	0 (0 , 0 , 0)	0 (0 , 0 , 0)
SLC	MTX	66	0.5	0 (0 , 0 , 0)	0 (0 , 0 , 0)	0 (0 , 0 , 0)
STL	LSX	29	0.5	0.89 (0.05 , 0.15 , 0.96)	0.70 (0.24 , 0 , 0.98)	0.31 (0.33 , 0 , 0.98)
TPA	TBW	33	0.5	0.95 (0.06 , 0.15 , 0.98)	0.79 (0.21 , 0 , 0.98)	0.44 (0.36 , 0 , 0.98)

Table A-3. Microburst Visibility for ASR-9 WSP

Airport	RadarID	Radar-Airport Distance (km)	Beam El. Angle (deg)	Mean (S.d., Min, Max) 10km	50km	100km
ATL	*					
BOS	*					
BWI	*					
CLE	*					
CLT	*					
CVG	*					
DCA	*					
DEN	*					
DFW	*					
DTW	*					
EWR	*					
FLL	*					
HNL	HNL	0.6	1.2	0.62 (0.32 , 0 , 0.98)	0.03 (0.14 , 0 , 0.98)	0.01 (0.07 , 0 , 0.98)
IAD	*					
IAH	*					
JFK	*					
LAS	*					
LAX	LAX	1.1	1.2	0.57 (0.25 , 0 , 0.98)	0.03 (0.13 , 0 , 0.98)	0.01 (0.06 , 0 , 0.98)
LGA	*					
MCO	*					
MDW	*					
MEM	*					
MIA	*					
MSP	*					
ORD	*					
PDX	PDX	2.2	1.2	0.39 (0.35 , 0 , 0.98)	0.02 (0.11 , 0 , 0.98)	0.01 (0.05 , 0 , 0.98)
PHL	*					
PHX	*					
PIT	*					
SAN	*					
SEA	SEA	0.4	1.2	0.56 (0.21 , 0.05 , 0.98)	0.03 (0.12 , 0 , 0.98)	0.01 (0.06 , 0 , 0.98)
SFO	*					
SLC	*					
STL	*					
TPA	*					

*No WSP

Table A-4. Microburst Visibility for Lidar

Airport	RadarID	Radar-Airport Distance (km)	Beam El. Angle (deg)	Mean (S.d., Min, Max) 10km
ATL	*			
BOS	*			
BWI	*			
CLE	*			
CLT	*			
CVG	*			
DCA	*			
DEN	*			
DFW	*			
DTW	*			
EWR	*			
FLL	*			
HNL	*			
IAD	*			
IAH	*			
JFK	*			
LAS	LAS	0.72	2.0	0.36 (0.28 , 0 , 0.90)
LAX	*			
LGA	*			
MCO	*			
MDW	*			
MEM	*			
MIA	*			
MSP	*			
ORD	*			
PDX	*			
PHL	*			
PHX	*			
PIT	*			
SAN	*			
SEA	*			
SFO	*			
SLC	*			
STL	*			
TPA	*			

*No LIDAR

APPENDIX B
GUST FRONT SUMMARY STATISTICS

Mean, standard deviation, minimum, and maximum values of the gust-front visibilities for ground-based wind-shear sensors in the 10, 50, and 100-km radius areas, respectively, around the individual OEP airports are listed in Tables B-1 (TDWR), B-2 (NEXRAD), B-3 (ASR-9 WSP), and B-4 (lidar, 10 km only). The areal resolution requirement is not considered in these tables.

Table B-1. Gust Front Visibility for TDWR

Airport	RadarID	Radar-Airport Distance (km)	Beam El. Angle (deg)	Mean (S.d., Min, Max) 10km	50km	100km
ATL	ATL	15	0.3	0.92 (0.11 , 0 , 0.95)	0.94 (0.04 , 0 , 0.95)	0.70 (0.38 , 0 , 0.95)
BOS	BOS	24	0.3	0.93 (0.07 , 0.13 , 0.95)	0.94 (0.05 , 0 , 0.95)	0.62 (0.41 , 0 , 0.95)
BWI	BWI	10	0.3	0.93 (0.08 , 0 , 0.95)	0.94 (0.05 , 0 , 0.95)	0.68 (0.37 , 0 , 0.95)
CLE	CLE	19	0.3	0.93 (0.10 , 0 , 0.95)	0.94 (0.06 , 0 , 0.95)	0.63 (0.41 , 0 , 0.95)
CLT	CLT	15	0.3	0.95 (0.03 , 0.12 , 0.95)	0.95 (0.03 , 0 , 0.95)	0.68 (0.38 , 0 , 0.95)
CVG	CVG	18	0.3	0.94 (0.06 , 0.16 , 0.95)	0.95 (0.02 , 0 , 0.95)	0.67 (0.39 , 0 , 0.95)
DCA	DCA	12	0.3	0.90 (0.13 , 0.07 , 0.95)	0.94 (0.05 , 0 , 0.95)	0.64 (0.39 , 0 , 0.95)
DEN	DEN	19	0.3	0.95 (0.01 , 0.88 , 0.95)	0.92 (0.14 , 0 , 0.95)	0.46 (0.45 , 0 , 0.95)
DFW	DFW	22	0.3	0.94 (0.05 , 0.26 , 0.95)	0.94 (0.04 , 0 , 0.95)	0.63 (0.42 , 0 , 0.95)
DTW	DTW	17	0.3	0.95 (0.01 , 0.87 , 0.95)	0.95 (0.02 , 0 , 0.95)	0.68 (0.39 , 0 , 0.95)
EWR	EWR	14	0.3	0.89 (0.16 , 0 , 0.95)	0.89 (0.21 , 0 , 0.95)	0.55 (0.43 , 0 , 0.95)
FLL	FLL	21	0.3	0.93 (0.09 , 0.03 , 0.95)	0.95 (0.03 , 0 , 0.95)	0.67 (0.39 , 0 , 0.95)
HNL	*					
IAD	IAD	17	0.3	0.93 (0.08 , 0.08 , 0.95)	0.89 (0.23 , 0 , 0.95)	0.49 (0.44 , 0 , 0.95)
IAH	IAH	24	0.3	0.95 (0.02 , 0.45 , 0.95)	0.95 (0.02 , 0 , 0.95)	0.65 (0.40 , 0 , 0.95)
JFK	JFK	10	0.3	0.87 (0.17 , 0 , 0.95)	0.93 (0.07 , 0 , 0.95)	0.68 (0.37 , 0 , 0.95)
LAS	LAS	15	0.3	0.68 (0.30 , 0 , 0.95)	0.16 (0.33 , 0 , 0.95)	0.05 (0.19 , 0 , 0.95)
LAX	*					
LGA	JFK	21	0.3	0.94 (0.06 , 0 , 0.95)	0.93 (0.07 , 0 , 0.95)	0.66 (0.40 , 0 , 0.95)
MCO	MCO	10	0.3	0.93 (0.07 , 0 , 0.95)	0.94 (0.10 , 0 , 0.95)	0.70 (0.37 , 0 , 0.95)
MDW	MDW	15	0.3	0.94 (0.02 , 0.76 , 0.95)	0.95 (0.02 , 0 , 0.95)	0.68 (0.38 , 0 , 0.95)
MEM	MEM	16	0.3	0.94 (0.05 , 0.31 , 0.95)	0.95 (0.03 , 0 , 0.95)	0.68 (0.38 , 0 , 0.95)
MIA	MIA	21	0.3	0.92 (0.10 , 0.02 , 0.95)	0.94 (0.04 , 0 , 0.95)	0.67 (0.39 , 0 , 0.95)
MSP	MSP	22	0.3	0.95 (0 , 0.90 , 0.95)	0.95 (0.02 , 0 , 0.95)	0.63 (0.40 , 0 , 0.95)
ORD	ORD	21	0.3	0.94 (0.05 , 0.14 , 0.95)	0.95 (0.02 , 0 , 0.95)	0.67 (0.39 , 0 , 0.95)
PDX	*					
PHL	PHL	17	0.3	0.91 (0.13 , 0 , 0.95)	0.94 (0.06 , 0 , 0.95)	0.65 (0.40 , 0 , 0.95)
PHX	PHX	14	0.3	0.70 (0.39 , 0 , 0.95)	0.47 (0.46 , 0 , 0.95)	0.24 (0.39 , 0 , 0.95)
PIT	PIT	21	0.3	0.95 (0.01 , 0.77 , 0.95)	0.95 (0.02 , 0 , 0.95)	0.66 (0.40 , 0 , 0.95)
SAN	*					
SEA	*					
SFO	*					
SLC	SLC	20	0.3	0.80 (0.33 , 0 , 0.95)	0.34 (0.44 , 0 , 0.95)	0.16 (0.34 , 0 , 0.95)
STL	STL	13	0.3	0.94 (0.03 , 0.47 , 0.95)	0.95 (0.02 , 0 , 0.95)	0.70 (0.37 , 0 , 0.95)
TPA	TPA	13	0.3	0.91 (0.11 , 0.06 , 0.95)	0.94 (0.05 , 0 , 0.95)	0.70 (0.37 , 0 , 0.95)

* No TDWR

Table B-2. Gust Front Visibility for NEXRAD

Airport	RadarID	Radar-Airport Distance (km)	Beam El. Angle (deg)	Mean (S.d., Min, Max) 10km	50km	100km
ATL	FFC	33	0.5	0.95 (0 , 0.95 , 0.95)	0.86 (0.18 , 0 , 0.95)	0.51 (0.42 , 0 , 0.95)
BOS	BOX	47	0.5	0.95 (0.01 , 0.92 , 0.95)	0.68 (0.36 , 0 , 0.95)	0.42 (0.43 , 0 , 0.95)
BWI	LWX	74	0.5	0.26 (0.21 , 0.01 , 0.75)	0.36 (0.41 , 0 , 0.95)	0.30 (0.41 , 0 , 0.95)
CLE	CLE	1	0.5	0.79 (0.26 , 0 , 0.95)	0.91 (0.14 , 0 , 0.95)	0.48 (0.41 , 0 , 0.95)
CLT	GSP	122	0.5	0 (0 , 0 , 0)	0.01 (0.04 , 0 , 0.42)	0.12 (0.29 , 0 , 0.95)
CVG	ILN	84	0.5	0.10 (0.09 , 0.01 , 0.38)	0.28 (0.37 , 0 , 0.95)	0.27 (0.40 , 0 , 0.95)
DCA	LWX	41	0.5	0.95 (0 , 0.93 , 0.95)	0.69 (0.36 , 0 , 0.95)	0.36 (0.42 , 0 , 0.95)
DEN	FTG	14	0.5	0.93 (0.06 , 0.13 , 0.95)	0.92 (0.11 , 0 , 0.95)	0.43 (0.42 , 0 , 0.95)
DFW	FWS	44	0.5	0.95 (0.02 , 0.34 , 0.95)	0.75 (0.31 , 0 , 0.95)	0.42 (0.43 , 0 , 0.95)
DTW	DTX	55	0.5	0.85 (0.10 , 0.56 , 0.95)	0.53 (0.41 , 0 , 0.95)	0.36 (0.42 , 0 , 0.95)
EWR	DIX	85	0.5	0.09 (0.08 , 0.01 , 0.36)	0.27 (0.37 , 0 , 0.95)	0.27 (0.40 , 0 , 0.95)
FLL	AMX	57	0.5	0.91 (0.04 , 0.77 , 0.95)	0.60 (0.39 , 0 , 0.95)	0.40 (0.43 , 0 , 0.95)
HNL	HMO	80	0.5	0 (0 , 0 , 0.01)	0.10 (0.23 , 0 , 0.95)	0.16 (0.32 , 0 , 0.95)
IAD	LWX	4	0.5	0.83 (0.22 , 0 , 0.95)	0.91 (0.17 , 0 , 0.95)	0.42 (0.42 , 0 , 0.95)
IAH	HGX	62	0.5	0.87 (0.07 , 0.63 , 0.95)	0.57 (0.40 , 0 , 0.95)	0.39 (0.43 , 0 , 0.95)
JFK	OKX	81	0.5	0.18 (0.15 , 0 , 0.56)	0.32 (0.39 , 0 , 0.95)	0.29 (0.40 , 0 , 0.95)
LAS	ESX	48	0.5	0 (0 , 0 , 0)	0 (0 , 0 , 0)	0 (0 , 0 , 0)
LAX	SOX	73	0.5	0 (0 , 0 , 0)	0 (0 , 0 , 0)	0 (0 , 0 , 0)
LGA	OKX	86	0.5	0.05 (0.06 , 0 , 0.33)	0.27 (0.37 , 0 , 0.95)	0.27 (0.40 , 0 , 0.95)
MCO	MLB	73	0.5	0.57 (0.20 , 0.19 , 0.89)	0.44 (0.41 , 0 , 0.95)	0.34 (0.42 , 0 , 0.95)
MDW	LOT	34	0.5	0.95 (0 , 0.95 , 0.95)	0.83 (0.22 , 0 , 0.95)	0.48 (0.42 , 0 , 0.95)
MEM	NQA	35	0.5	0.95 (0 , 0.89 , 0.95)	0.85 (0.19 , 0 , 0.95)	0.50 (0.42 , 0 , 0.95)
MIA	AMX	24	0.5	0.94 (0.08 , 0.01 , 0.95)	0.91 (0.10 , 0 , 0.95)	0.52 (0.41 , 0 , 0.95)
MSP	MPX	28	0.5	0.94 (0.05 , 0.05 , 0.95)	0.88 (0.14 , 0.05 , 0.95)	0.49 (0.41 , 0 , 0.95)
ORD	LOT	44	0.5	0.95 (0 , 0.94 , 0.95)	0.75 (0.30 , 0 , 0.95)	0.45 (0.43 , 0 , 0.95)
PDX	RTX	32	0.5	0.81 (0.15 , 0.04 , 0.95)	0.42 (0.40 , 0 , 0.95)	0.13 (0.29 , 0 , 0.95)
PHL	DIX	71	0.5	0.53 (0.21 , 0.14 , 0.88)	0.43 (0.41 , 0 , 0.95)	0.33 (0.42 , 0 , 0.95)
PHX	IWA	36	0.5	0.90 (0.17 , 0 , 0.95)	0.61 (0.38 , 0 , 0.95)	0.24 (0.38 , 0 , 0.95)
PIT	PBZ	5	0.5	0.91 (0.10 , 0.15 , 0.95)	0.94 (0.06 , 0.01 , 0.95)	0.54 (0.40 , 0 , 0.95)
SAN	NKX	25	0.5	0.94 (0.04 , 0.38 , 0.95)	0.58 (0.40 , 0 , 0.95)	0.17 (0.33 , 0 , 0.95)
SEA	ATX	84	0.5	0.13 (0.11 , 0.01 , 0.46)	0.29 (0.38 , 0 , 0.95)	0.22 (0.37 , 0 , 0.95)
SFO	MUX	67	0.5	0 (0 , 0 , 0)	0 (0 , 0 , 0)	0 (0 , 0 , 0)
SLC	MTX	66	0.5	0 (0 , 0 , 0)	0 (0.01 , 0 , 0.06)	0 (0.02 , 0 , 0.89)
STL	LSX	29	0.5	0.94 (0.06 , 0 , 0.95)	0.90 (0.12 , 0 , 0.95)	0.50 (0.42 , 0 , 0.95)
TPA	TBW	33	0.5	0.93 (0.10 , 0 , 0.95)	0.86 (0.18 , 0 , 0.95)	0.50 (0.42 , 0 , 0.95)

Table B-3. Gust Front Visibility for ASR-9 WSP

Airport	RadarID	Radar-Airport Distance (km)	Beam El. Angle (deg)	Mean (S.d., Min, Max) 10km	50km	100km
ATL	*					
BOS	*					
BWI	*					
CLE	*					
CLT	*					
CVG	*					
DCA	*					
DEN	*					
DFW	*					
DTW	*					
EWR	*					
FLL	*					
HNL	HNL	0.6	1.2	0.73 (0.26 , 0 , 0.92)	0.09 (0.22 , 0 , 0.92)	0.02 (0.12 , 0 , 0.92)
IAD	*					
IAH	*					
JFK	*					
LAS	*					
LAX	LAX	1.1	1.2	0.85 (0.2 , 0 , 0.92)	0.12 (0.27 , 0 , 0.92)	0.03 (0.14 , 0 , 0.92)
LGA	*					
MCO	*					
MDW	*					
MEM	*					
MIA	*					
MSP	*					
ORD	*					
PDX	PDX	2.2	1.2	0.81 (0.24 , 0 , 0.92)	0.11 (0.25 , 0 , 0.92)	0.03 (0.14 , 0 , 0.92)
PHL	*					
PHX	*					
PIT	*					
SAN	*					
SEA	SEA	0.4	1.2	0.85 (0.20 , 0 , 0.92)	0.13 (0.27 , 0 , 0.92)	0.03 (0.15 , 0 , 0.92)
SFO	*					
SLC	*					
STL	*					
TPA	*					

*No WSP

Table B-4. Gust Front Visibility for Lidar

Airport	RadarID	Radar-Airport Distance (km)	Beam El. Angle (deg)	Mean (S.d., Min, Max) 10km
ATL	*			
BOS	*			
BWI	*			
CLE	*			
CLT	*			
CVG	*			
DCA	*			
DEN	*			
DFW	*			
DTW	*			
EWR	*			
FLL	*			
HNL	*			
IAD	*			
IAH	*			
JFK	*			
LAS	LAS	0.72	2.0	0.95 (0 , 0 , 0.95)
LAX	*			
LGA	*			
MCO	*			
MDW	*			
MEM	*			
MIA	*			
MSP	*			
ORD	*			
PDX	*			
PHL	*			
PHX	*			
PIT	*			
SAN	*			
SEA	*			
SFO	*			
SLC	*			
STL	*			
TPA	*			

*No LIDAR

APPENDIX C
COMPOSITE BEST WIND-SHEAR VISIBILITY MAPS AT INDIVIDUAL OEP AIRPORTS

The composite maps of the best wind-shear visibility satisfying the areal resolution requirement of 0.25 km^2 for the OEP terminal airspaces are generated for different ground-based wind-shear sensors. The "o" is the airport location and the "x" is the sensor location. The individual sensors are labeled with "T" (for TDWR), "N" (for NEXRAD), "A" (for ASR-9 WSP), and "L" (for lidar).

ATL

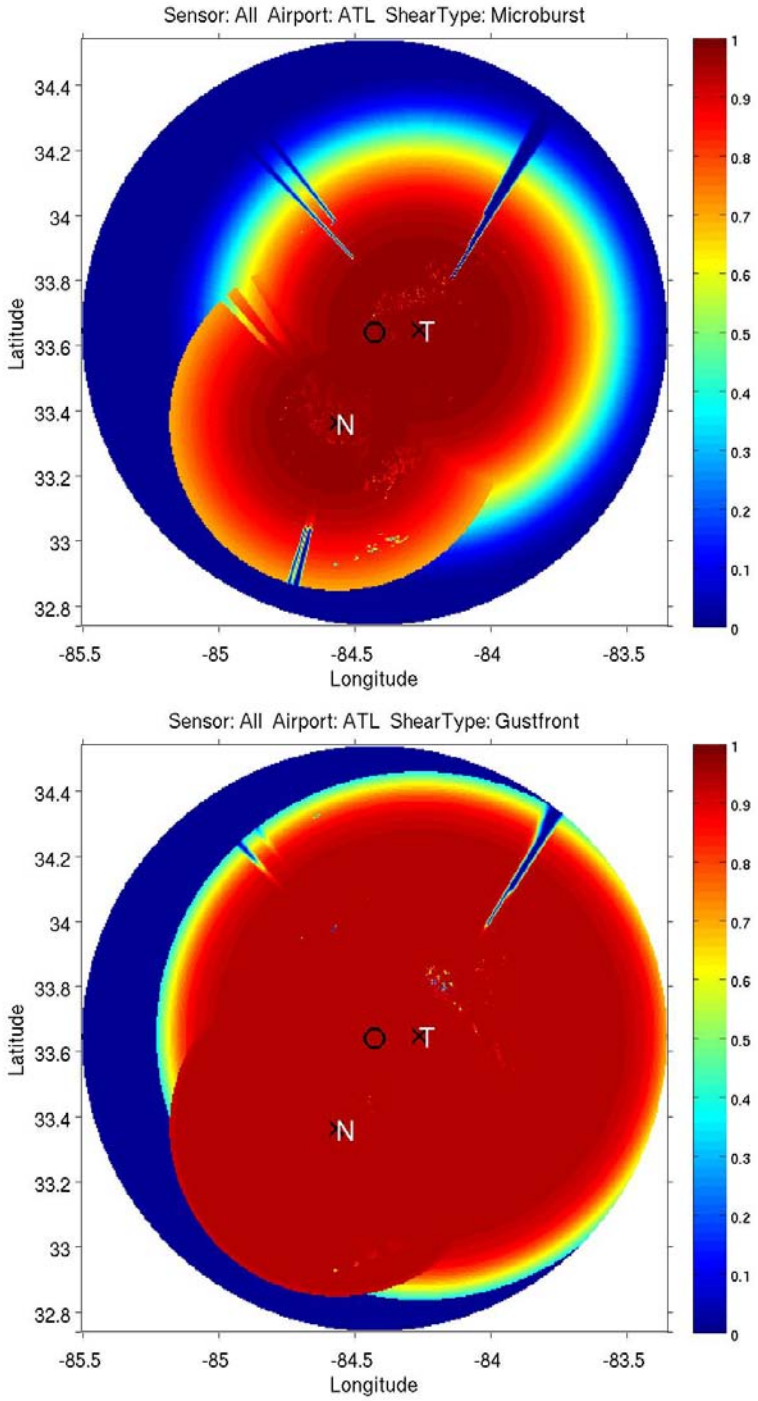

Figure C-1. Wind-shear visibility maps for ATL. Top: Microburst. Bottom: Gust front.

BOS

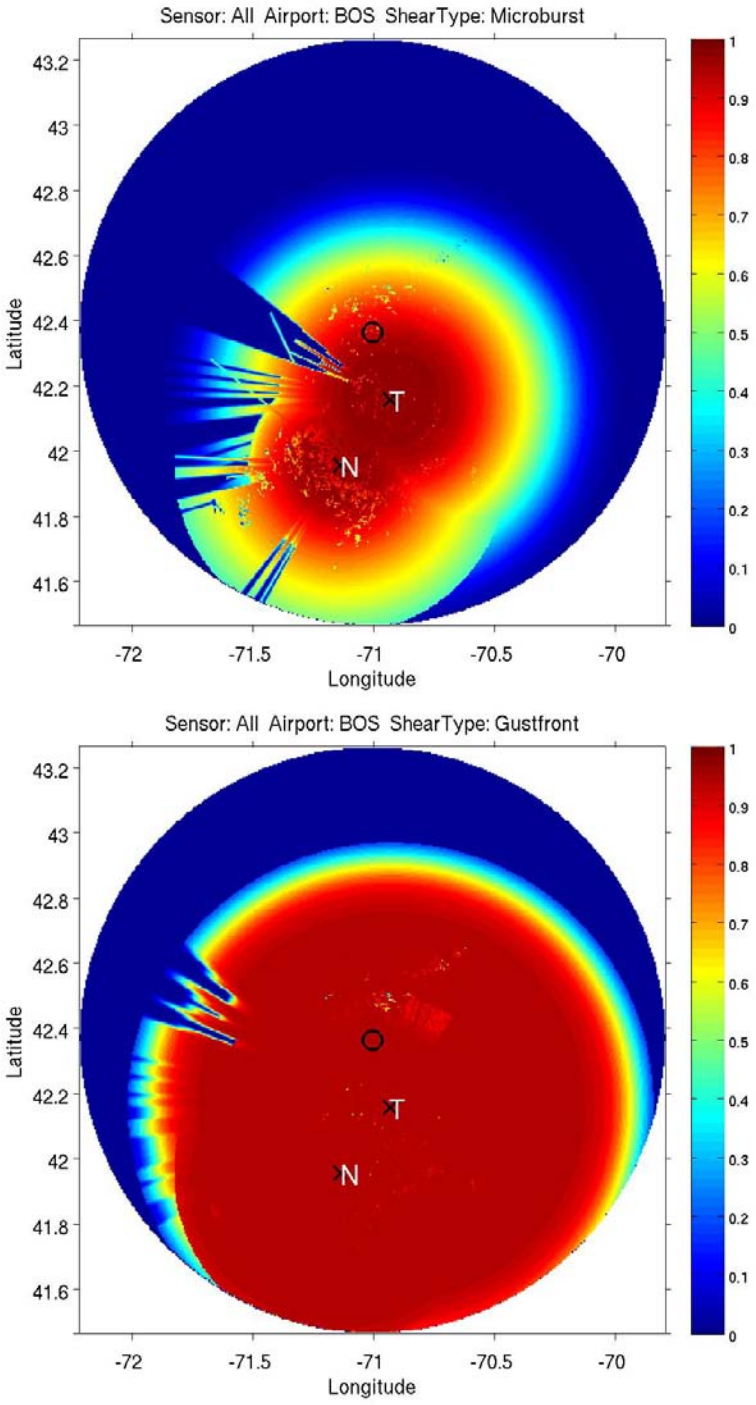

Figure C-2. Wind-shear visibility maps for BOS. Top: Microburst. Bottom: Gust front.

BWI

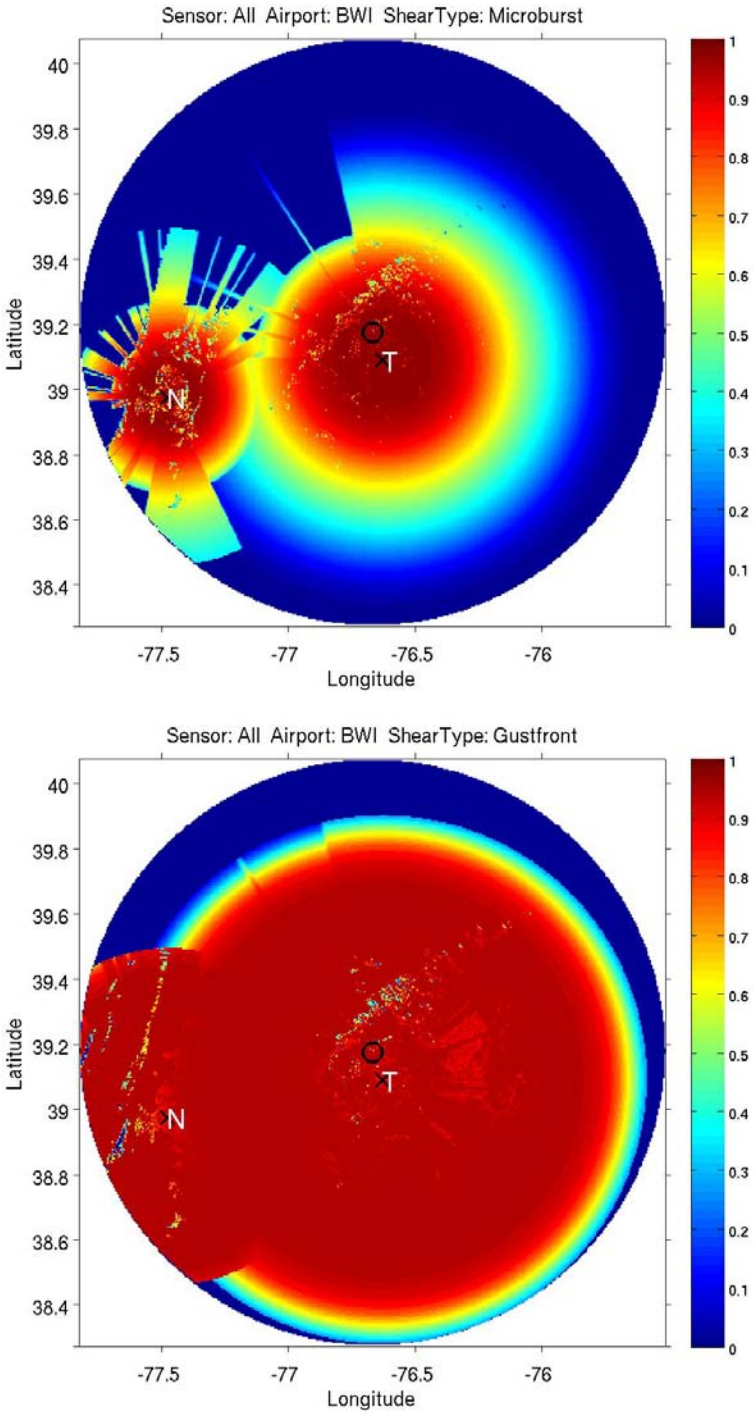

Figure C-3. Wind-shear visibility maps for BWI. Top: Microburst. Bottom: Gust front.

CLE

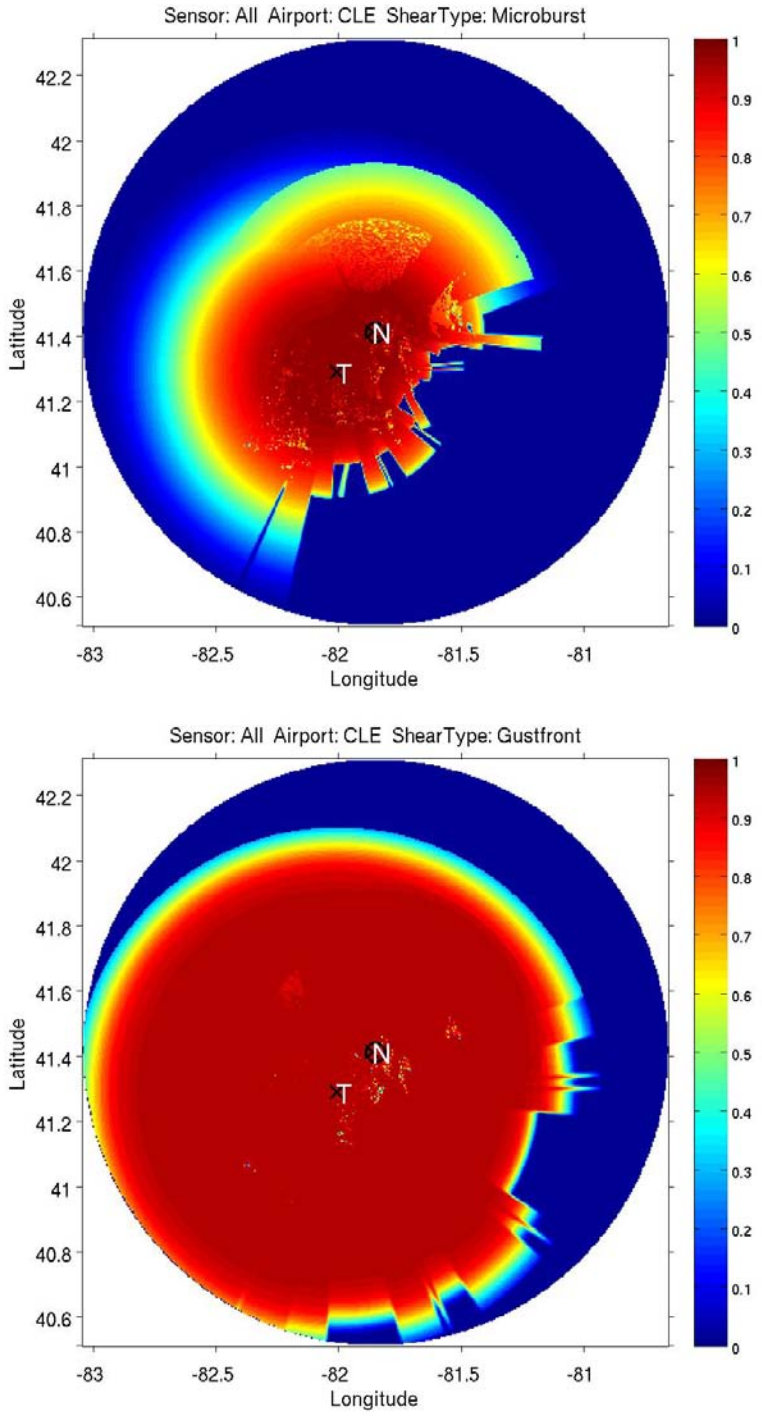

Figure C-4. Wind-shear visibility maps for CLE. Top: Microburst. Bottom: Gust front.

CLT

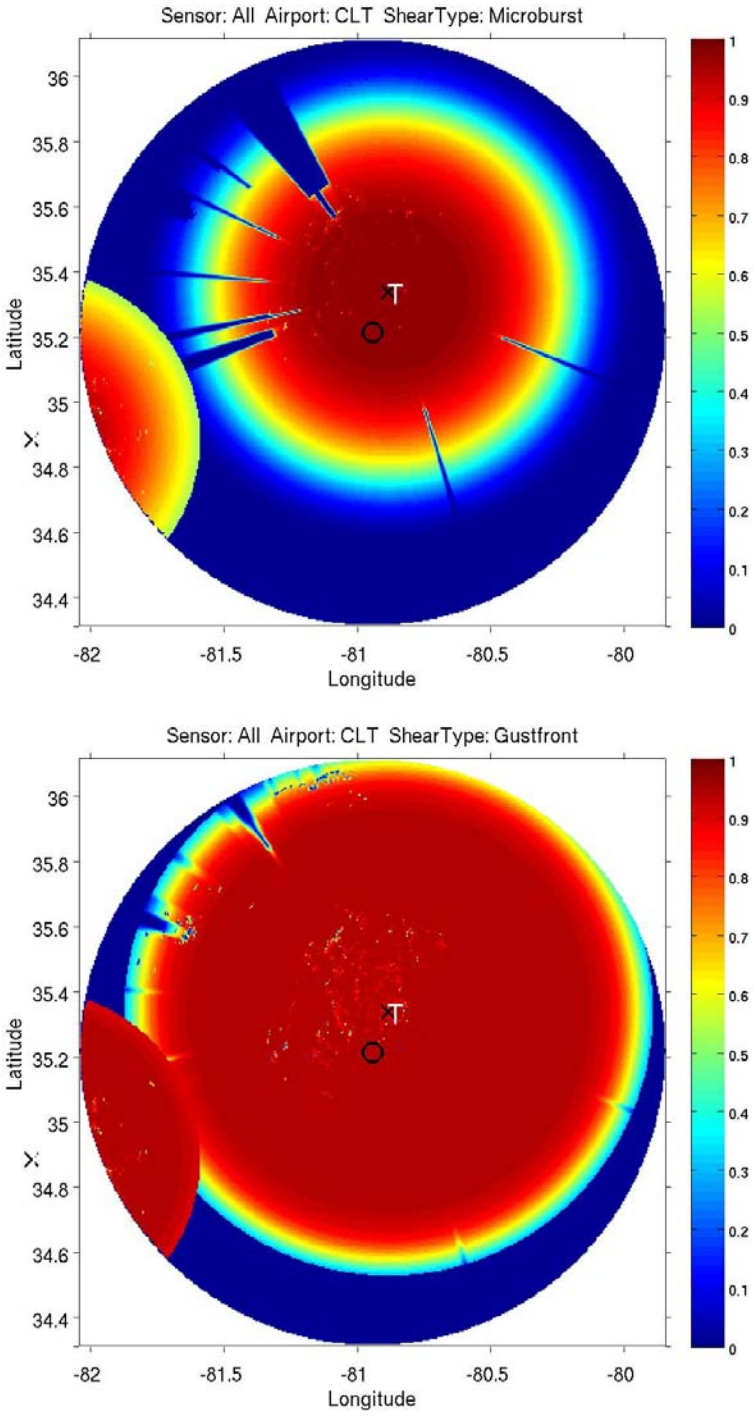

Figure C-5. Wind-shear visibility maps for CLT. Top: Microburst. Bottom: Gust front.

CVG

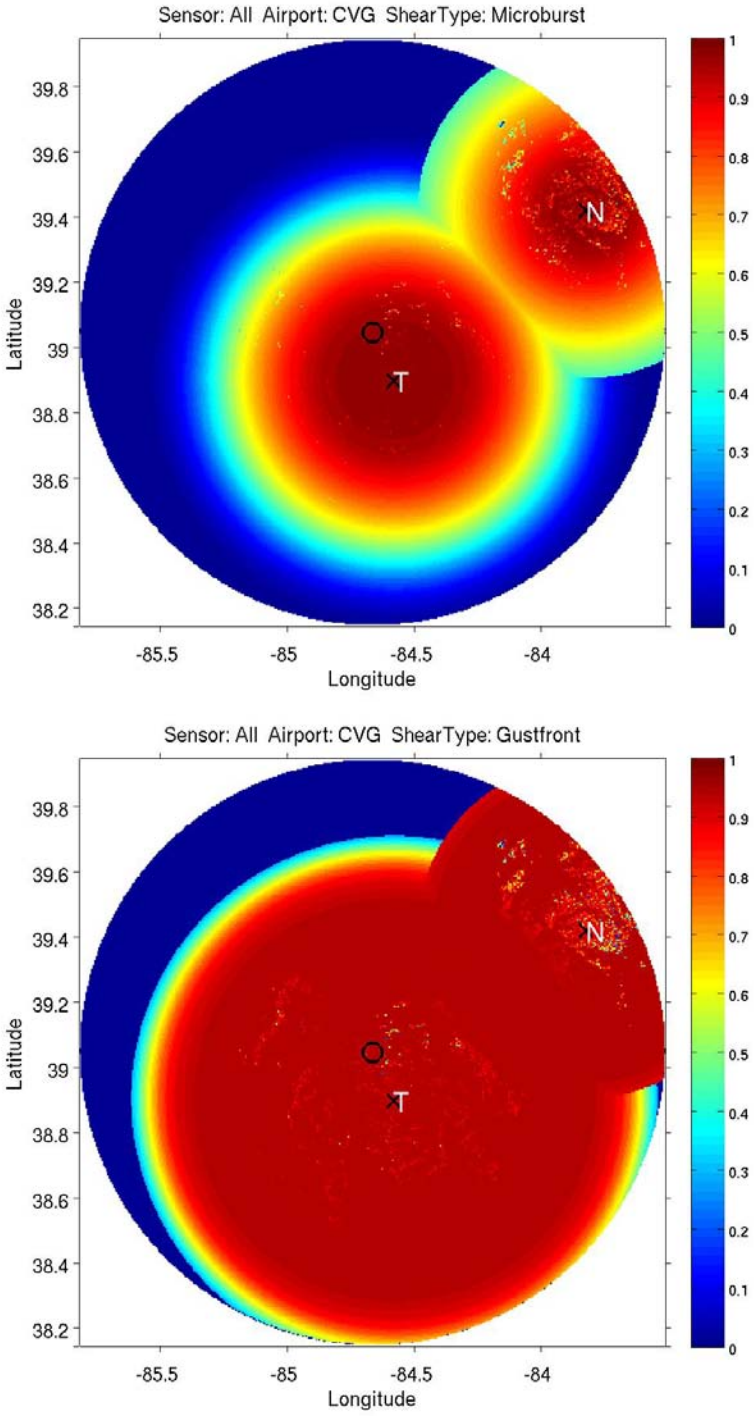

Figure C-6. Wind-shear visibility maps for CVG. Top: Microburst. Bottom: Gust front.

DCA

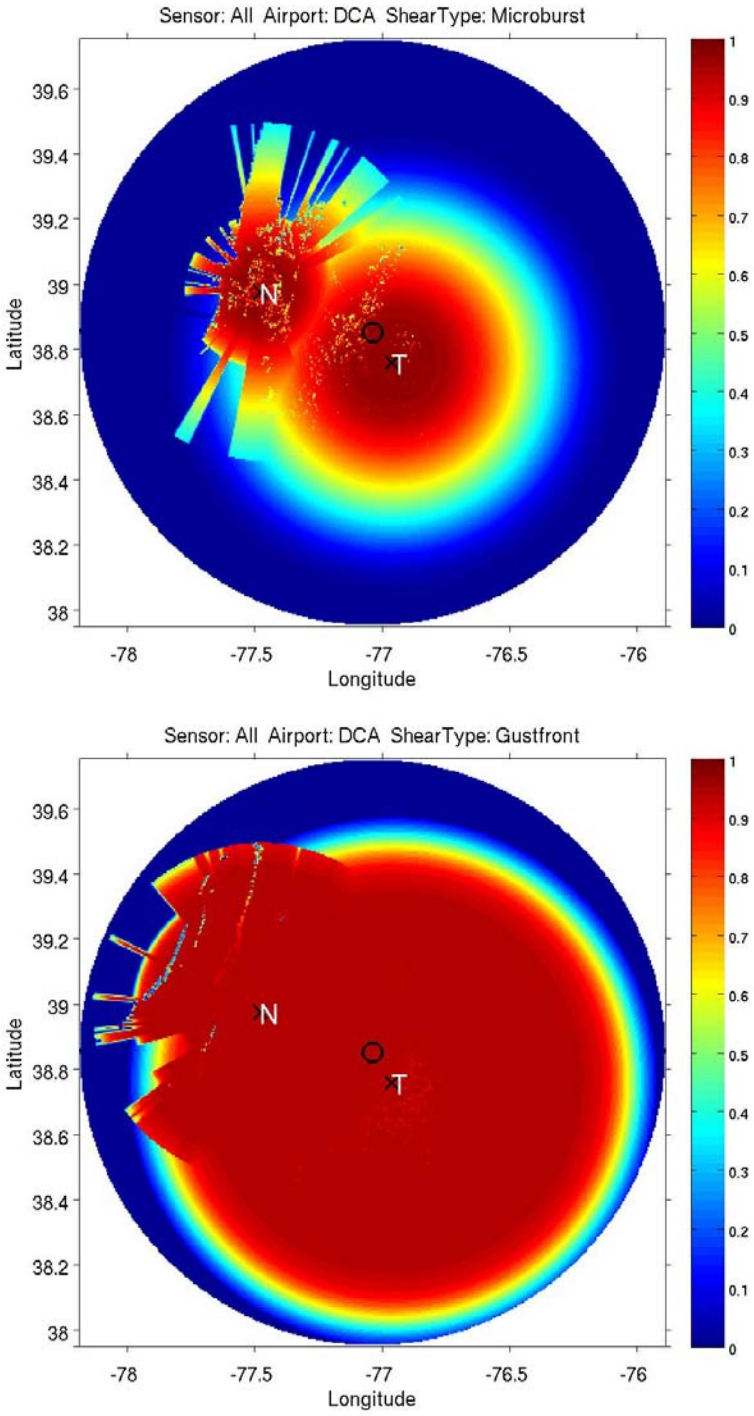

Figure C-7. Wind-shear visibility maps for DCA. Top: Microburst. Bottom: Gust front.

DEN

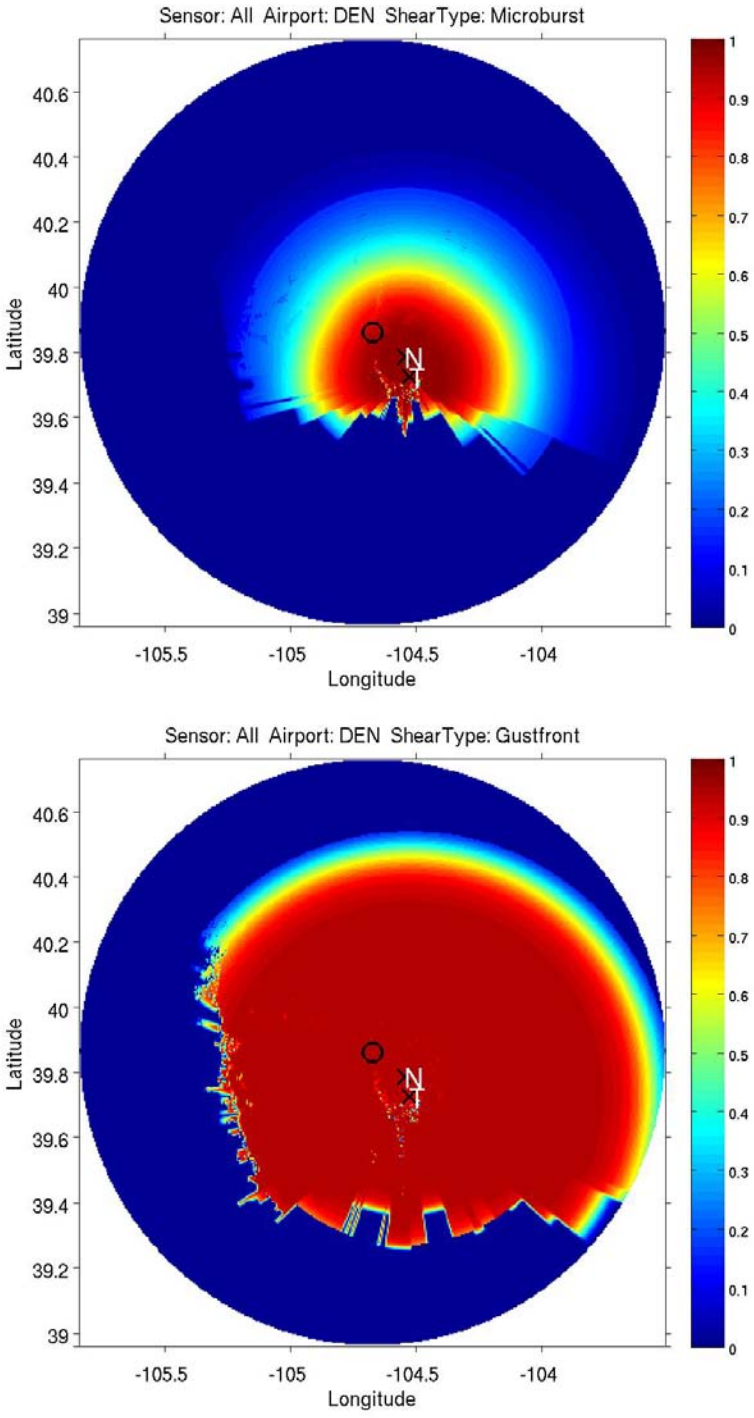

Figure C-8. Wind-shear visibility maps for DEN. Top: Microburst. Bottom: Gust front.

DFW

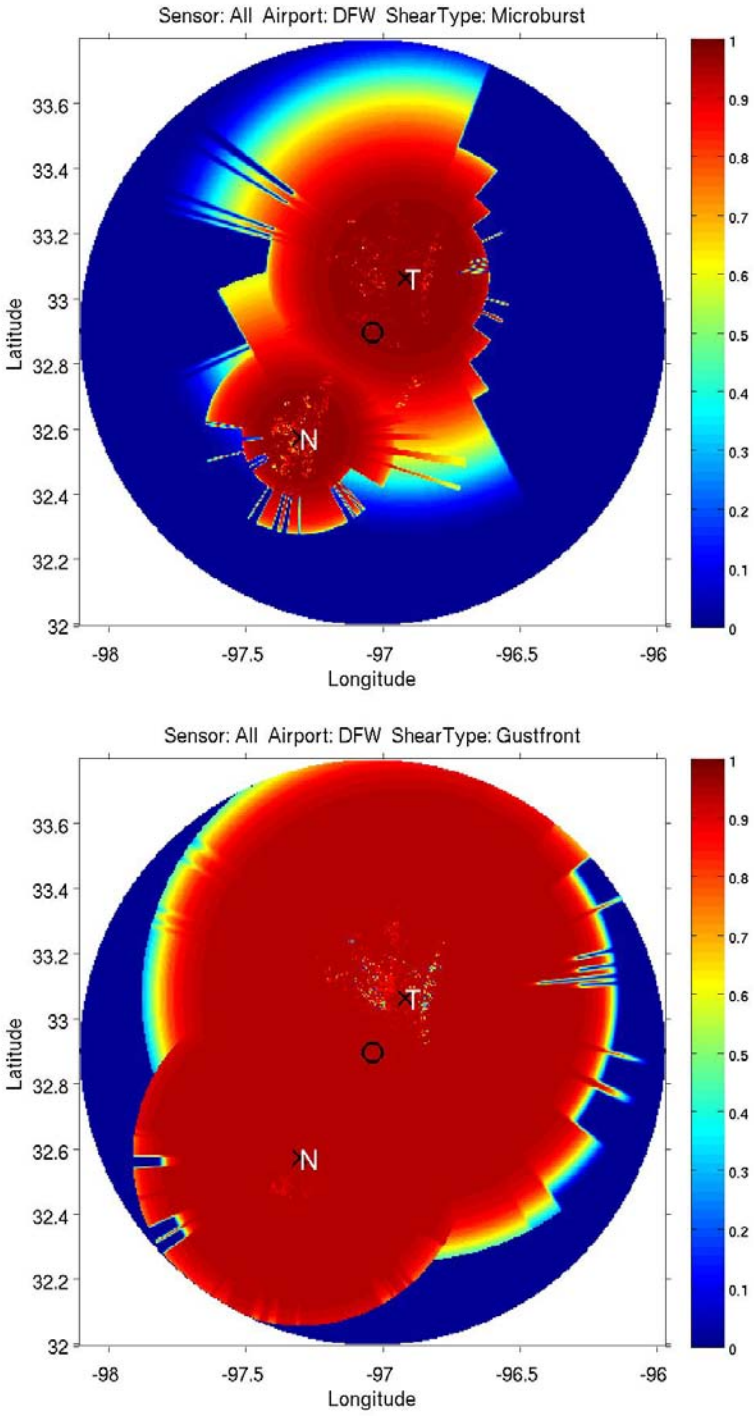

Figure C-9. Wind-shear visibility maps for DFW. Top: Microburst. Bottom: Gust front.

DTW

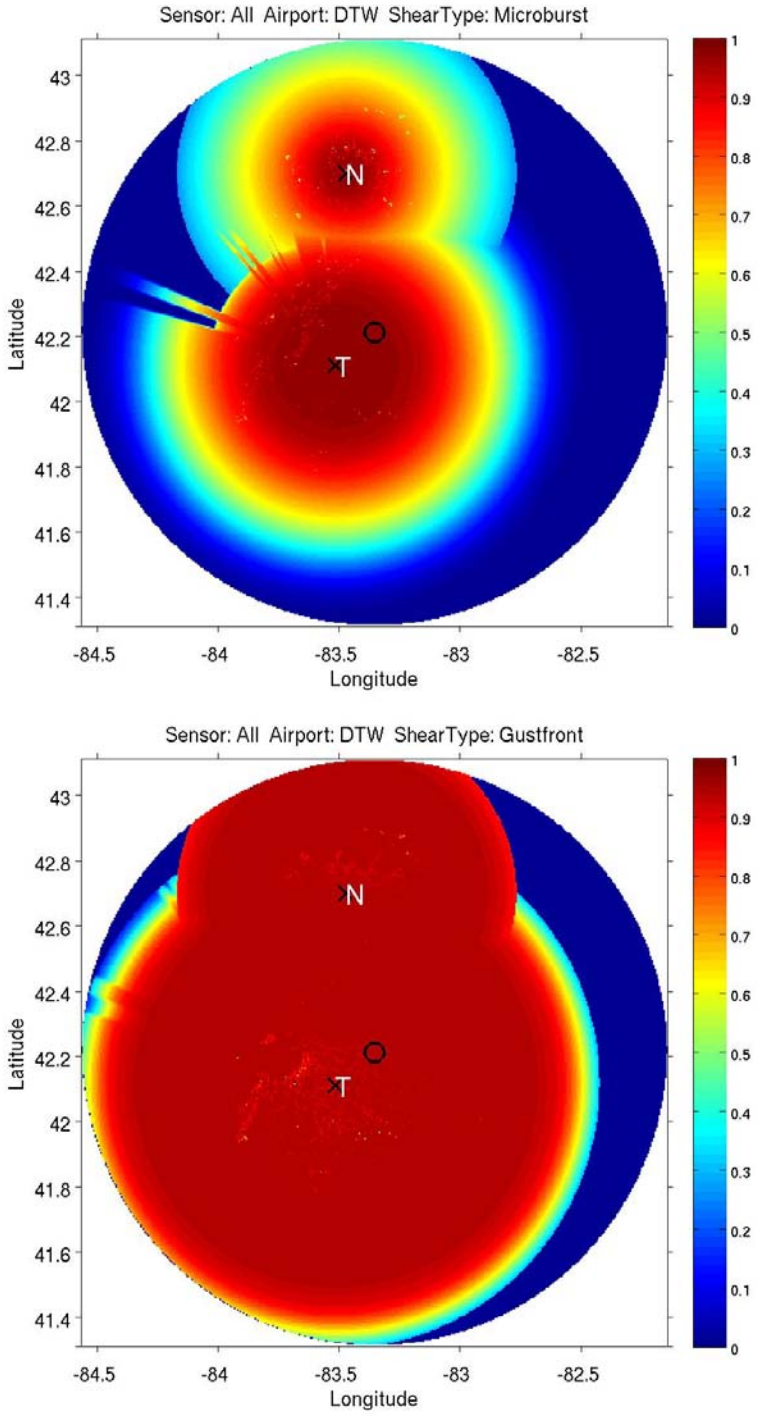

Figure C-10. Wind-shear visibility maps for DTW. Top: Microburst. Bottom: Gust front.

EWR

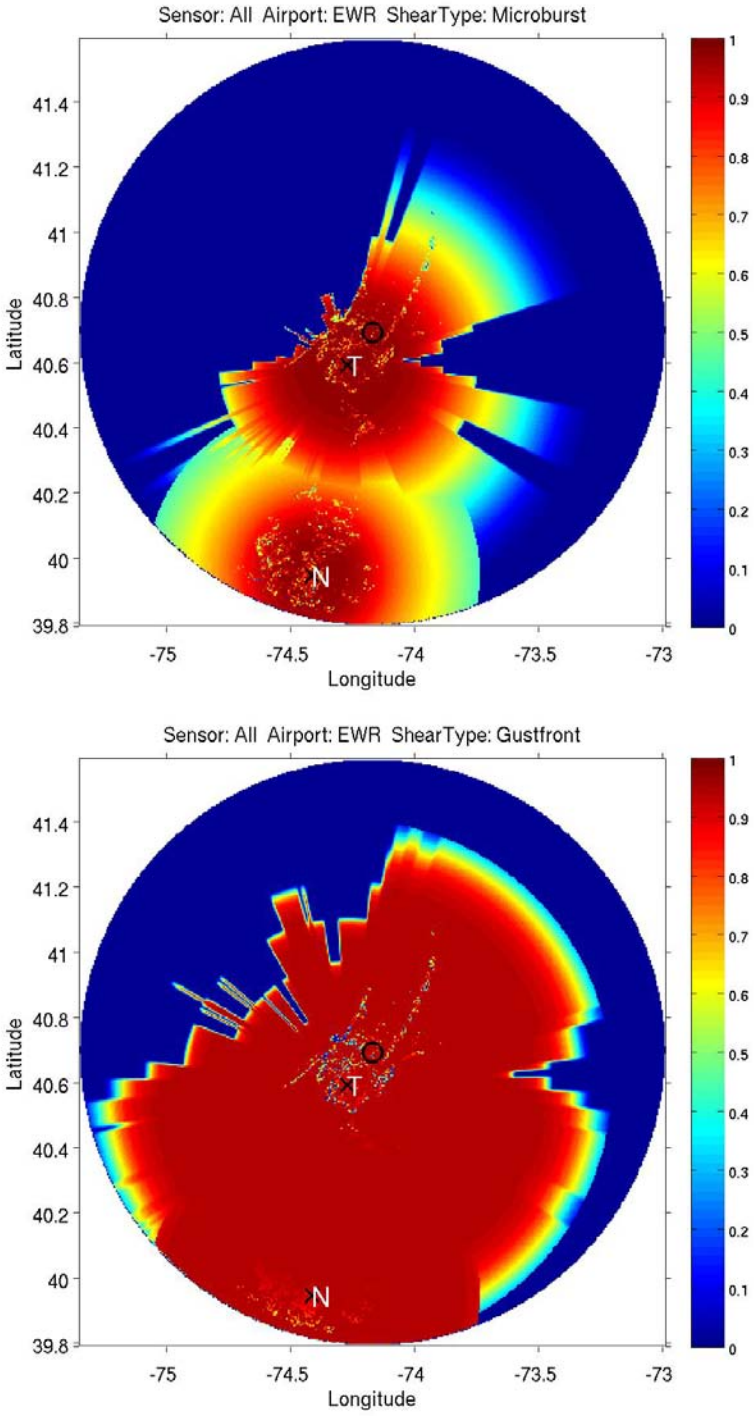

Figure C-11. Wind-shear visibility maps for EWR. Top: Microburst. Bottom: Gust front.

FLL

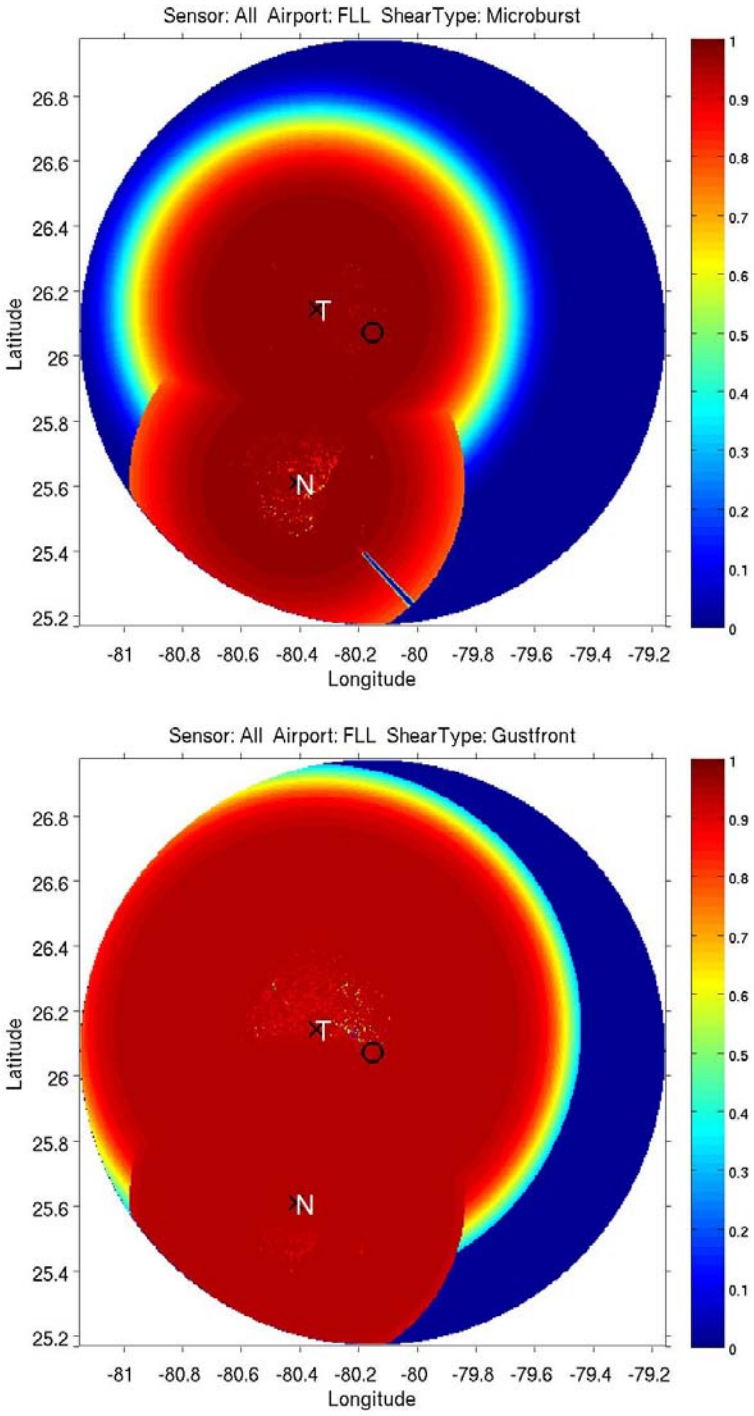

Figure C-12. Wind-shear visibility maps for FLL. Top: Microburst. Bottom: Gust front.

HNL

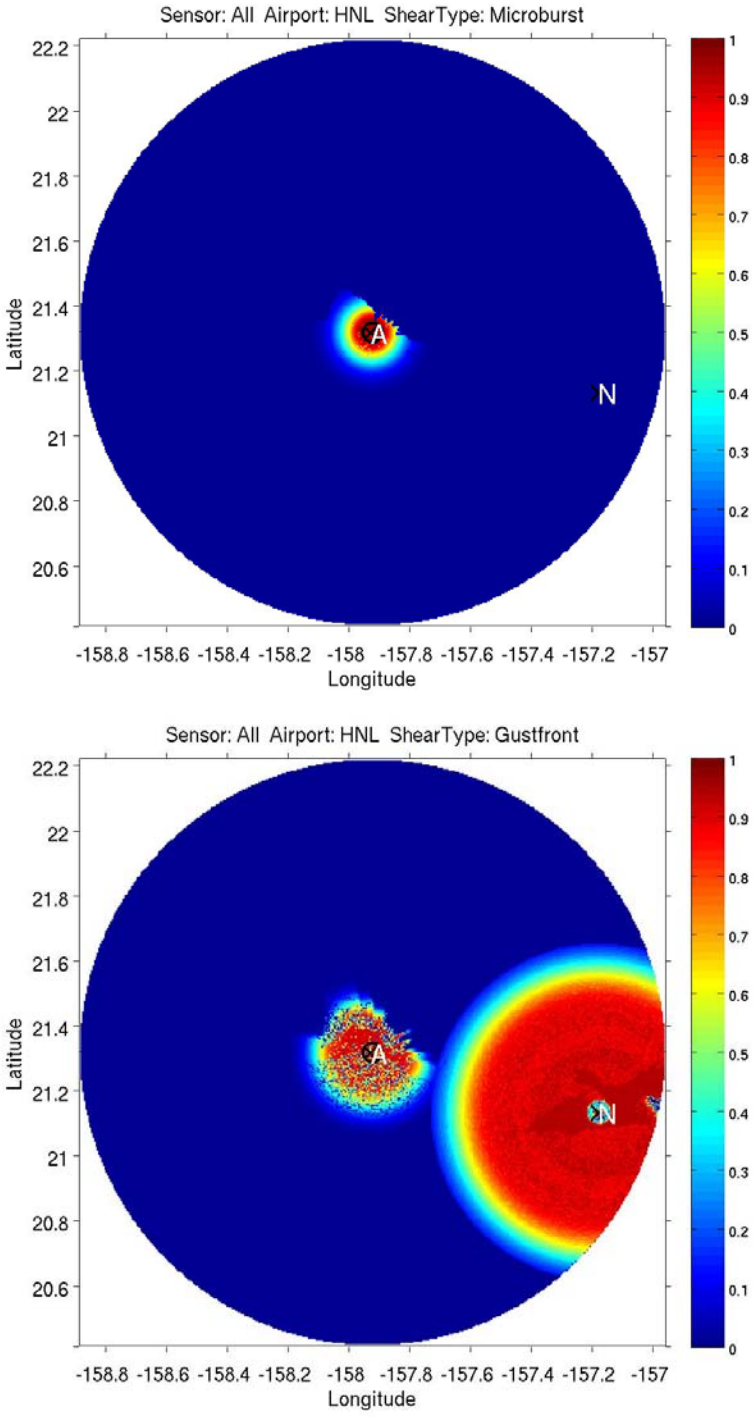

Figure C-13. Wind-shear visibility maps for HNL. Top: NEXRAD. Bottom: Gust front.

IAD

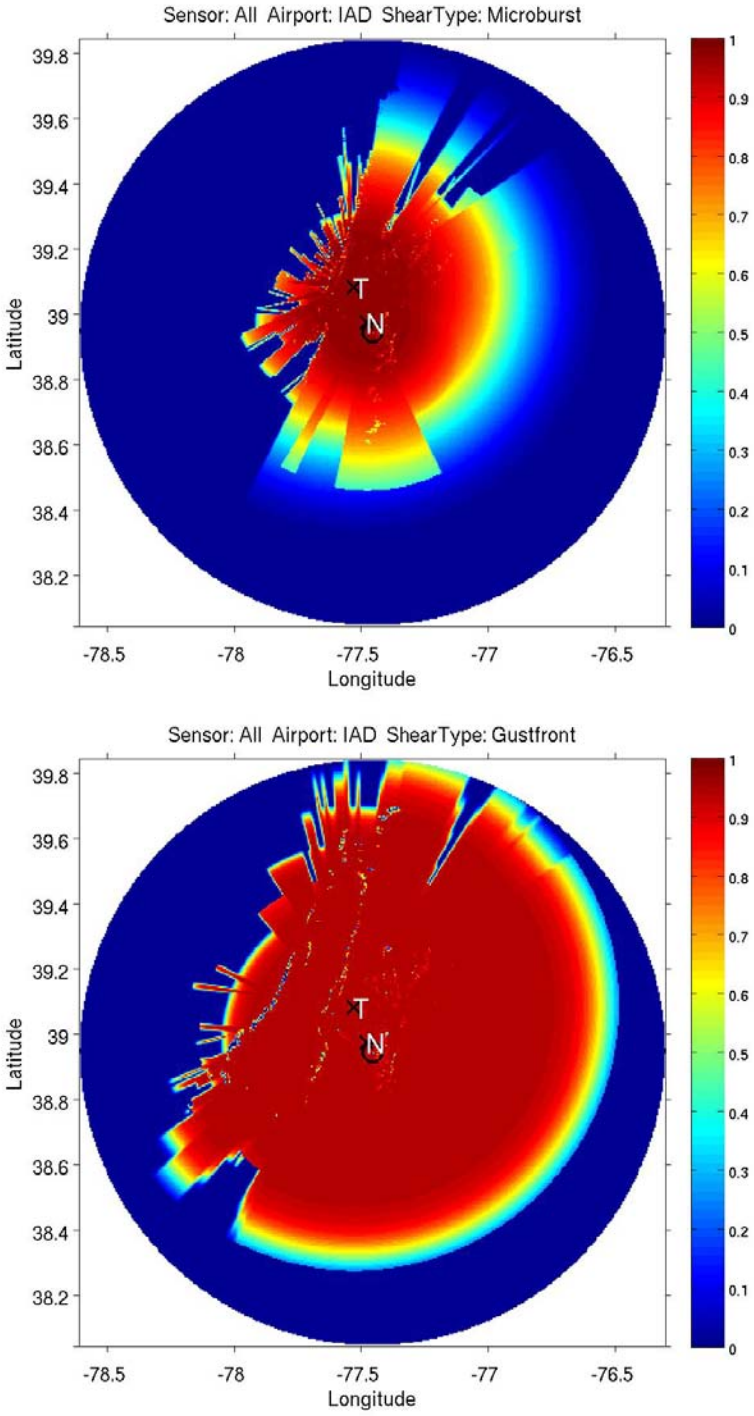

Figure C-14. Wind-shear visibility maps for IAD. Top: Microburst. Bottom: Gust front.

IAH

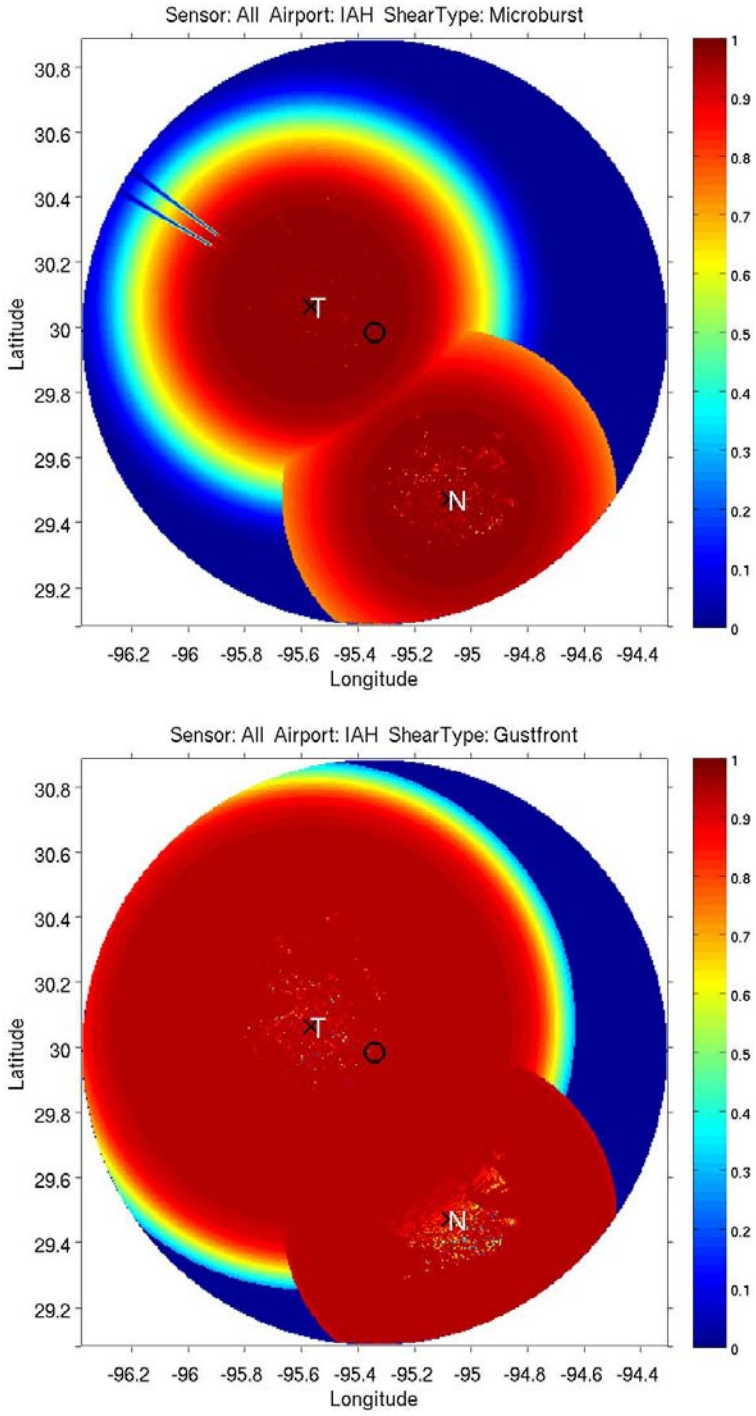

Figure C-15. Wind-shear visibility maps for IAH. Top: Microburst. Bottom: Gust front.

JFK

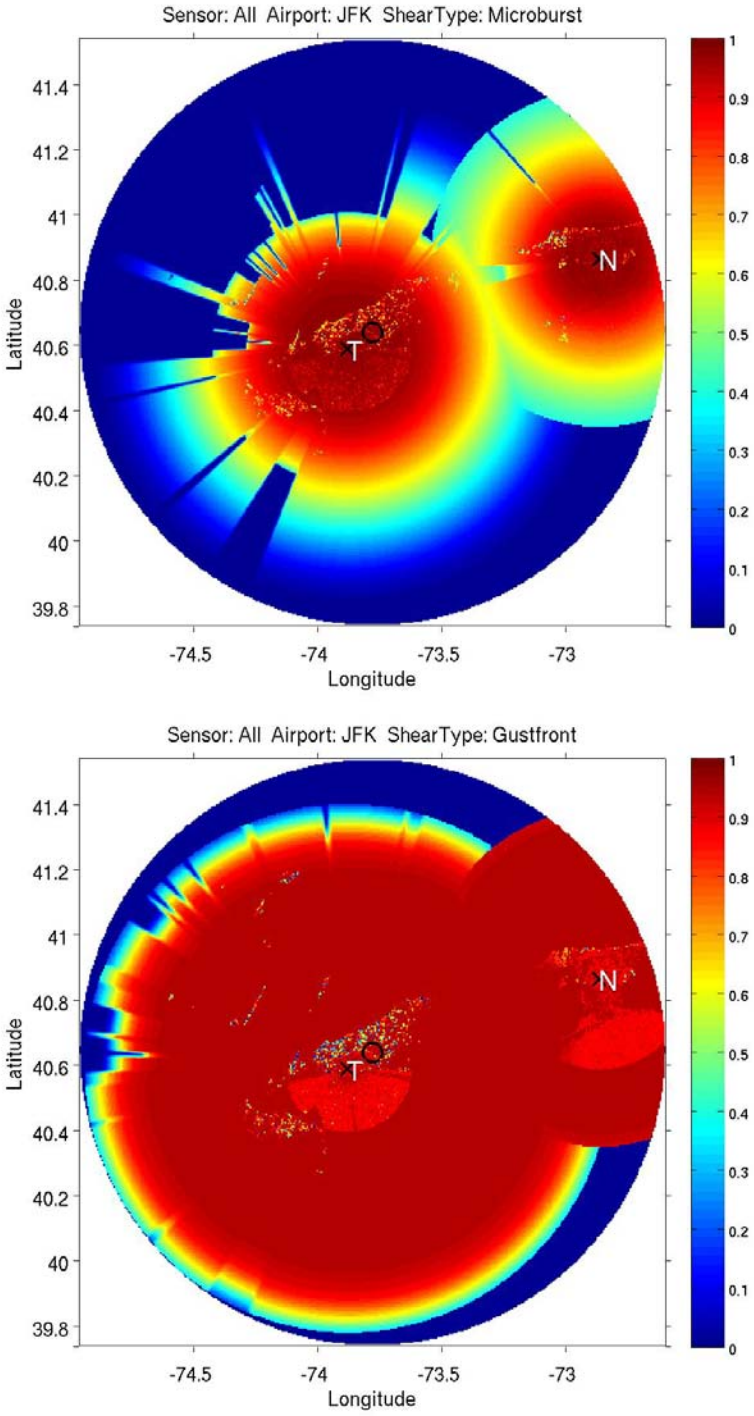

Figure C-16. Wind-shear visibility maps for JFK. Top: Microburst. Bottom: Gust front.

LAS

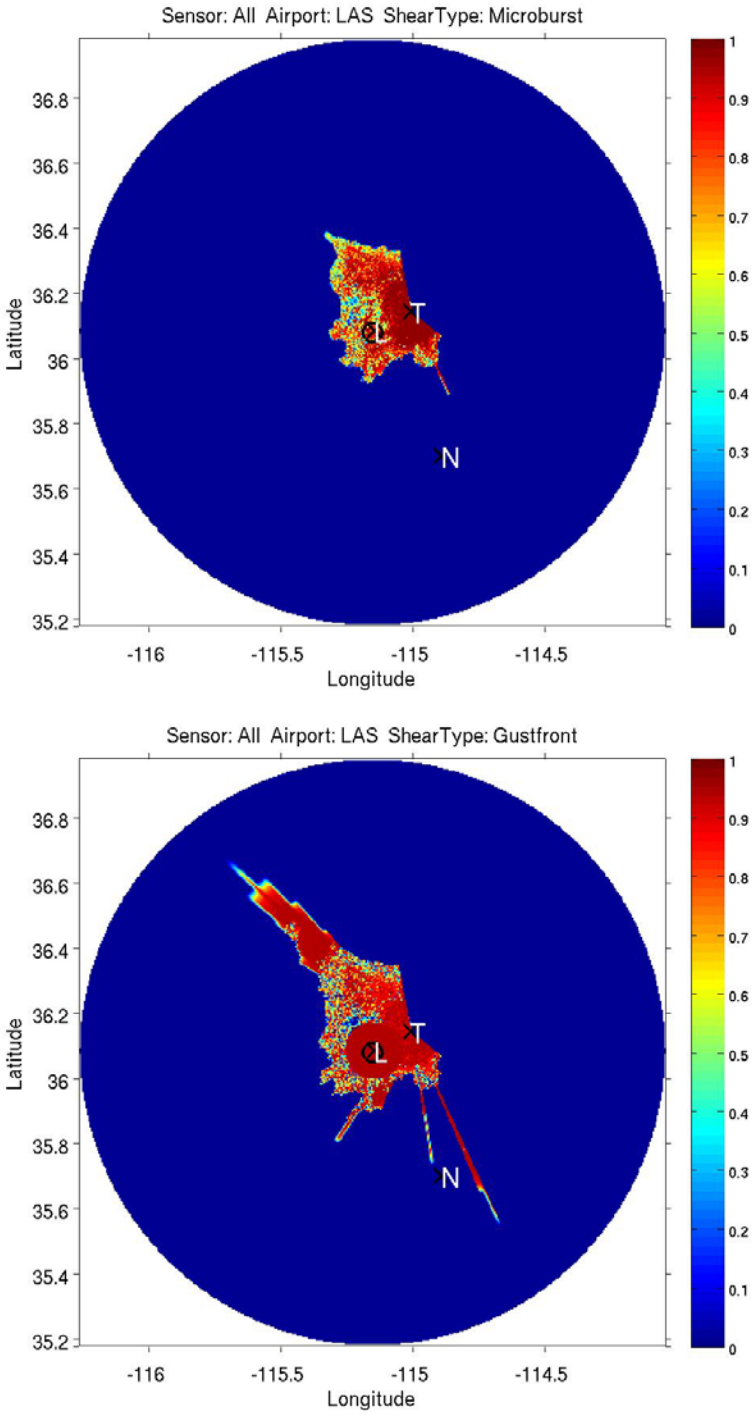

Figure C-17. Wind-shear visibility maps for LAS. Top: Microburst. Bottom: Gust front.

LAX

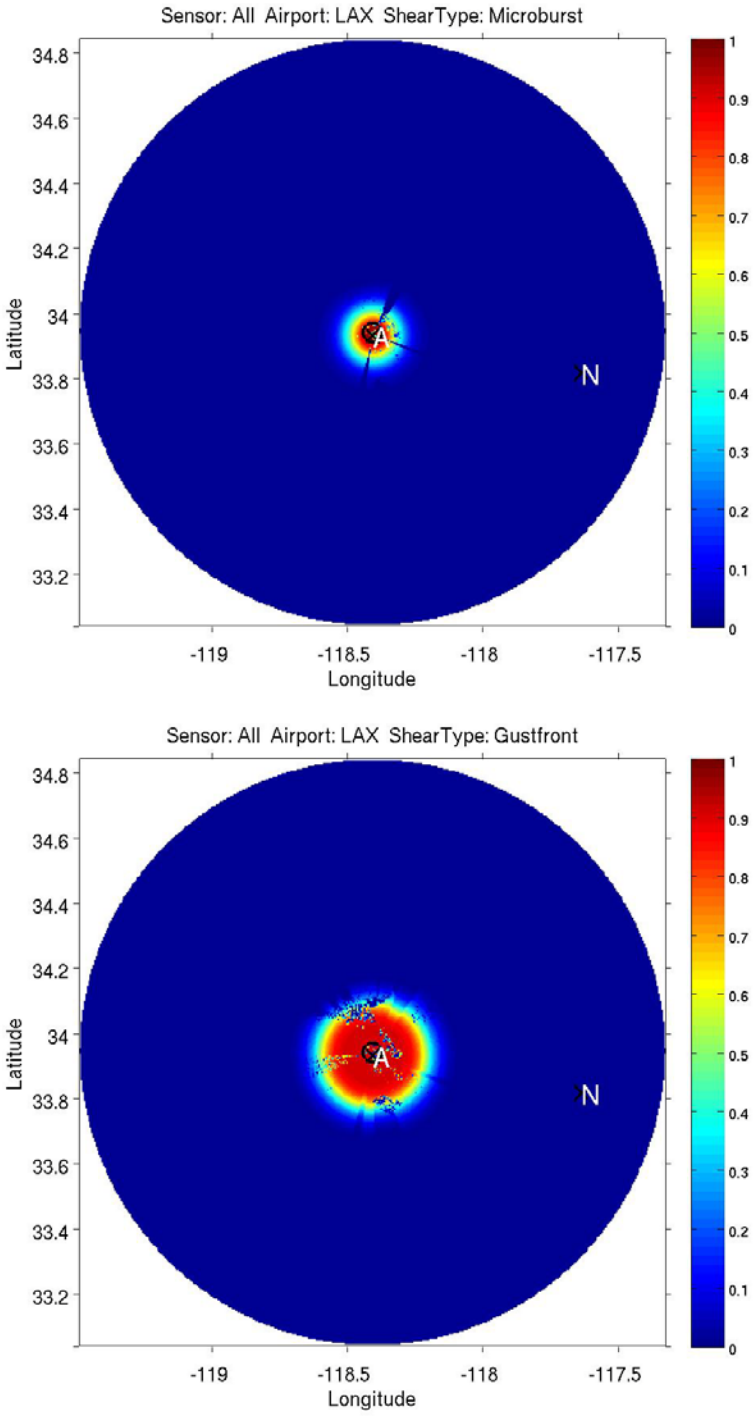

Figure C-18. Wind-shear visibility maps for LAX. Top: NEXRAD. Bottom: Gust front.

LGA

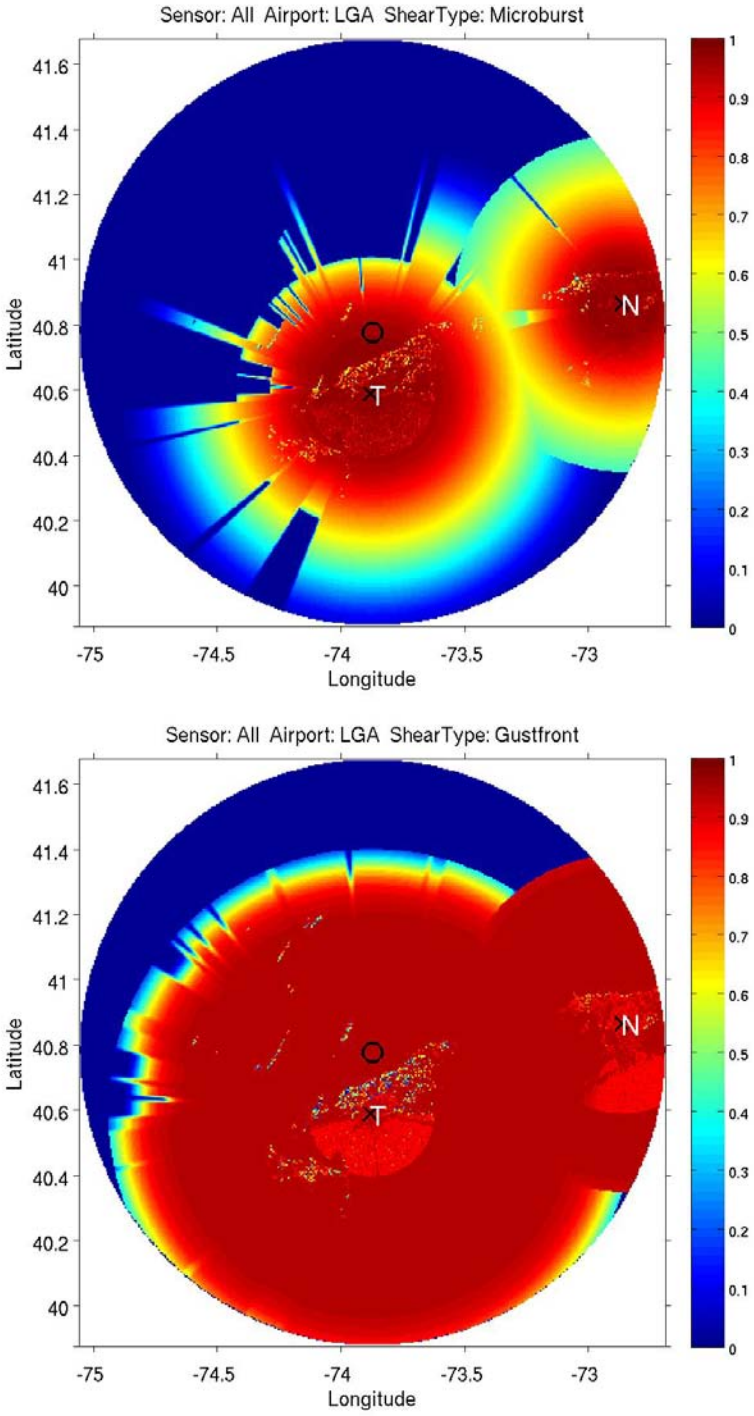

Figure C-19. Wind-shear visibility maps for LGA. Top: Microburst. Bottom: Gust front.

MCO

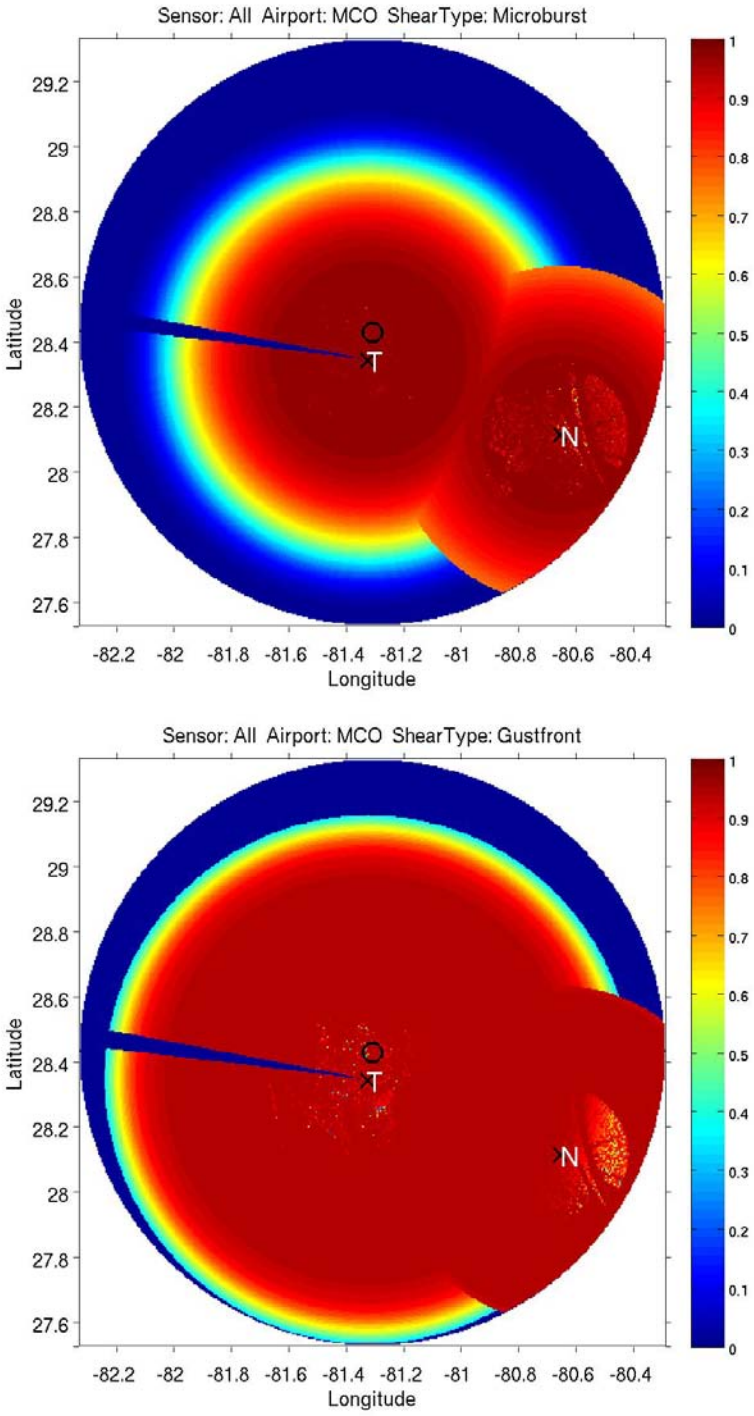

Figure C-20. Wind-shear visibility maps for MCO. Top: Microburst. Bottom: Gust front.

MDW

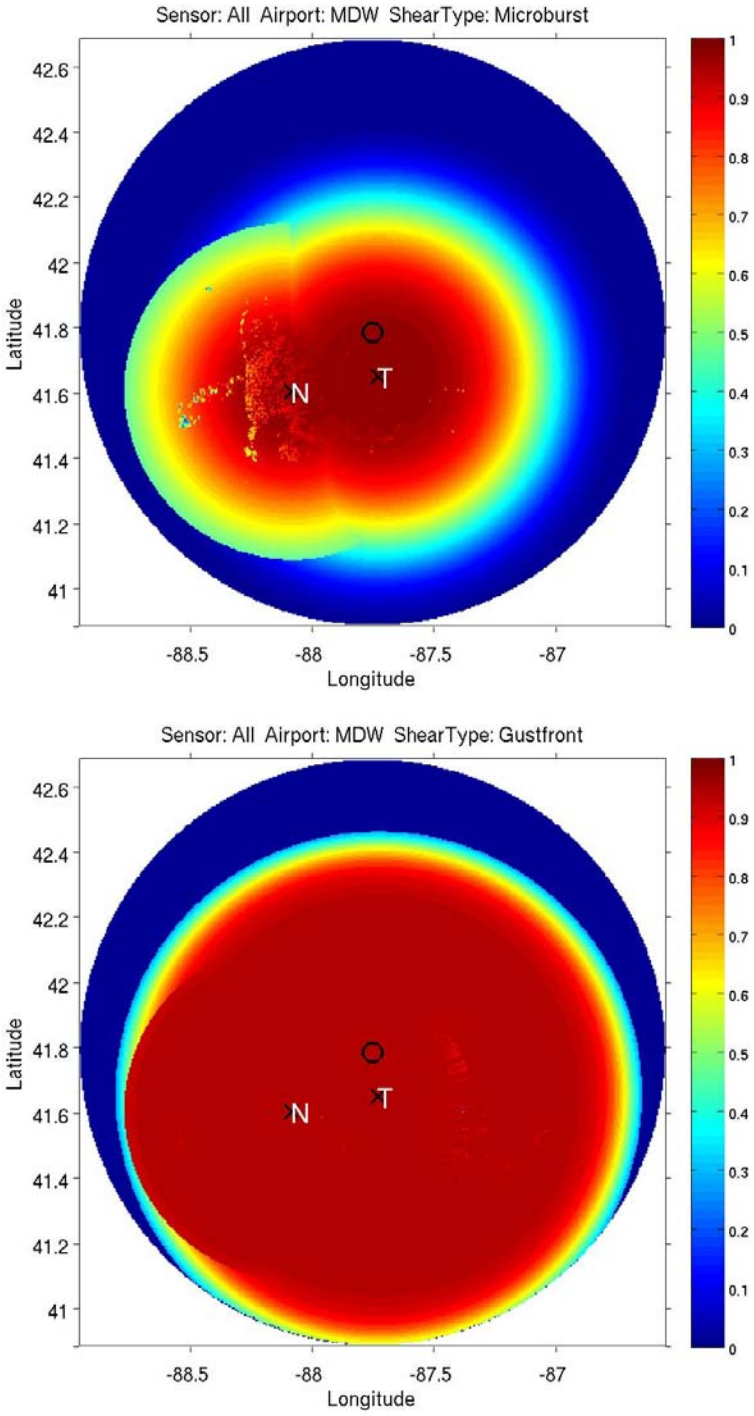

Figure C-21. Wind-shear visibility maps for MDW. Top: Microburst. Bottom: Gust front.

MEM

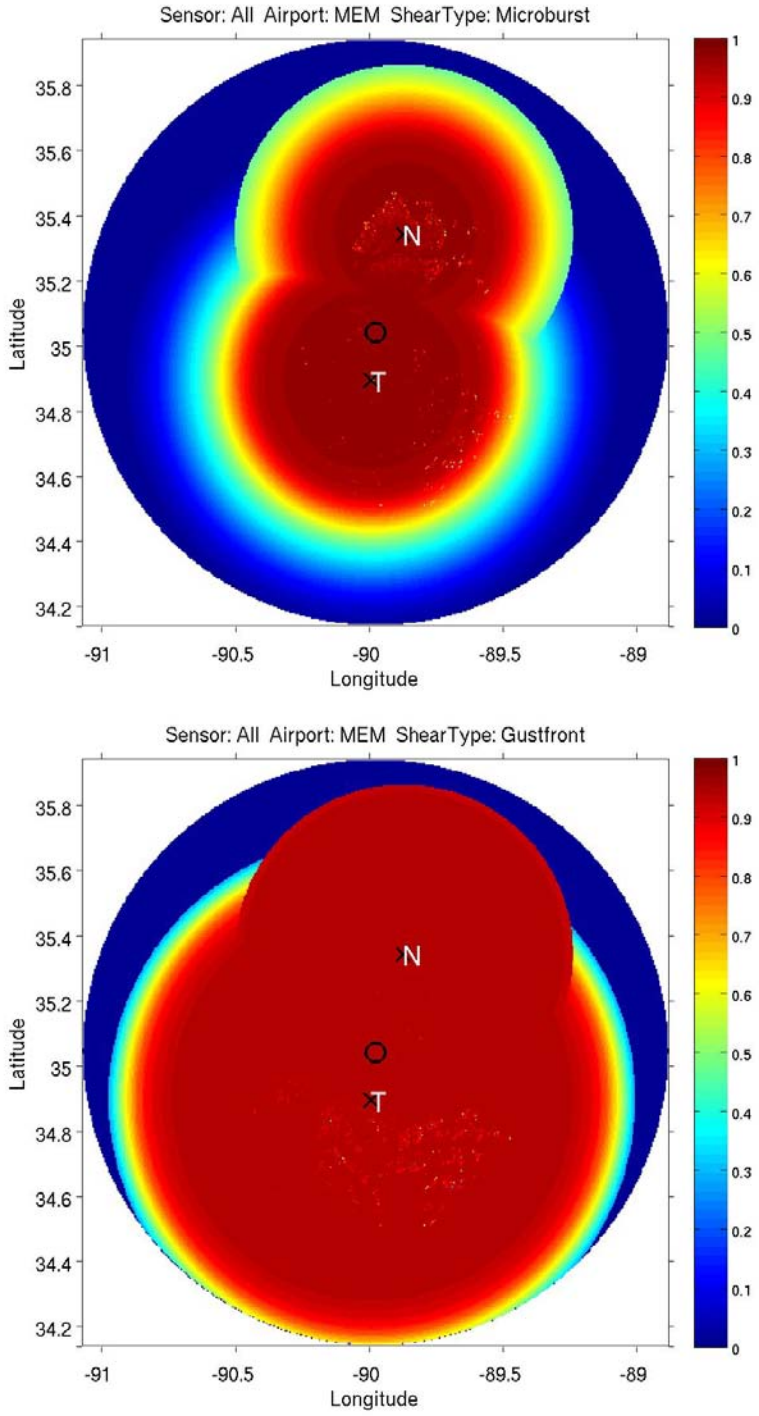

Figure C-22. Wind-shear visibility maps for MEM. Top: Microburst. Bottom: Gust front.

MIA

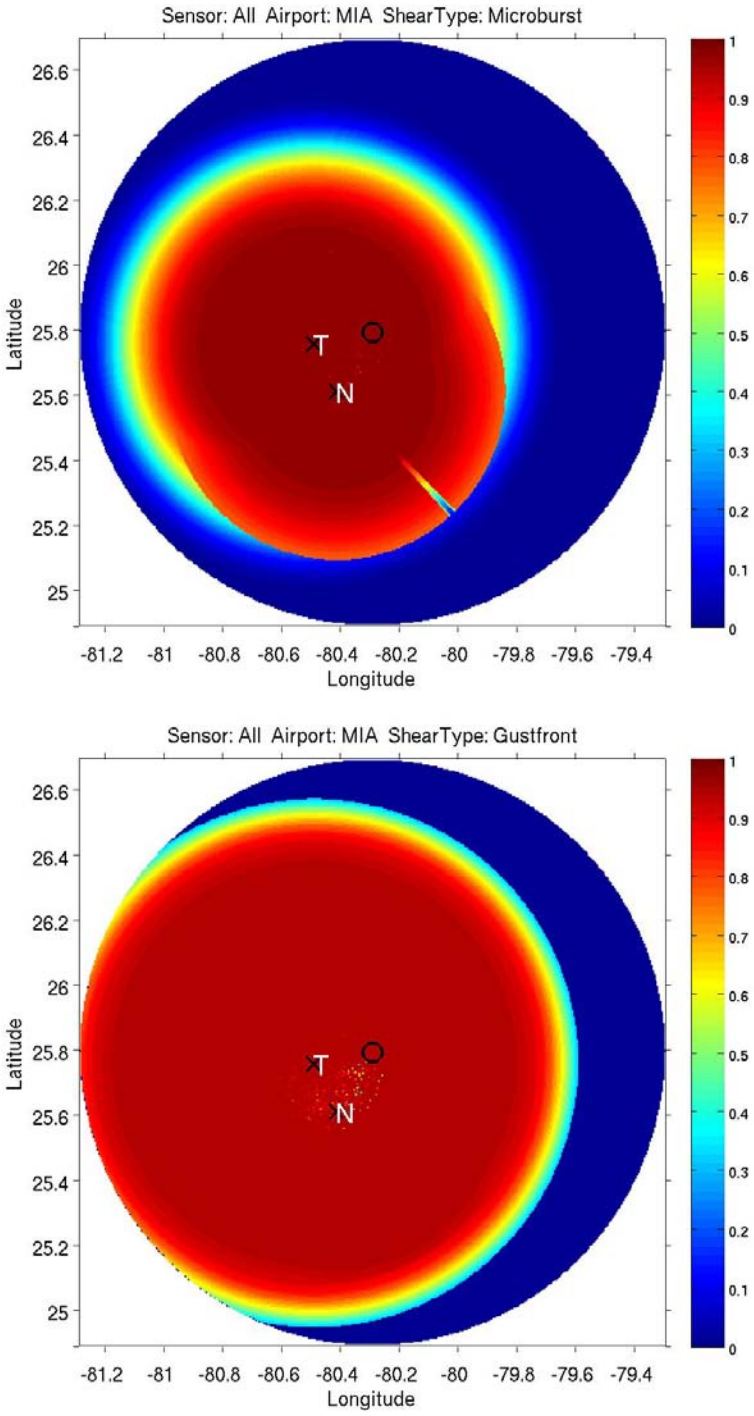

Figure C-23. Wind-shear visibility maps for MIA. Top: Microburst. Bottom: Gust front.

MSP

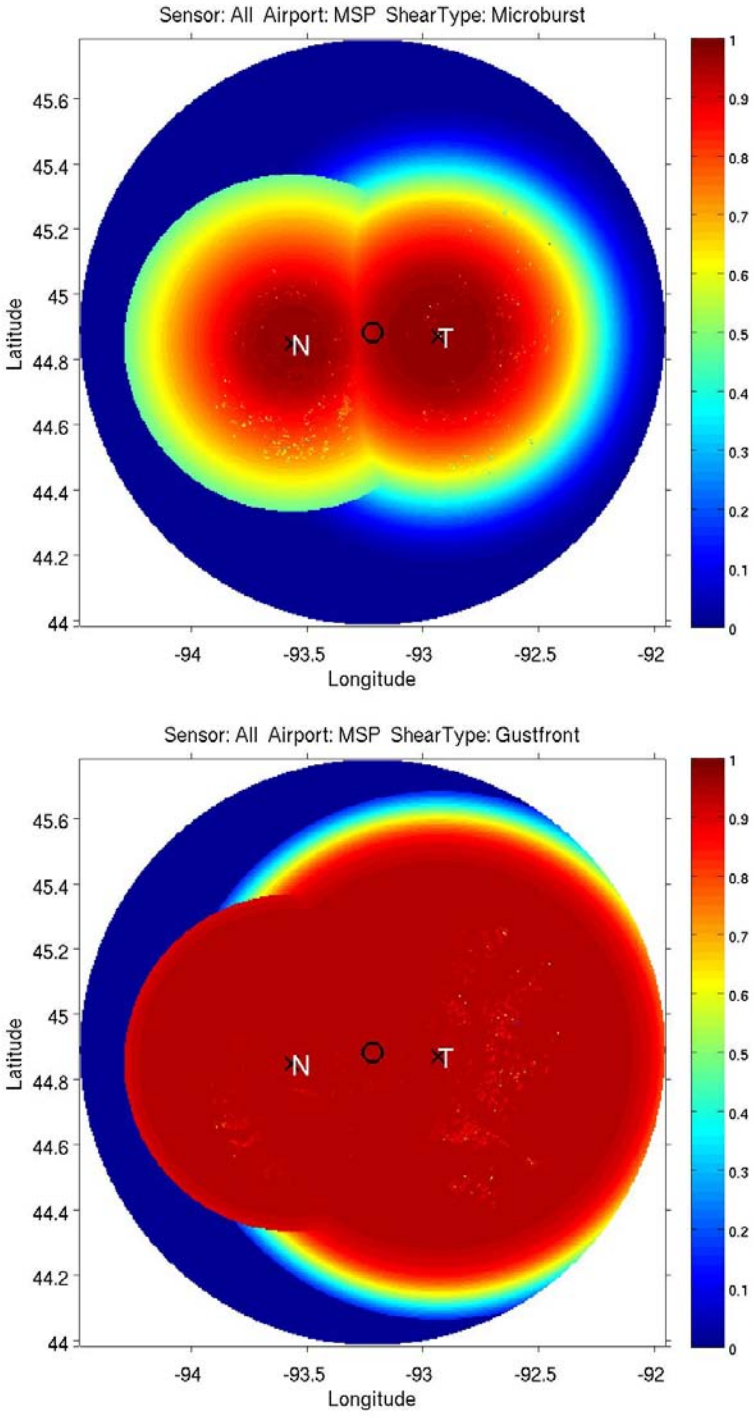

Figure C-24. Wind-shear visibility maps for MSP. Top: Microburst. Bottom: Gust front.

ORD

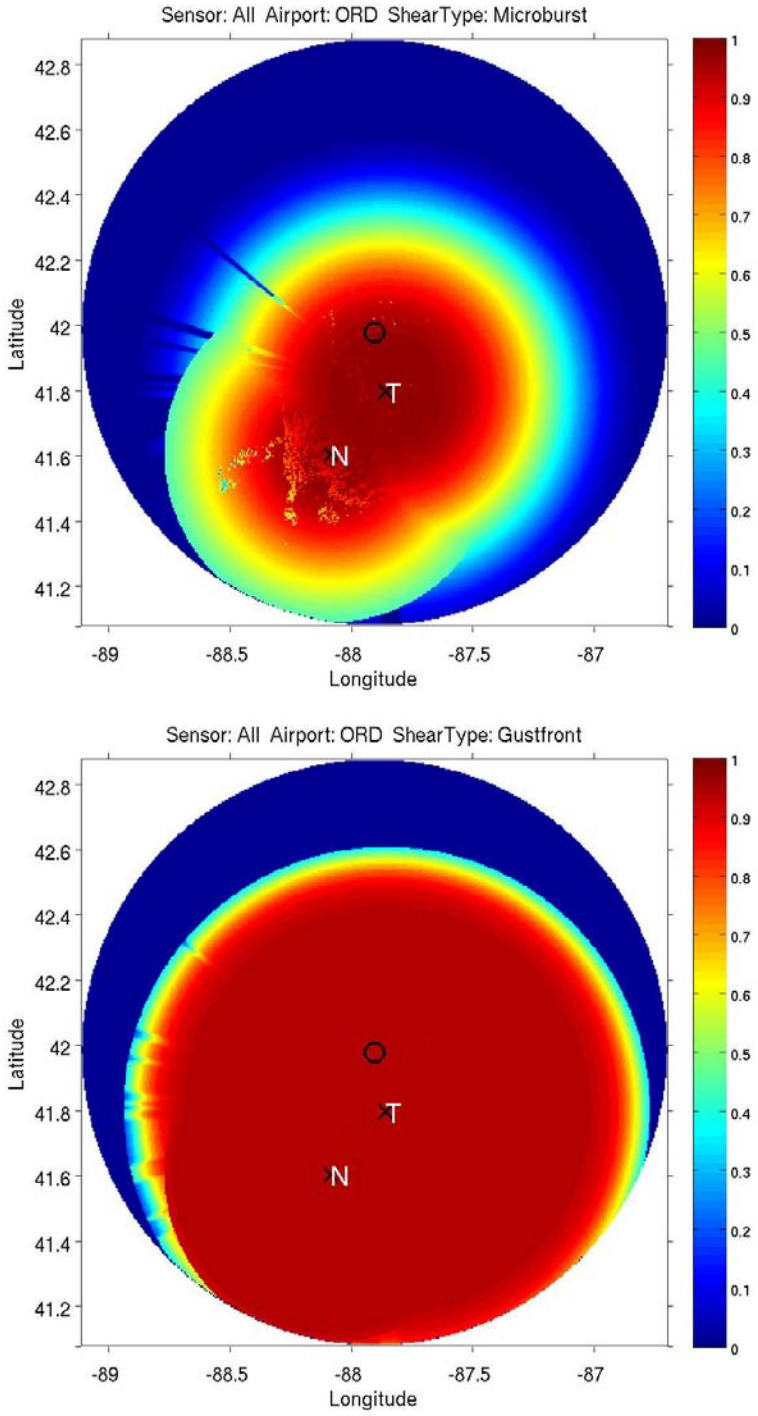

Figure C-25. Wind-shear visibility maps for ORD. Top: Microburst. Bottom: Gust front.

PDX

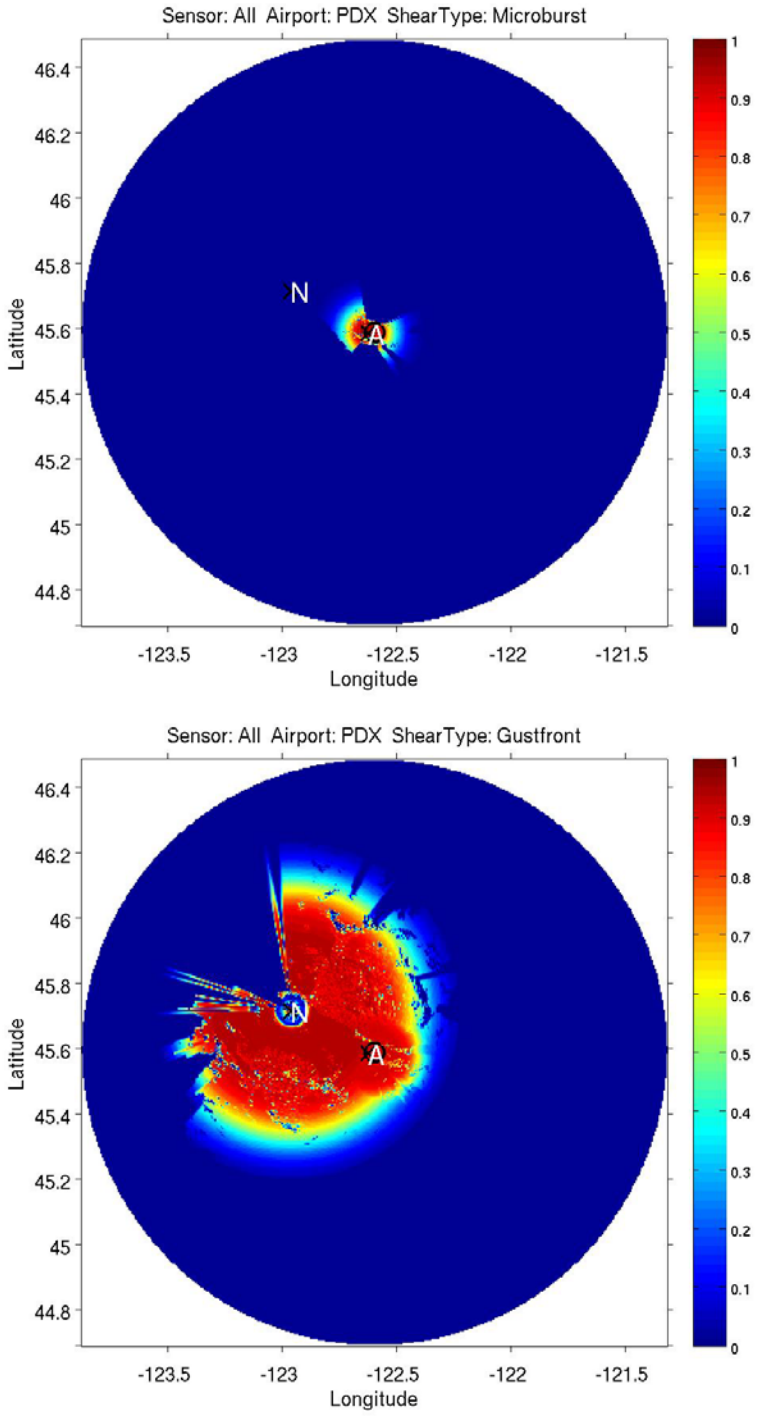

Figure C-26. Wind-shear visibility maps for PDX. Top: NEXRAD. Bottom: Gust front.

PHL

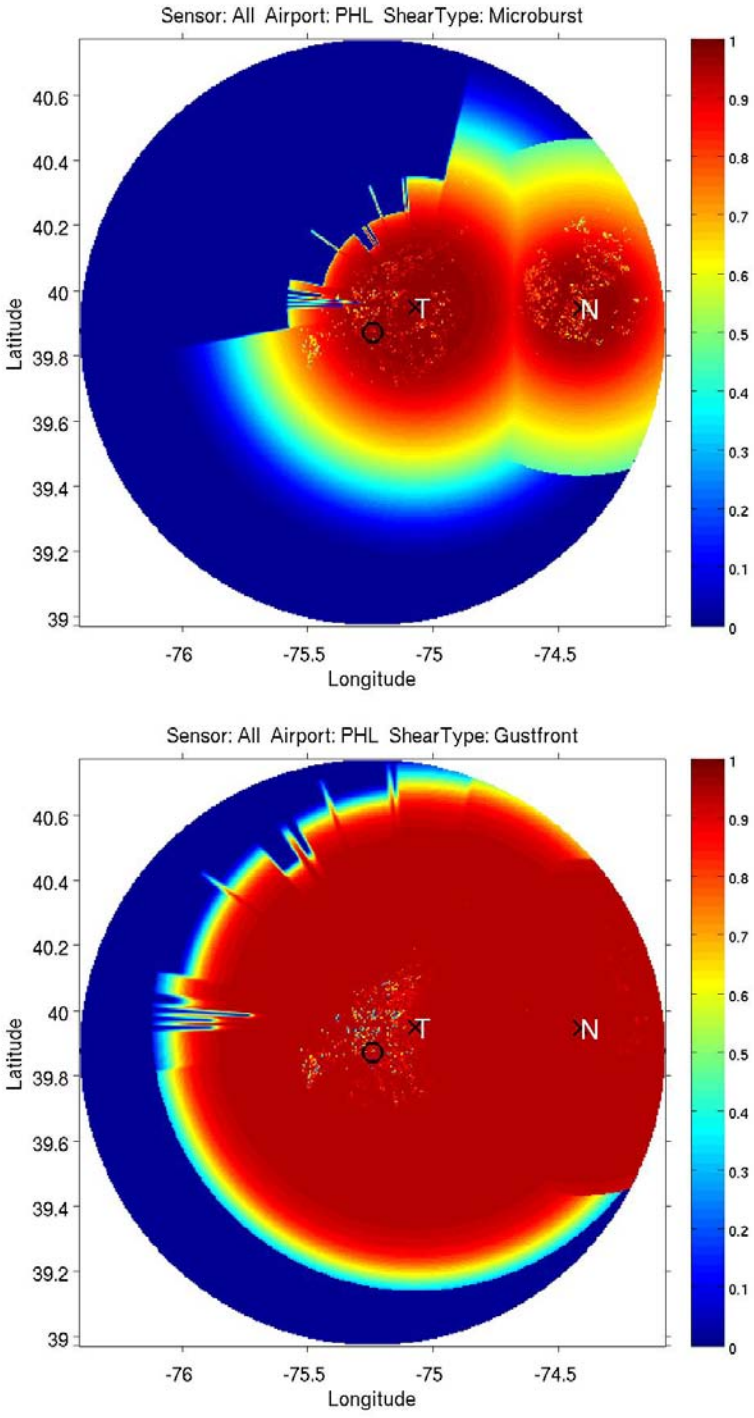

Figure C-27. Wind-shear visibility maps for PHL. Top: Microburst. Bottom: Gust front.

PHX

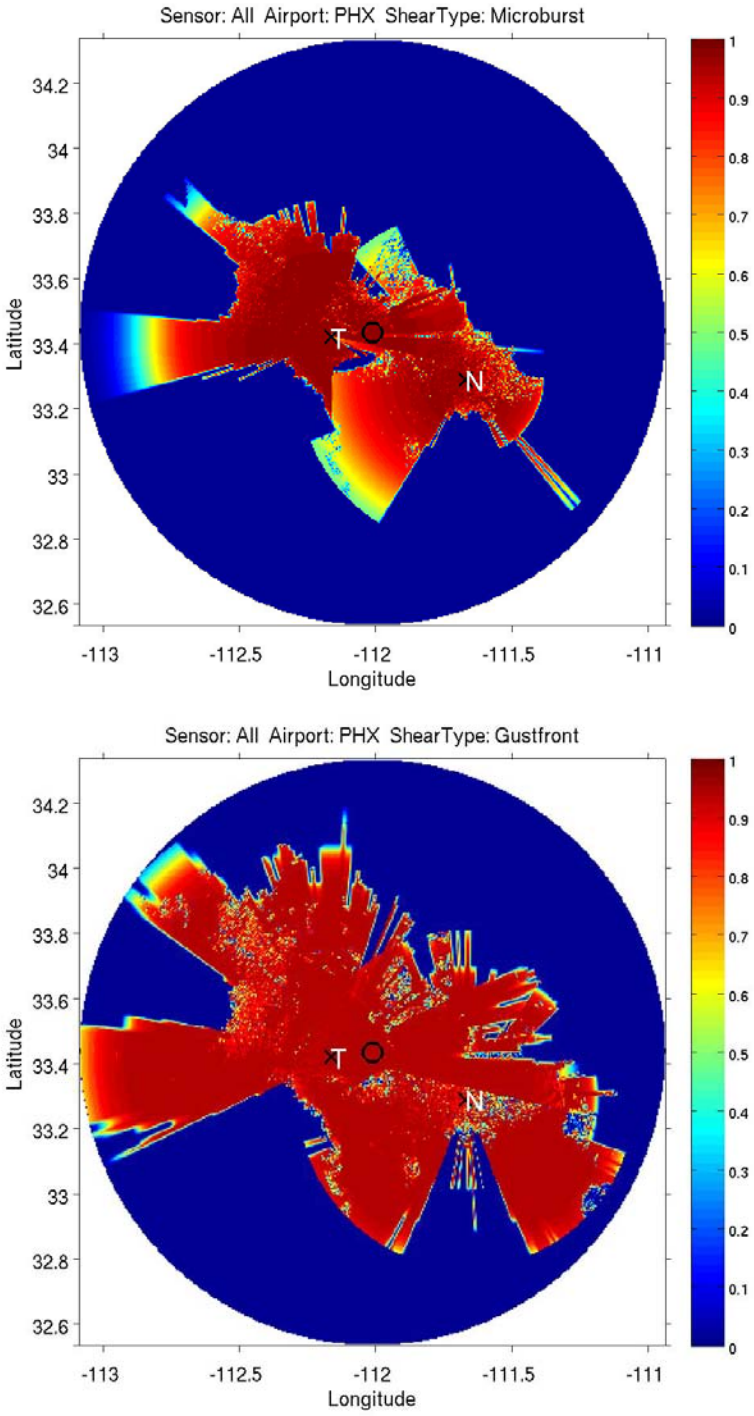

Figure C-28. Wind-shear visibility maps for PHX. Top: Microburst. Bottom: Gust front.

PIT

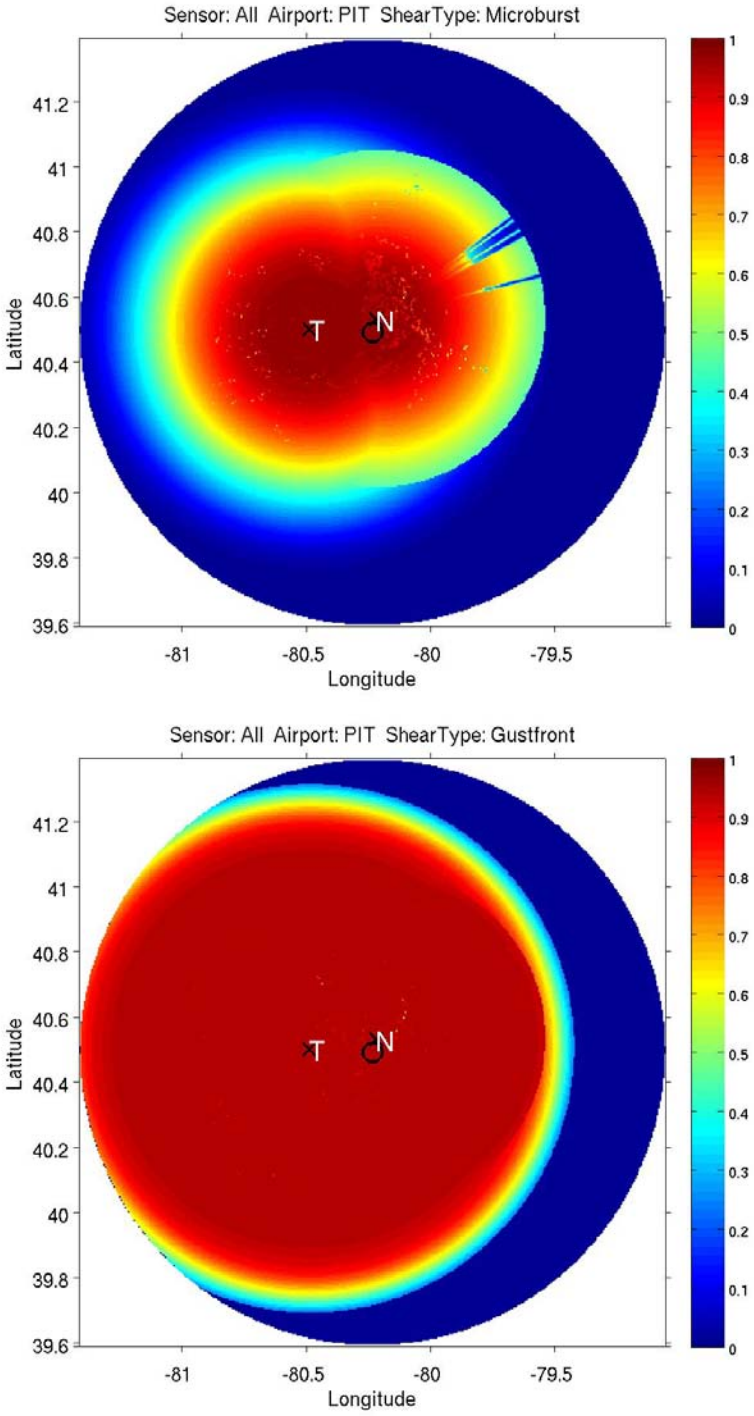

Figure C-29. Wind-shear visibility maps for PIT. Top: Microburst. Bottom: Gust front.

SAN

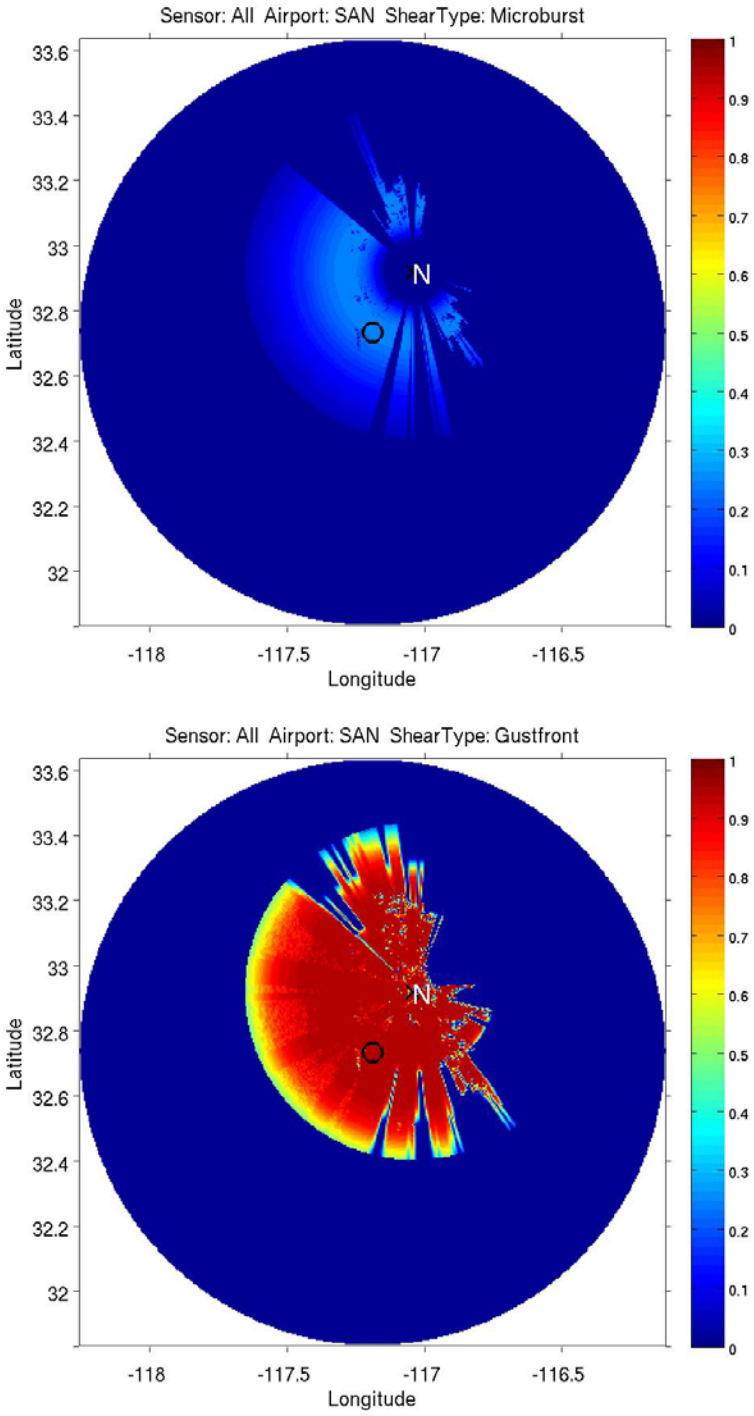

Figure C-30. Wind-shear visibility maps for SAN. Top: Microburst. Bottom: Gust front.

SEA

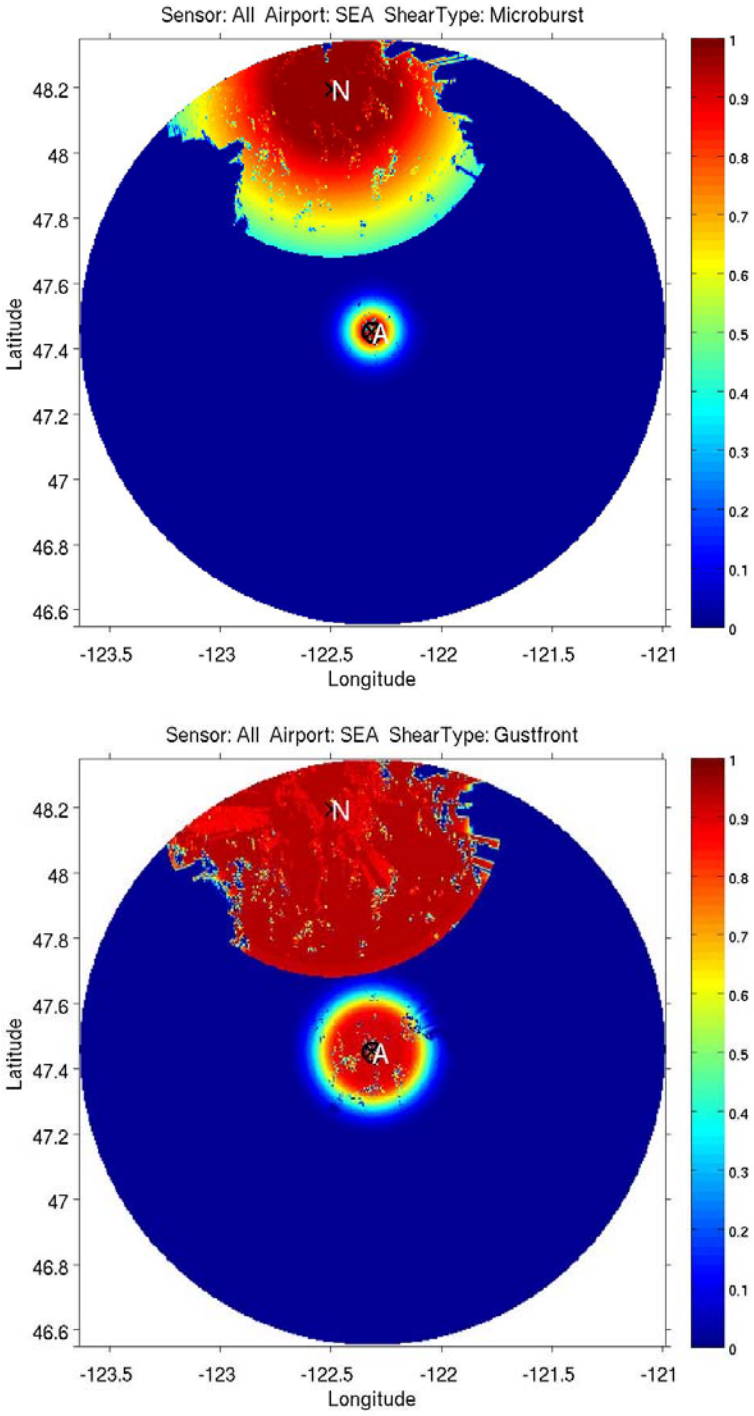

Figure C-31. Wind-shear visibility maps for SEA. Top: Microburst. Bottom: Gust front.

SFO

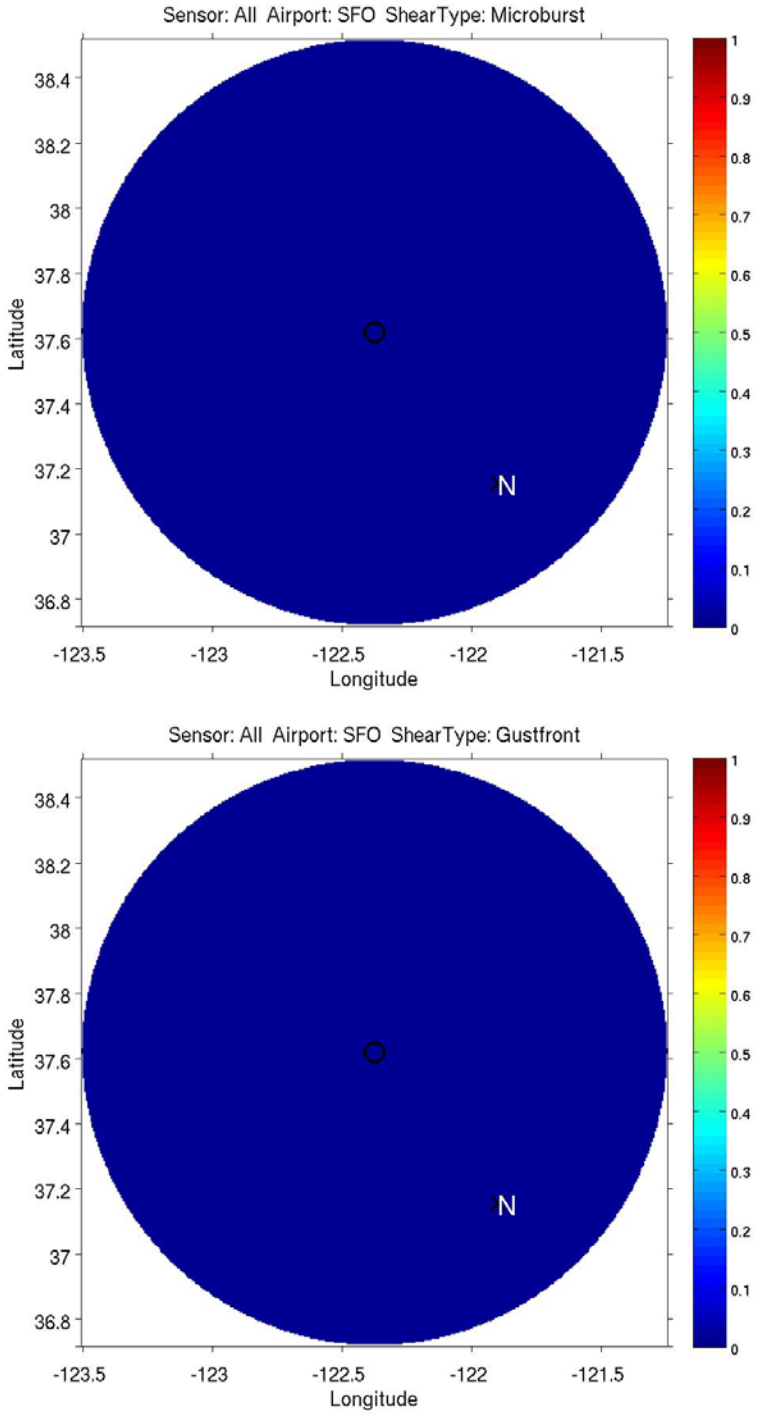

Figure C-32. Wind-shear visibility maps for SFO. Top: Microburst. Bottom: Gust front.

SLC

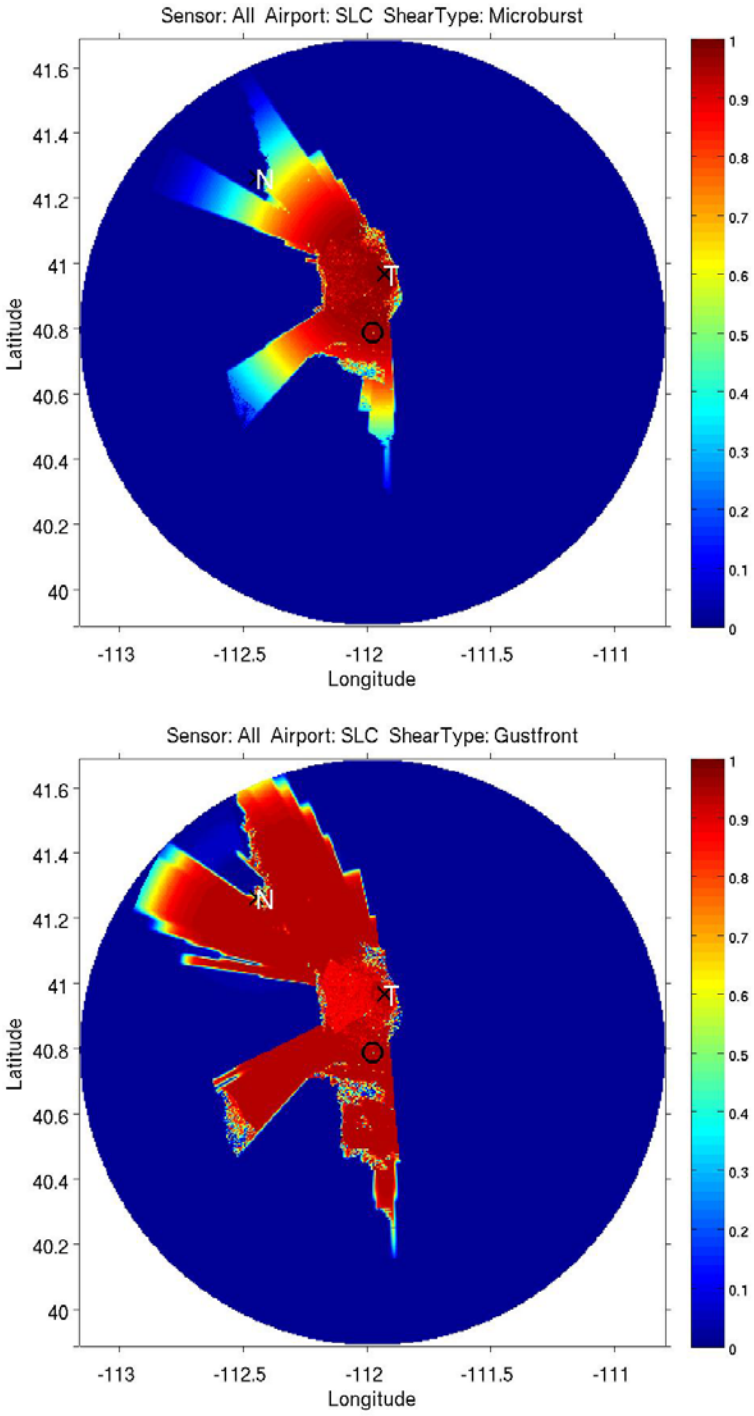

Figure C-33. Wind-shear visibility maps for SLC. Top: Microburst. Bottom: Gust front.

STL

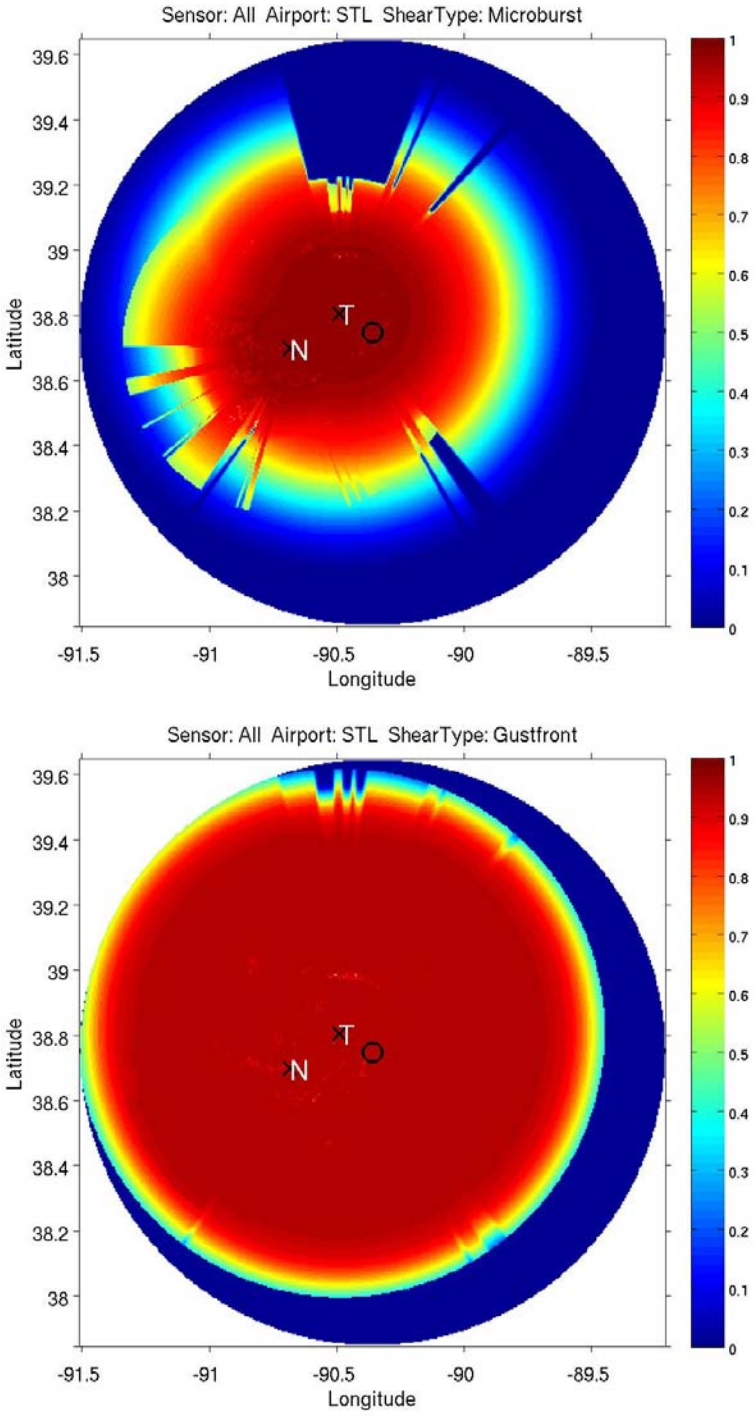

Figure C-34. Wind-shear visibility maps for STL. Top: Microburst. Bottom: Gust front.

TPA

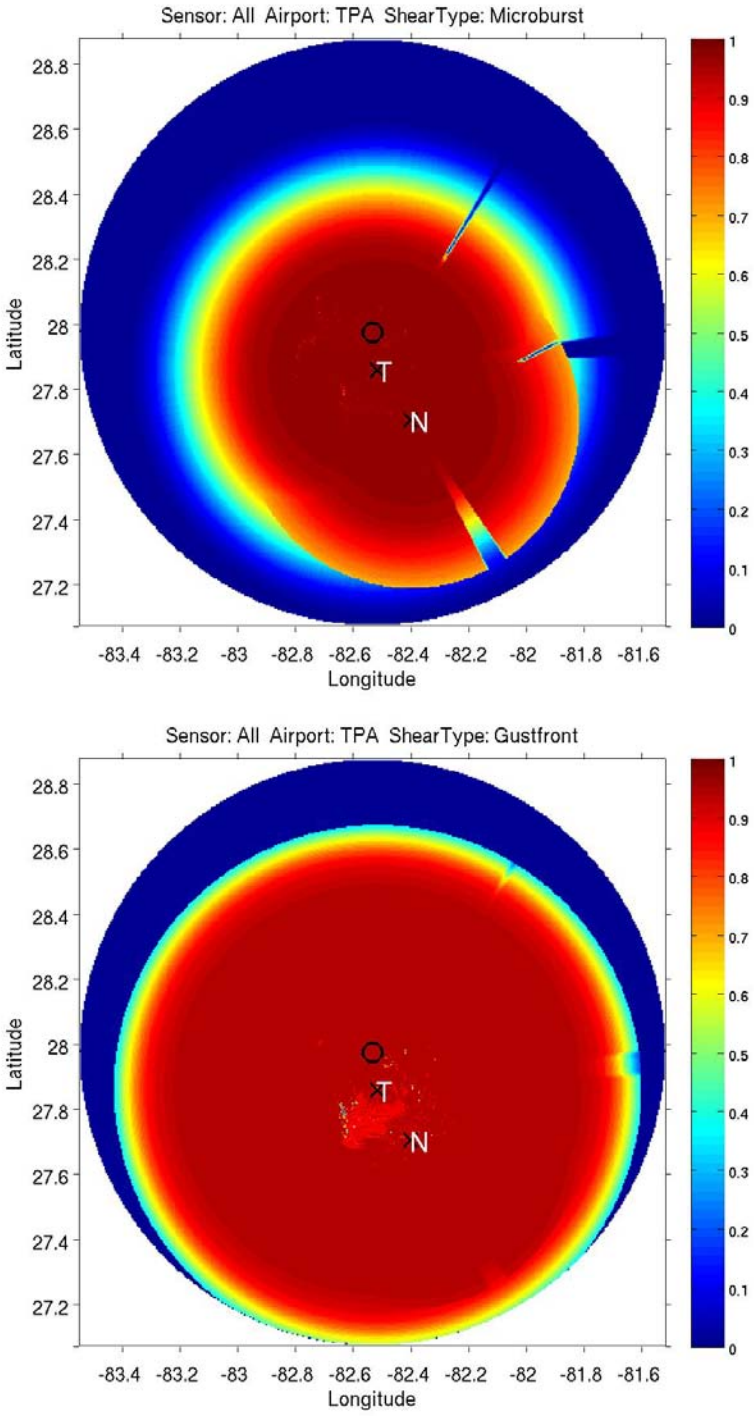

Figure C-35. Wind-shear visibility maps for TPA. Top: Microburst. Bottom: Gust front.